NASA TECHNICAL NOTE

NASA TN D-4844

NASA TN D-4844

WIND-TUNNEL INVESTIGATION OF THE LOW-SPEED HIGH-LIFT AERODYNAMICS OF A ONE-FIFTH SCALE VARIABLE-SWEEP SUPERSONIC TRANSPORT

by Anthony M. Cook

Ames Research Center
Moffett Field, Calif.

NATIONAL AERONAUTICS AND SPACE ADMINISTRATION • WASHINGTON, D. C. • OCTOBER 1968

WIND-TUNNEL INVESTIGATION OF THE LOW-SPEED HIGH-LIFT AERODYNAMICS OF A ONE-FIFTH SCALE VARIABLE-SWEEP SUPERSONIC TRANSPORT

By Anthony M. Cook

Ames Research Center
Moffett Field, Calif.

NATIONAL AERONAUTICS AND SPACE ADMINISTRATION

For sale by the Clearinghouse for Federal Scientific and Technical Information
Springfield, Virginia 22151 – CFSTI price $3.00

WIND-TUNNEL INVESTIGATION OF THE LOW-SPEED HIGH-LIFT AERODYNAMICS OF A ONE-FIFTH SCALE VARIABLE-SWEEP SUPERSONIC TRANSPORT

By Anthony M. Cook

Ames Research Center

SUMMARY

Low-speed aerodynamic characteristics of a large-scale variable-sweep supersonic transport model have been determined in the Ames 40- by 80-Foot Wind Tunnel. Included are data for the model both in and out of ground effect.

The results are presented as six-component aerodynamic force and moment data obtained at various angles of attack and sideslip. The investigation was made at a free-stream dynamic pressure of 25 pounds per square foot, corresponding to a Reynolds number of 11 million, based upon the mean aerodynamic chord of the fully swept wing. The majority of testing was directed toward the optimization of high-lift configurations and the investigation of longitudinal stability and control characteristics for the take-off and landing configurations. Data concerning low-speed flight at higher wing sweeps of 30°, 42° and 72° are also presented.

It is shown that the model maintained acceptable levels of longitudinal stability up to 13° angle of attack at high lift in both the landing and take-off configurations. The model also exhibited lateral and directional stability up to high angles of sideslip.

INTRODUCTION

A continuing series of investigations into the low-speed aerodynamics of supersonic transport configurations with wings of variable sweep is being conducted in the Ames 40- by 80-Foot Wind Tunnel. This paper presents the results of a recent investigation of a one-fifth scale model of a proposed 200-passenger version. Results pertaining to earlier (SCAT 14) configurations are to be found in reference 1.

The primary purpose of these tests was to investigate the longitudinal stability and lift characteristics of low-speed high-lift configurations in and out of ground effect with wings swept 20°. Included in the high-lift data are:

(1) Optimization studies for wing trailing-edge flap deflection and wing leading-edge slat configurations

(2) Effects of horizontal-tail incidence and elevator deflection, and

(3) Lateral control effectiveness of ailerons and spoilers.

The latter portion of this report contains longitudinal and lateral characteristics, at low speed, for configurations with higher angles of wing sweepback. Data are presented for sweep angles of 30° and 42°, representing low-speed-holding and subsonic cruise configurations, respectively. In addition, possible low-speed lift improvements at 72° wing sweep are shown for the emergency landing with wings fully swept.

The model had a movable outer wing panel with the pivot point at 42 percent of the fully swept wing semispan.

Six-component force and moment data are presented. Free-stream dynamic pressure was 25 pounds per square foot, corresponding to a Reynolds number of 11 million, based upon the mean aerodynamic chord of the fully swept wing.

NOMENCLATURE

b	wing span, ft
C_D	drag coefficient, $\frac{\text{drag}}{qS}$
C_L	lift coefficient, $\frac{\text{lift}}{qS}$
C_l	rolling-moment coefficient, $\frac{\text{rolling moment}}{qSb}$
C_m	pitching-moment coefficient, $\frac{\text{pitching moment}}{qS\bar{c}}$
C_n	yawing-moment coefficient, $\frac{\text{yawing moment}}{qSb}$
C_Y	side-force coefficient, $\frac{\text{side force}}{qS}$
c	chord
$\bar{c}$	mean aerodynamic chord of fully swept wing, $\frac{2}{S}\int_0^{b/2} c^2\,dy$, ft
$\bar{c}_T$	mean aerodynamic chord of horizontal tail, ft
$\bar{c}_V$	mean aerodynamic chord of vertical tail, ft
Droop	additional 25° leading-edge droop on all wing leading-edge slats
Ext	extended chord wing LE slats, number of segments indicated by subscript

G_a	gap of auxiliary wing TE flap, percent of streamwise wing chord
G_m	gap of main wing TE flap, percent of streamwise wing chord
h	distance from ground plane to model moment center at $\alpha = 0^\circ$, ft
i_T	horizontal-tail incidence, positive trailing edge down, deg
LE	leading edge
l_T	tail length, measured from 40 percent $\bar{c}$ to 25 percent of the tail mean aerodynamic chord, ft
q	free-stream dynamic pressure, lb/ft^2
S	total planform area of fully swept wing, ft^2
strake	fixed, inboard portion of the wing
TE	trailing edge
$\overline{V}_T$	tail volume coefficient, $\frac{S_T}{S}\frac{l_T}{\bar{c}}$
x	streamwise distance along airfoil chord, ft
y	spanwise distance perpendicular to the plane of symmetry, ft
z	perpendicular distance above the wing chord plane, ft
α	angle of attack of body reference axis, deg
β	angle of sideslip of plane of symmetry, deg
δ	angle of deflection of control surface, or flap, or slat, measured normal to hinge line, deg
δ_A	angle of aileron deflection (positive for right wing down roll)
δ_e	angle of elevator deflection (negative, TE up), deg
δ_F	angle of wing TE flap deflection (stated as: "Main flap deflection-auxiliary flap deflection") relative to wing chord plane, deg
δ_R	angle of rudder deflection (positive, TE left), deg
δ_S	angle of wing LE slat deflection, deg
δ_{SF}	angle of strake TE flap deflection, deg
δ_{SP}	angle of wing spoiler deflection (positive, TE up), deg

δ_{SS} angle of strake LE slat deflection, deg

η wing semispan station, $\frac{2y}{b}$

Λ angle of sweepback of outer wing leading edge, deg

Sample Configuration Legend:

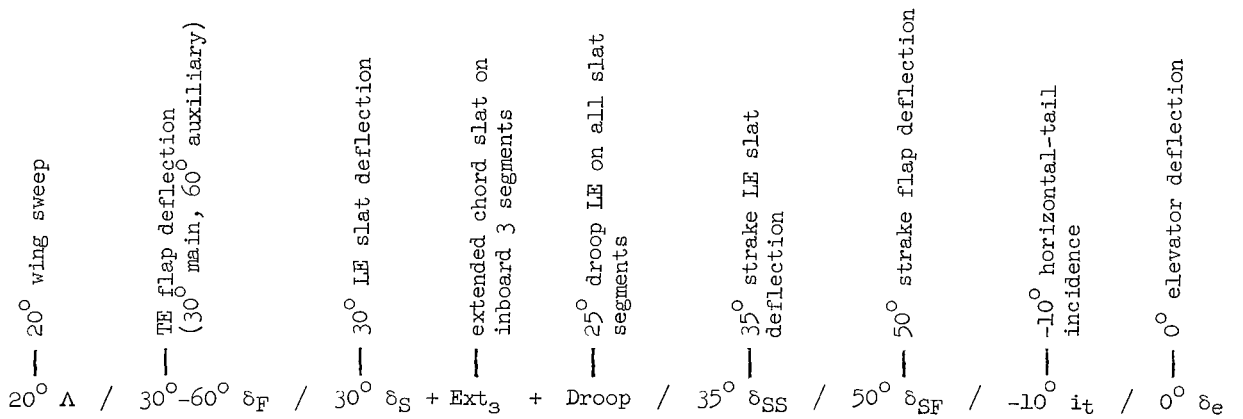

MODEL AND APPARATUS

The model was installed in the wind tunnel as shown in figure 1.

The model represented, to one-fifth scale, a typical 200-passenger version of a low-wing, variable-sweep supersonic transport configuration. Wing leading-edge sweepback angles were variable from 20° to 72°, with intermediate positions of 25°, 30°, and 42°. The inboard, fixed portion of the wing, hereafter referred to as the strake, had a leading-edge sweep of 72°. Thus, with the outer panel fully swept to 72°, the leading edges of both strake and wing were continuous, forming an arrow-wing planform.

Planform

The aerodynamic reference dimensions of the model are listed in table I. Geometric details of the model and component parts are shown in figure 2.

Wing.- The wing-strake airfoil sections of the fully swept wing were those of a previously optimized supersonic wing. Typical airfoil sections at various spanwise stations are shown in figure 2(b), and the corresponding airfoil ordinates are listed in table II. The wing was fabricated to represent the twist and camber for a 1 g take-off condition with 20° of wing sweep, and a wing loading of 100 pounds per square foot. The resultant wing twist

is shown in the curve of figure 2(e). The wing pivot on the fully swept wing was located at 42 percent semispan and 57 percent mean aerodynamic chord. The strake leading-edge radius was tapered from 0.015 $\bar{c}$ at the forward (fuselage) juncture, to 0.0012 $\bar{c}$ (outer wing leading-edge radius) at the wing-strake juncture. Typical strake sections for three longitudinal body stations are shown in figure 2(b).

High-Lift Devices

Wing trailing-edge flaps.- A typical cross section of the double-slotted trailing-edge flaps is shown in figure 2(c). Total flap system chord was 30 percent of the wing chord and the auxiliary flap comprised 40 percent of the total flap chord. The flaps were built in three sections on each wing, extending from 25 to 80 percent of the unswept semispan, measured from the plane of symmetry. Flap deflection and gap were adjustable. The notation used gives the flap deflections relative to the wing reference plane of both the main and auxiliary flaps. For example, 30°-50° δ_F denotes 30° and 50° deflection of the main and auxiliary flaps, respectively (see fig. 2(c)). Flap gaps, optimized in a previous exploratory investigation, were set as follows: For flap deflections of 30°-50° and higher (representative of landing flap deflections) gaps of 1.5 and 0.6 percent wing chord were set for the main and auxiliary flaps, respectively; for take-off deflections, 20°-50° or lower, gaps of 2.5 and 1.0 percent c were used.

Wing leading-edge slat.- Four wing leading-edge slat configurations were tested and are shown in figure 2(d).

Slat deflections of 20°, 30°, and 40° were tested with a gap of 1.2 percent wing chord (see fig. 2(c)).

For purposes of identification, it should be noted that slat configurations were altered by slat segment, there being four segments, numbered 1 through 4 starting inboard, as shown in figure 2(a). The basic slat (see fig. 2(d)) was used unless otherwise noted. When the slat with leading-edge droop was installed, data legends indicate "droop," signifying leading-edge droop on all slat segments. Thus, for example, a data legend of 30° δ_S + Ext_3 + Droop indicates all slat segments deflected 30°, extended chord slat on inboard 3 segments, and leading-edge droop on all four segments.

Wing leading-edge chord extension.- For wings swept 30° and 42°, with flaps and slats up, a wing leading-edge chord extension was tested. This chord extension, from 67 to 84 percent semispan, extended the wing chord 10 percent, with a droop of 10° and had no gap.

Strake leading-edge slat.- A constant 6-inch chord slat (fig. 2(c)), 4.25 percent $\bar{c}$ (perpendicular to the leading edge), was installed along the strake leading edge for flow control during high-lift testing. The slat geometry was the same as that of the strake leading edge. The slat was adjustable for deflections of 35° and 40°, relative to the wing reference plane. Strake slat gap was a constant 1.5 inches (0.011 $\bar{c}$).

Strake trailing-edge flap.- A plain flap of 11-inch chord (0.078 $\bar{c}$) and 6-inch span (0.042 $\bar{c}$) was installed at the trailing edge of the strake. This flap, designed to deflect between the inboard and outboard engine nacelles, was adjustable for deflections of 0°, 20°, 40°, and 50° from the wing reference plane.

Controls

Longitudinal.- The horizontal-tail airfoil section consisted of a symmetrical 3 percent hexagonal section with contour breaks at 35 and 65 percent chord. The leading-edge radius was 0.2 percent chord. The tail was mounted on the fuselage with a negative dihedral of 10°. In addition, a plain-flap-type elevator was incorporated on the horizontal tail. The elevator chord had a linear taper from 25 percent tail chord at the root to 30 percent tail chord at the tip.

Lateral directional.- The model was equipped with ailerons for lateral control at low flight speeds. Aileron span (relative to 20° wing sweep) was 20 percent of wing semispan, extending from 80 percent semispan to the wing tip fairing. Aileron chord was 25 percent of the local wing chord.

The remainder of the lateral control system for low speed consisted of wing upper surface spoilers just ahead of the flaps as shown in figure 2(c). Three spanwise spoiler sections on each wing could be deflected in 5° increments, separately or together.

The vertical tail had the same section definition as the horizontal tail. Incorporated was a rudder of 35 percent tail chord, extending from the root to 71 percent of the vertical tail height. Directional characteristics were obtained for 0° and 25° left rudder.

Other Model Components

Fuselage.- Typical fuselage cross sections, for various body stations, are shown in figure 2(a).

Nacelles.- The model was equipped with four hollow, flow-through nacelles, mounted on the underside of the strake, to simulate a four-engine side-by-side arrangement. The nozzle exit diameter represented a fully expanded nozzle condition. This nozzle shape and the nacelle interior contour were designed to provide a minimum of flow separation.

Landing gear.- In order to investigate wake and interference effects of landing gear, mock-ups of representative gear assemblies were installed on the model during ground-effect testing. The gear system included wheels, gear doors, and tubing to scale size simulating gear support members and struts.

TESTS

The data presented in this paper resulted from a series of three wind-tunnel tests. Two of the tests were made with the model mounted on the vertical center line of the wind tunnel, out of ground effect, with the data corrected to free-air conditions. The third test was made with the wind-tunnel ground plane installed and the model in ground effect at a height-to-wing-span ratio (at 20° wing sweep) of 0.11.

Six-component force and moment data were obtained through angle-of-attack ranges from -4° to +40° out of ground effect, and -4° to +12° in ground effect. Data were obtained for angles of sideslip from -12° to +8° out of ground effect. Free-stream dynamic pressure was 25 pounds per square foot, corresponding to a Reynolds number of 11 million, based upon the fully swept wing mean aerodynamic chord.

The majority of tests were directed toward the optimization of high-lift devices for landing and take-off and the investigation of longitudinal stability characteristics for the optimized take-off and landing configurations.

Partial-span, double-slotted trailing-edge flaps were tested on the 20° swept wing to optimize the deflection angles for both the take-off and landing configurations. Various combinations of the four spanwise wing leading-edge slat configurations were tested to adjust to local flow conditions for optimum slat effectiveness. The wing slat study obtained the effects of deflection angle, slat chord length, and slat nose droop.

Longitudinal control data were obtained from horizontal-tail incidence positions from +5° to -20° in 5° increments, and elevator deflections of 0°, -10°, and -20°.

Ailerons and spoilers were also tested to determine the lateral characteristics of the take-off and landing configurations and to assess the effectiveness of these devices for lateral control. Ailerons were always deflected equally in opposite directions, positive deflection indicating positive roll.

REDUCTION OF DATA

Corrections

Out of ground effect (free air).- Standard corrections were applied to the longitudinal data to account for wind-tunnel wall effects. The corrections accounted for variations in span due to wing sweep, as follows (all corrections additive):

Wing sweep	20°	25°	30°	42°	72°
$\Delta\alpha/C_L$	0.44	0.44	0.45	0.46	0.51
$\Delta C_D/C_L^2$	.008	.008	.008	.008	.009
$\Delta C_m/C_L$	.0034	.0034	.0034	.0035	.0038

In addition, the following additive corrections were applied to account for the combination of tares resulting from wind forces on the exposed portions of the model support struts:

$$\Delta C_D = -0.0225$$

$$\Delta C_m = 0.0188$$

In ground effect (h/b = 0.11).- No boundary corrections were applied to the ground-effect data since the method of reference 2 indicated that subtracting the floor correction from the total boundary correction results in a negligible correction for the remaining tunnel boundaries.

An angle-of-attack correction to account for the upwash created by the presence of the ground plane was applied to all ground-effect data as follows:

$$\alpha = \alpha_u + 0.5^\circ$$

Additive corrections for exposed strut tares were as follows:

$$\Delta C_L = 0.0025$$

$$\Delta C_D = -0.030$$

$$\Delta C_m = -0.038$$

Reference Dimensions

The computation of force and moment coefficients was based upon the dimensions corresponding to the fully swept wing configuration, as follows:

$$S = 200.76 \text{ ft}^2$$

$$\bar{c} = 11.81 \text{ ft}$$

$$b = 19.68 \text{ ft}$$

Moment Center Location

Two moment center locations were used for data computation. The first, relating to an aft center of gravity, was located at 52 percent $\bar{c}$. The second, shown only in selected data, relates to a forward center-of-gravity location of 42 percent $\bar{c}$. The vertical location of both moment centers was 3.25 inches below the wing reference plane.

RESULTS

The results are arranged by configuration as shown in the index to data, table III.

Low-Speed Configurations

The majority of the data pertain to configurations with 20° of wing sweep. The longitudinal characteristics of the basic model (20° wing sweep, clean wing, horizontal tail off), both in and out of ground effect, are shown in figure 3. Similar results for the take-off and landing configurations are presented in figures 4 and 5. Also included in figure 5 is the effect of horizontal tail. The results of studies to optimize the configurations for best take-off and landing performance are presented in figures 6 through 11. The effects of wing sweep, wing trailing-edge flaps, wing leading-edge slats, and strake slats are shown. Longitudinal and lateral stability and control characteristics for the low-speed configurations are provided in figures 12 through 21. Configuration variables included horizontal-tail incidence, and elevator, aileron, and spoiler deflection. Similar data showing the effect of ground proximity, Reynolds number, and landing gear are presented in figures 22 through 26.

Low-Speed Characteristics of High-Speed Configurations

General low-speed aerodynamic characteristics of selected subsonic flight configurations comprise the latter portion of this paper, and are presented without discussion. Data shown for wing sweeps of 30° and 42° include the effects of wing leading-edge segment extension, horizontal-tail incidence, and both longitudinal and lateral-directional characteristics of the model. These results are shown in figures 27 through 32.

The last data presented (figs. 33 through 37) are from an investigation of an emergency landing with fully swept wings. Possible low-speed lift improvements from partial wing flap and strake flap deflection, as well as the effects of sideslip, ground proximity, and longitudinal control deflections, are shown.

DISCUSSION

The data presented herein resulted from a comprehensive study of the low-speed longitudinal and lateral-directional characteristics of a specific supersonic transport model. The results are presented almost in entirety. However, the following discussion will expand only upon the data considered most pertinent to the major areas of investigation, optimization of low-speed high-lift characteristics and assessment of longitudinal stability and control at a wing sweepback angle of 20°.

Aerodynamic Characteristics

Ground effect.- Figures 3, 4, and 5 present the effects of ground proximity, at an approximate landing gear height, on the clean (tail off), take-off, and landing configurations, respectively. The slope of the lift curve increased 30 percent at low angles of attack. With the high-lift configurations, however, this increase became an almost constant average lift increment of 0.15 C_L above 4° angle of attack. Analysis of the pitching moments of the three figures reveals that ground proximity had a slight stabilizing effect in the clean wing-body combination. With flaps down, tail off, however (fig. 5), ground effect was destabilizing by approximately 4-1/2 percent of static margin. Finally, with the horizontal tail on and flaps down, there was only a negative shift in C_{m_o} equal to that produced by approximately $2\text{-}1/2^\circ$ of horizontal-tail incidence, due to ground effect. In other words, the tail contribution to stability is larger in ground effect, as is usually the case. However, the effect of ground proximity on the wing canceled this stabilizing tail contribution, resulting in no net change in stability level for the complete, flaps down configuration in ground effect.

Wing trailing-edge flaps.- The effects of wing trailing-edge flap deflection are depicted in the curves of figure 7 for various flap angles for take-off. (Optimum deflection was considered to be 15°-45° (15° main flap, 45° aft flap), based upon the most favorable combination of trimmed lift coefficient (0.94) and lift-drag ratio (8.5) at a 10° rotation attitude.) The selection of 30°-60° (fig. 8) as the flap deflection for landing was based upon the superior pitching-moment linearity between 8° and 12° angle of attack associated with the 30°-60° deflection, even though higher maximum lift coefficients were available with higher deflections.

Wing leading-edge slats.- The selection of a 20° deflection of the wing leading-edge slat for take-off was based upon earlier tests to optimize the leading-edge configuration. Figure 9 presents the effects of an extended chord slat (see figs. 2(a) and (d) for details). This build-up of wing slat configuration on the inboard segment was found to be an effective means of delaying separation at the wing-strake juncture caused by the strake vortex. A small improvement in pitching moment at constant angle of attack is shown for the use of extended chord slats on the inboard three segments (20° δ_S + Ext_3). The drooped slat leading edge (in figs. 9(c), (d)) resulted in

extending the stall attitude 8° and increasing $C_{L_{max}}$ by 11-1/2 percent (0.2 C_L). The droop also appears to remove most of the undesirable pitch-up "in deep stall." There was, however, a lift loss of 5 percent attributed to the drooped slat leading edge at the lower take-off lift coefficients. This slat shape was therefore adopted for the landing configuration only. A slat deflection of 30° is shown (fig. 10) to have a higher $C_{L_{max}}$ than 40° deflection. Furthermore, the extension of slat chord in addition to the 25° slat leading-edge droop yielded a landing-slat configuration with the highest $C_{L_{max}}$ and most favorable pitching-moment linearity.

Wing sweep.- The effects of wing sweep angles of 20° and 25° for the landing configuration are shown in figure 6. There was a lift advantage to the 20° wing sweep of 0.1 C_L at 10° angle of attack (approximate angle for lift-off); $C_{L_{max}}$, however, remained the same. On the other hand, a slight improvement in stability level at low angles of attack was obtained by increasing the wing sweep to 25°, with a lesser pitch-up tendency at higher angles of attack. The choice then depends upon the trade off between C_L required at a given angle of attack and the importance assigned to the pitch-up.

Stability and Control

The model exhibited a pitch-up instability above 14° angle of attack in all low-speed configurations. As discussed in reference 1, a pitch-up approaching stall is inherent in a variable-sweep airplane with an outboard wing pivot and a highly swept inboard fixed wing, or strake. This longitudinal instability is generally known to be caused by vortex flow generated along a sharp, highly swept (strake) leading edge.

This model, therefore, was equipped with a strake leading-edge slat to reduce adverse spanwise pressure gradients and thus delay vortex formation. The effect of this strake slat, on the characteristics of a typical landing configuration, is shown in figure 11. With the strake slat retracted, the combination of wing-tip separation and added vortex-induced lift on the strake caused a forward shift in aerodynamic center and, hence, pitch-up at 10° angle of attack. However, with a 35° strake slat deflection, this vortex-induced lift is reduced to the extent that the pitching moment continued linearly to 13° angle of attack, and the break was much less severe. Further deflection to 40° produced no additional benefit and, in fact, aggravated stability recovery in the deep stall range.

Longitudinal control.- The characteristics of longitudinal control as a function of horizontal-tail incidence and elevator deflection are presented in figures 12 and 13 for take-off and landing configurations, respectively. Control power of the tail has been summarized from these data and is presented in figure 14. As shown, control power was essentially constant up to an angle of attack of 30°. In addition, longitudinal control for a forward center-of-gravity location, in ground effect, is presented in figure 22(c). Calculations indicate that longitudinal control power is sufficient, at a tail angle of attack of -12°, to rotate such an airplane on take-off at this forward center of gravity.

Lateral-directional characteristics.- The effects of sideslip are shown in figures 15, 16, and 17. The effects of aileron and spoiler deflection for lateral control are shown in figures 18 through 21. The model had positive effective dihedral up to the stall angle of attack. Directional stability was low, but stable, up to 12° angle of attack, became neutrally stable, and finally unstable above 16° angle of attack.

Ames Research Center
National Aeronautics and Space Administration
Moffett Field, Calif. 94035, June 12, 1968
720-01-00-01-00-21

REFERENCES

1. Cook, Anthony M.; Greif, Richard K.; and Aoyagi, Kiyoshi: Large-Scale Wind-Tunnel Investigation of the Low-Speed Aerodynamic Characteristics of a Supersonic Transport Model Having Variable-Sweep Wings. NASA TN D-2824, 1965.

2. Recant, Isidore G.: Wind-Tunnel Investigation of Ground Effect on Wings With Flaps. NACA TN 705, 1939.

TABLE I.- AERODYNAMIC REFERENCE DIMENSIONS

Wing	
Area (Arrow wing, $72^{\circ}\Lambda$), ft^2	200.76
Span	
$20^{\circ}\Lambda$, ft	33.85
$25^{\circ}\Lambda$, ft	33.00
$30^{\circ}\Lambda$, ft	32.50
$42^{\circ}\Lambda$, ft	29.93
$72^{\circ}\Lambda$, ft	19.68
Aspect ratio	
$20^{\circ}\Lambda$	5.71
$25^{\circ}\Lambda$	5.50
$30^{\circ}\Lambda$	5.26
$42^{\circ}\Lambda$	4.46
$72^{\circ}\Lambda$	1.93
$\bar{c}$ (Arrow wing, $72^{\circ}\Lambda$), ft	11.81
Fuselage	
Length, ft	54.17
Maximum width, ft	2.67
Horizontal tail	
Area (exposed), ft^2	36.40
Span, ft	9.73
Aspect ratio	2.00
Taper ratio	0.20
Tail length (0.40 $\bar{c}$ to 0.25 $\bar{c}_T$), ft	16.90
$\bar{c}_T$, ft	4.90
V_T	0.257
Vertical tail	
Area, ft^2	17.84
Span (exposed), ft	4.46
Aspect ratio	1.11
Taper ratio	0.254
Tail length (0.40 $\bar{c}$ to 0.25 $\bar{c}_V$), ft	16.33
$\bar{c}_V$, ft	4.48

TABLE II.- WING AIRFOIL ORDINATES

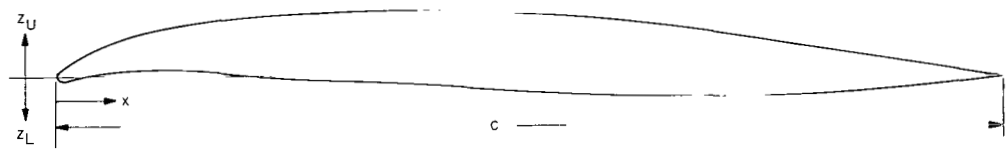

Typical sections perpendicular to the wing leading edge as in figure 2(b).

x/c	Section D-D		Section E-E		Section G-G	
	z_U/c	z_L/c	z_U/c	z_L/c	z_U/c	z_L/c
0	0	0	0	0	0	0
.05	.0386	.0015	.0338	-.0035	.0296	-.0035
.10	.0546	.0035	.0492	-.0050	.0423	-.0072
.15	.0627	.0066	.0570	-.0042	.0485	-.0081
.20	.0674	.0105	.0639	-.0017	.0515	-.0074
.30	.0717	.0181	.0701	.0037	.0554	-.0051
.40	.0700	.0255	.0716	.0089	.0578	-.0046
.50	.0640	.0334	.0694	.0142	.0568	-.0039
.60	.0524	.0411	.0602	.0202	.0534	-.0023
.70	.0401	.0427	.0467	.0221	.0462	0
.80	.0262	.0343	.0303	.0186	.0351	0
.90	.0128	.0195	.0145	.0109	.0199	0
1.00	0	0	0	0	0	0
	LE radius = 0.0035c		LE radius = 0.0035c		LE radius = 0.0035c	

TABLE III.- INDEX TO DATA FIGURES

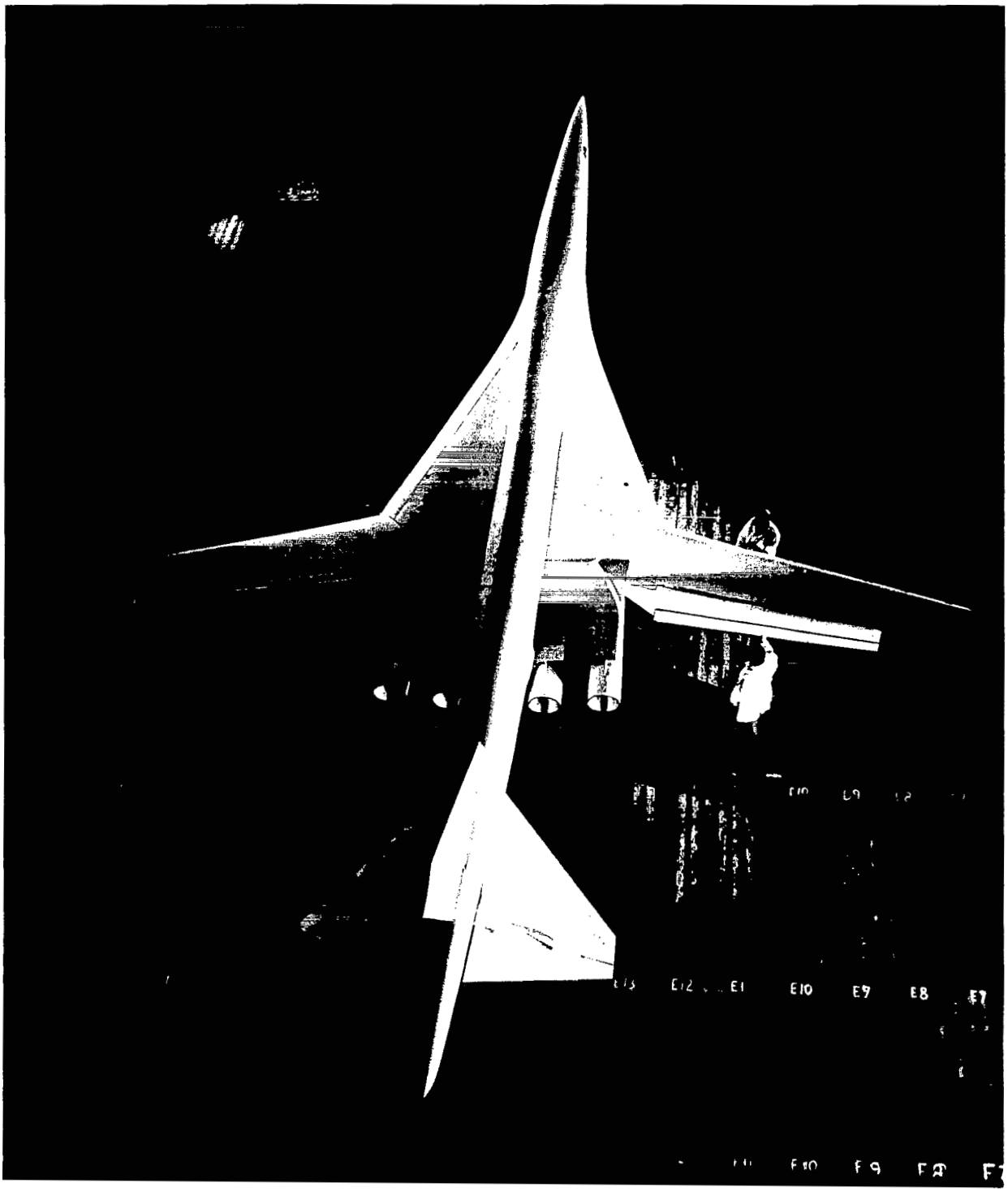

A-36782

(a) Top view.

Figure 1.- Photographs of the model mounted in the 40- by 80 foot wind tunnel.

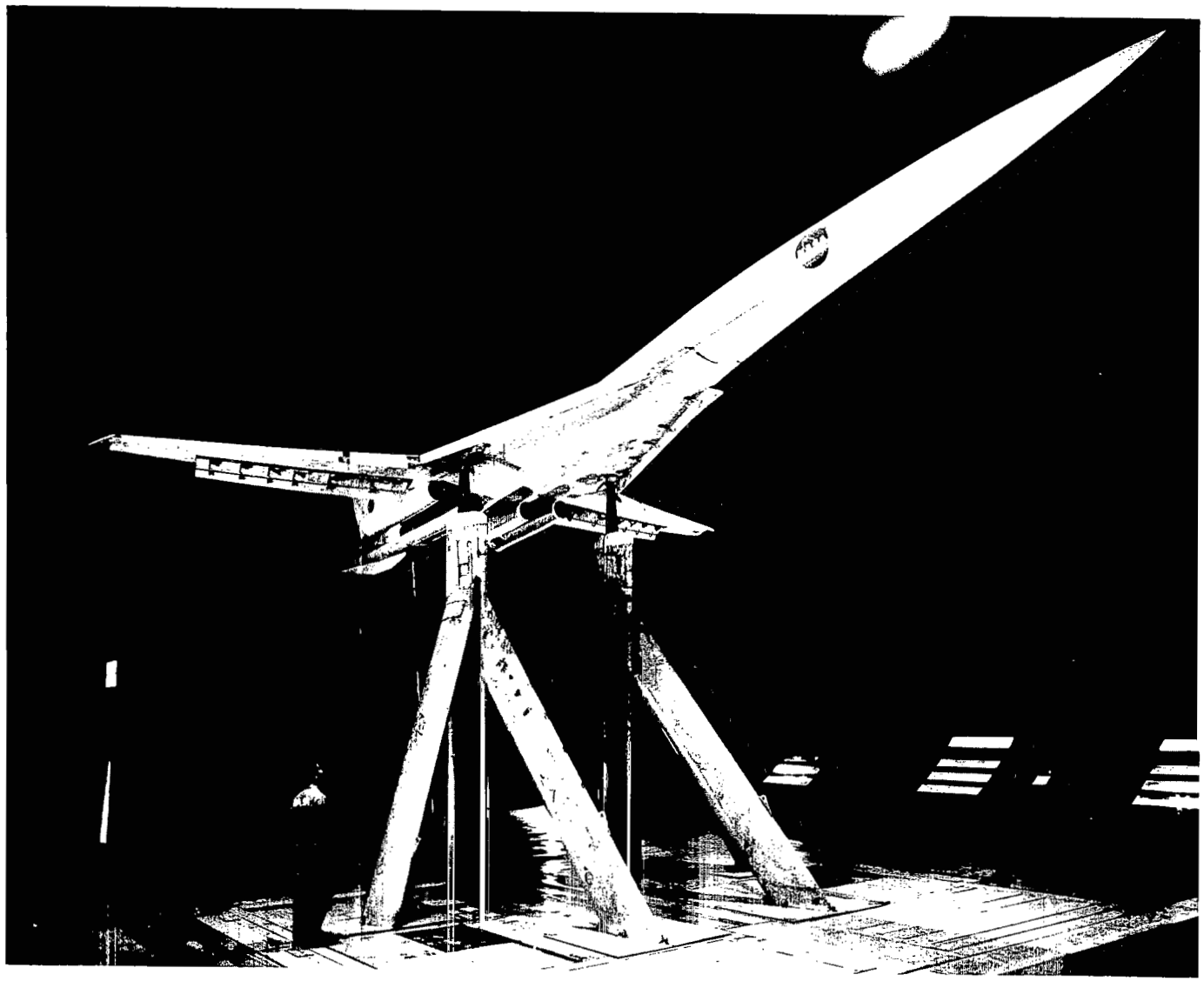

A-34759

(b) Three-quarter front view.

Figure 1.- Continued.

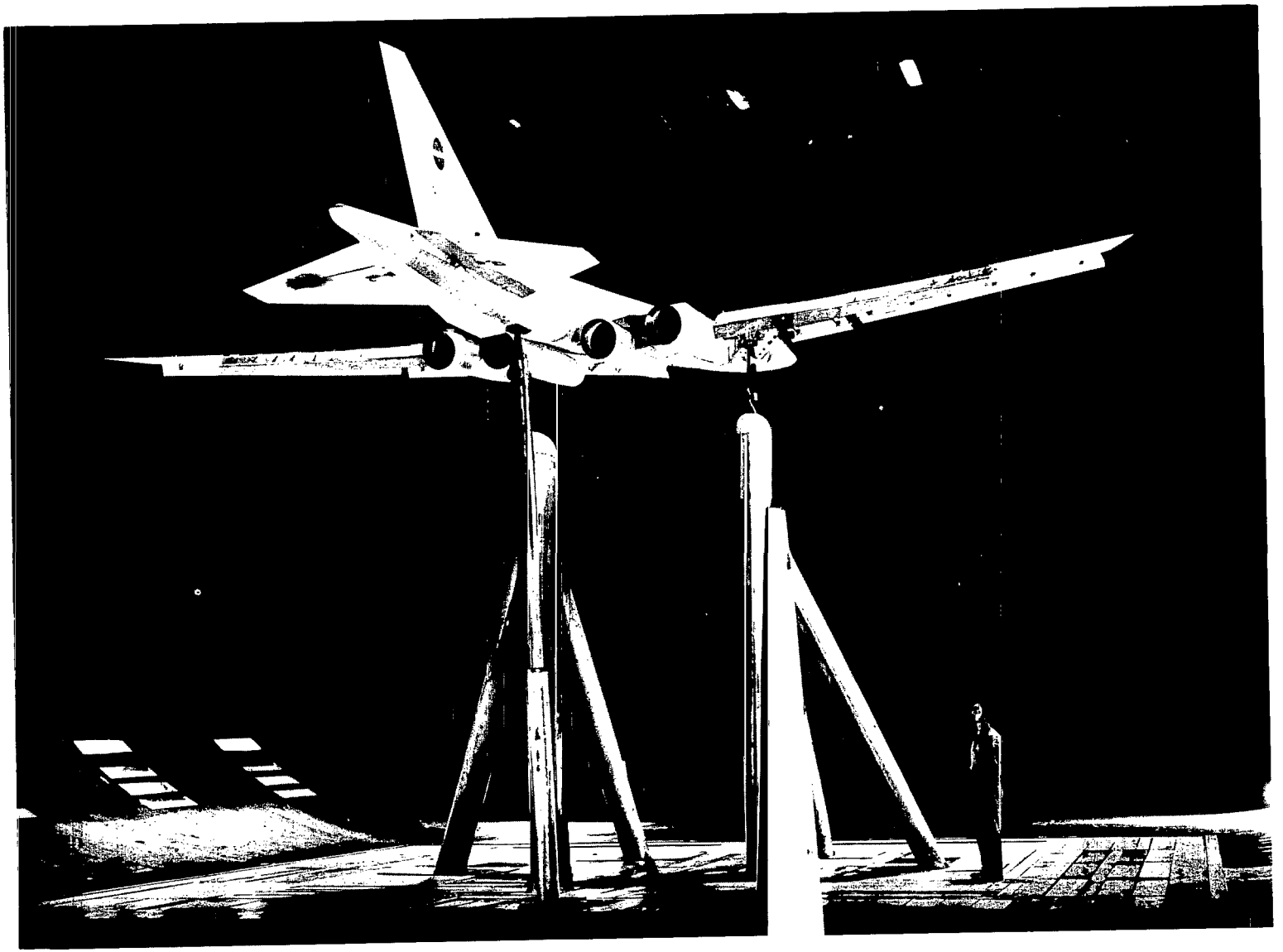

A-34760

(c) Three-quarter rear view.

Figure 1.- Concluded.

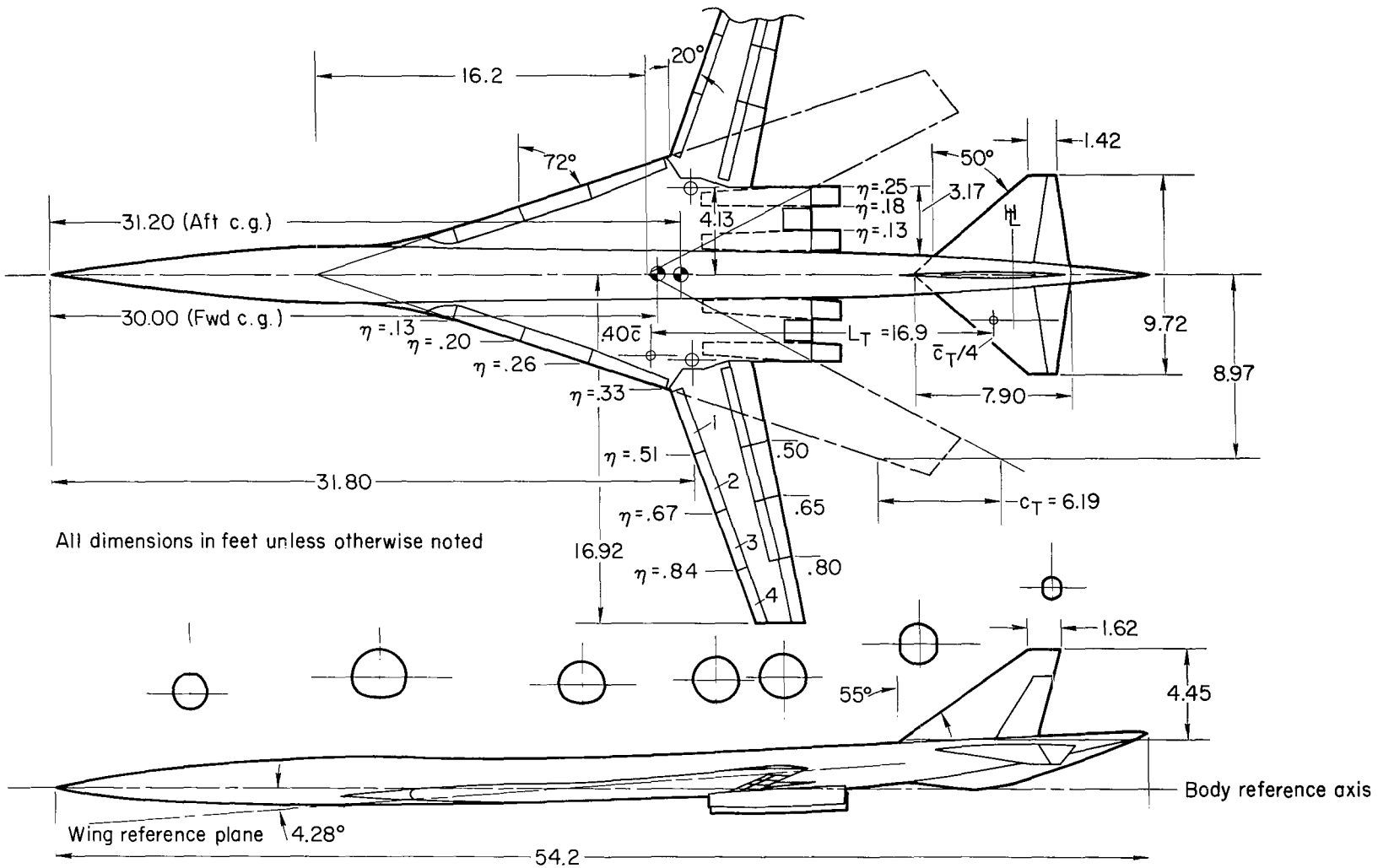

(a) Complete model.

Figure 2.- Geometric details of the model.

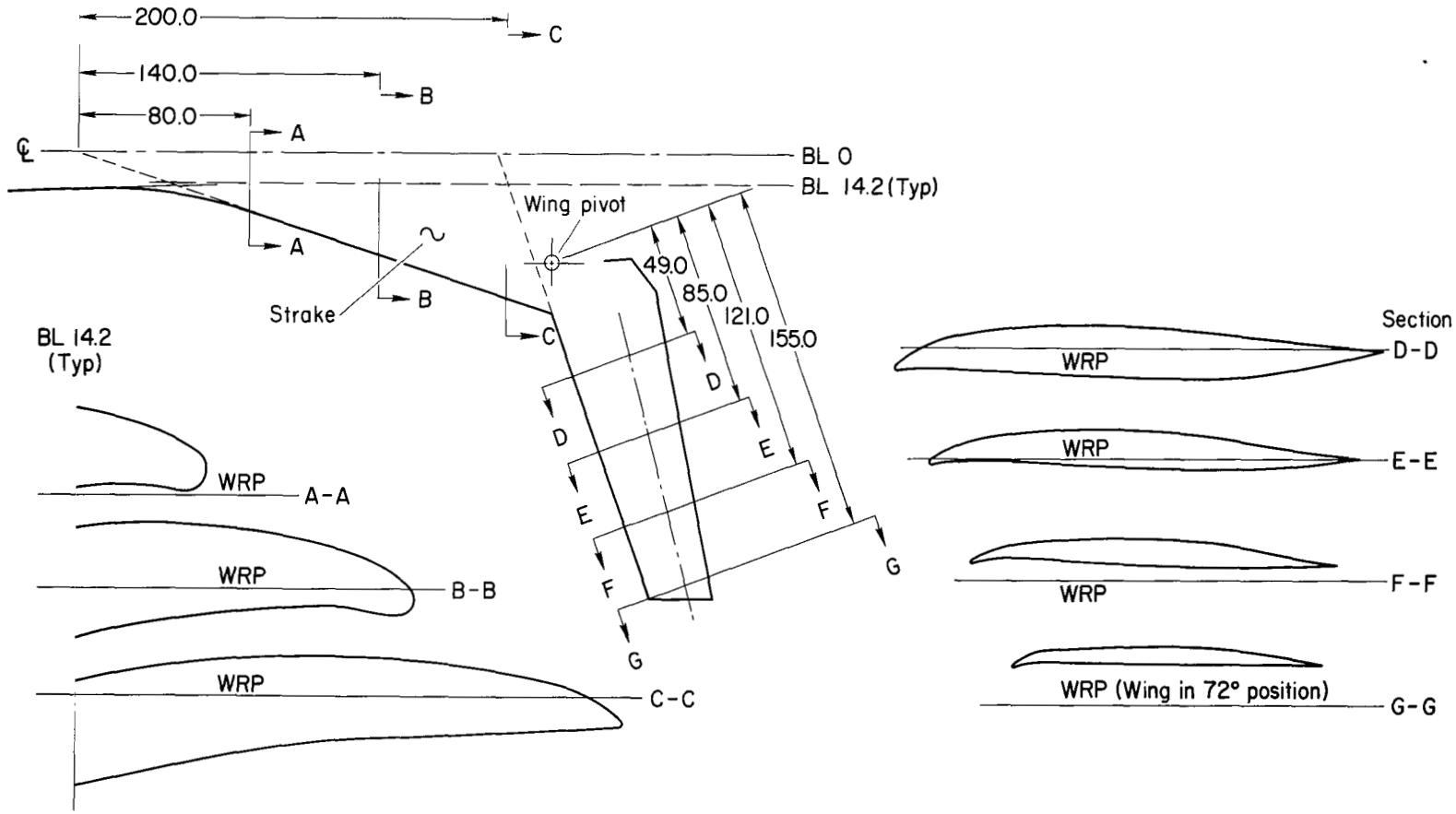

(b) Strake and wing airfoil sections.

Figure 2.- Continued.

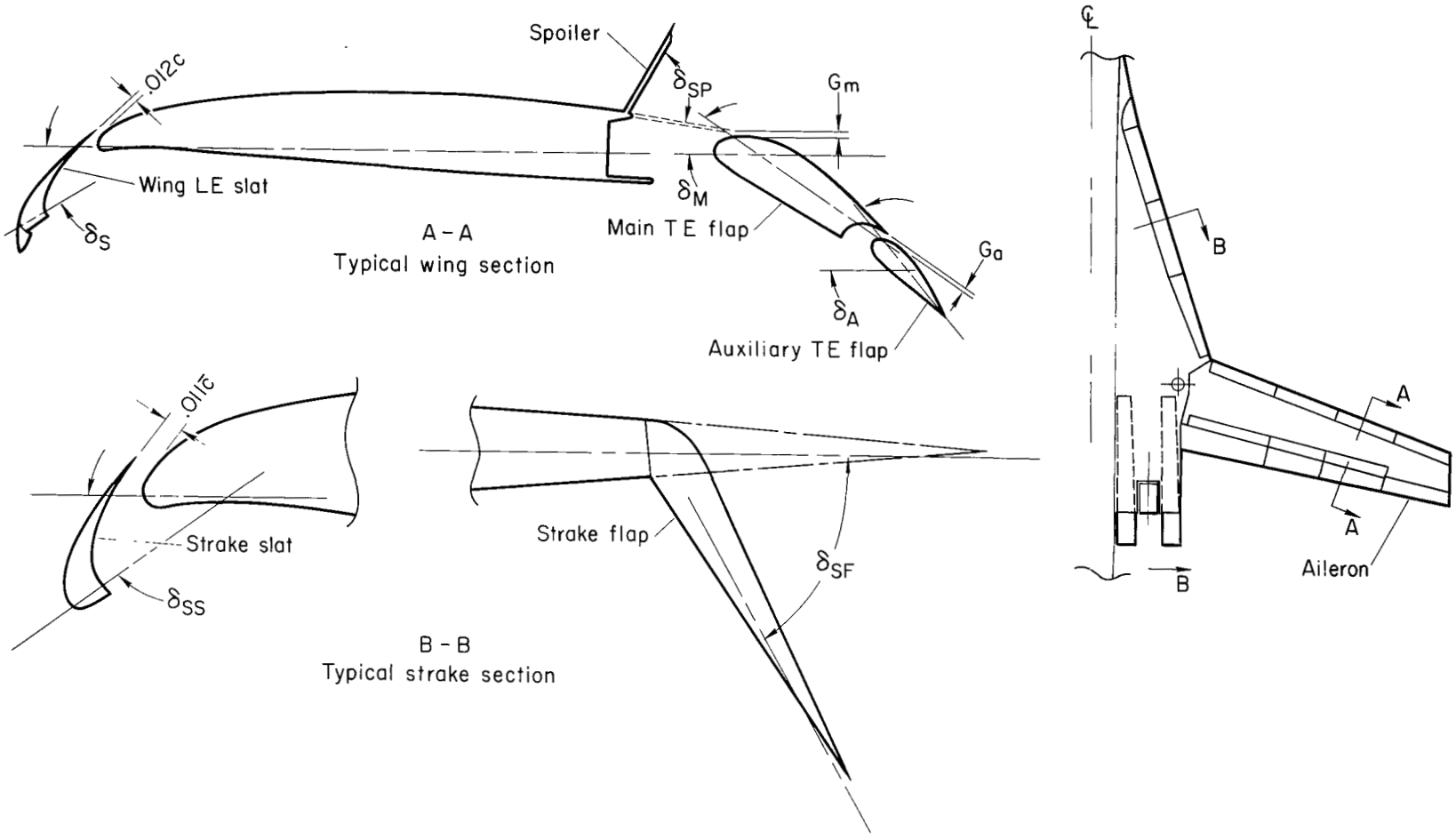

(c) Typical sections of high-lift devices.

Figure 2.- Continued.

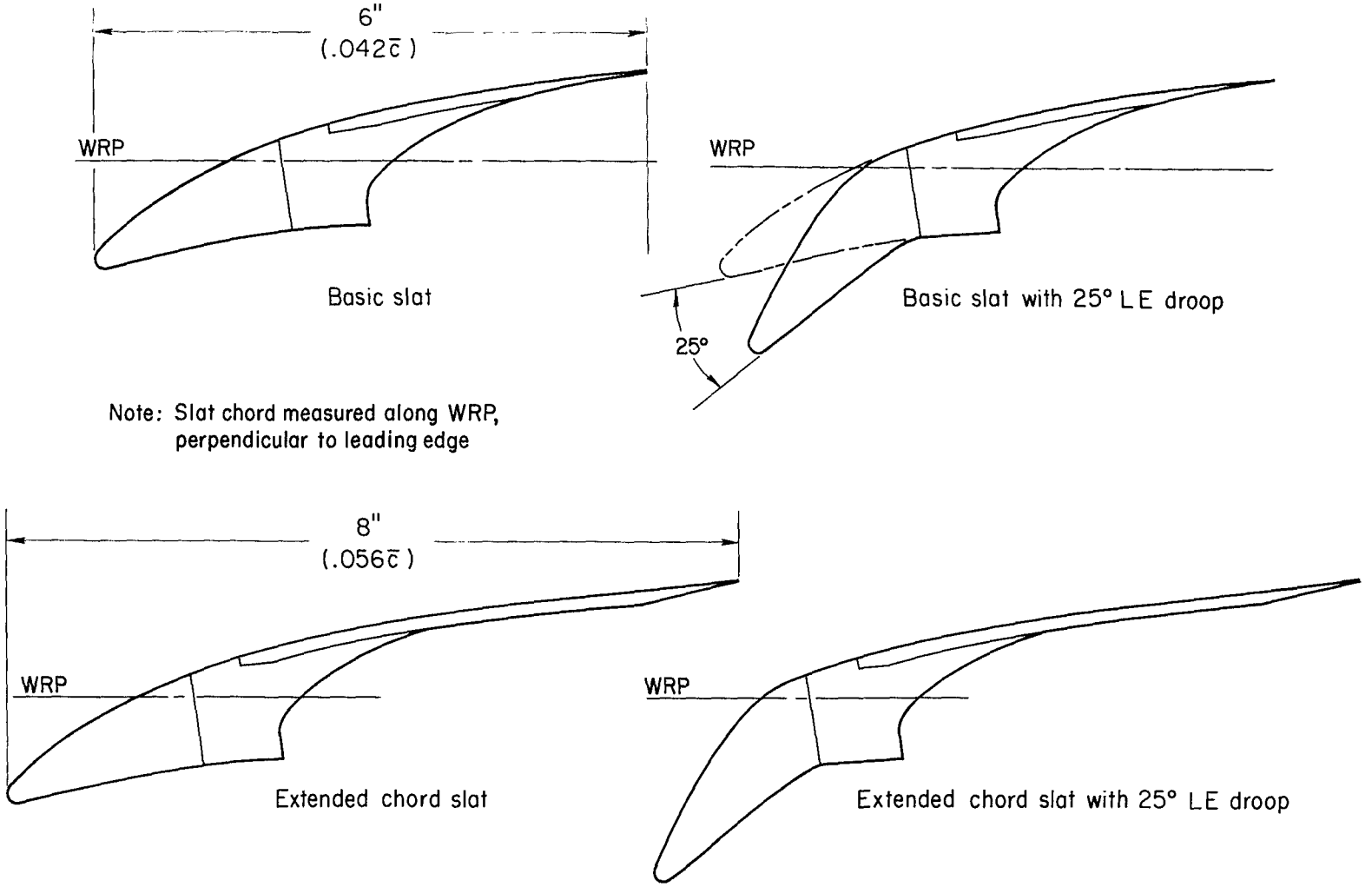

(d) Wing leading-edge slat details.

Figure 2.- Continued.

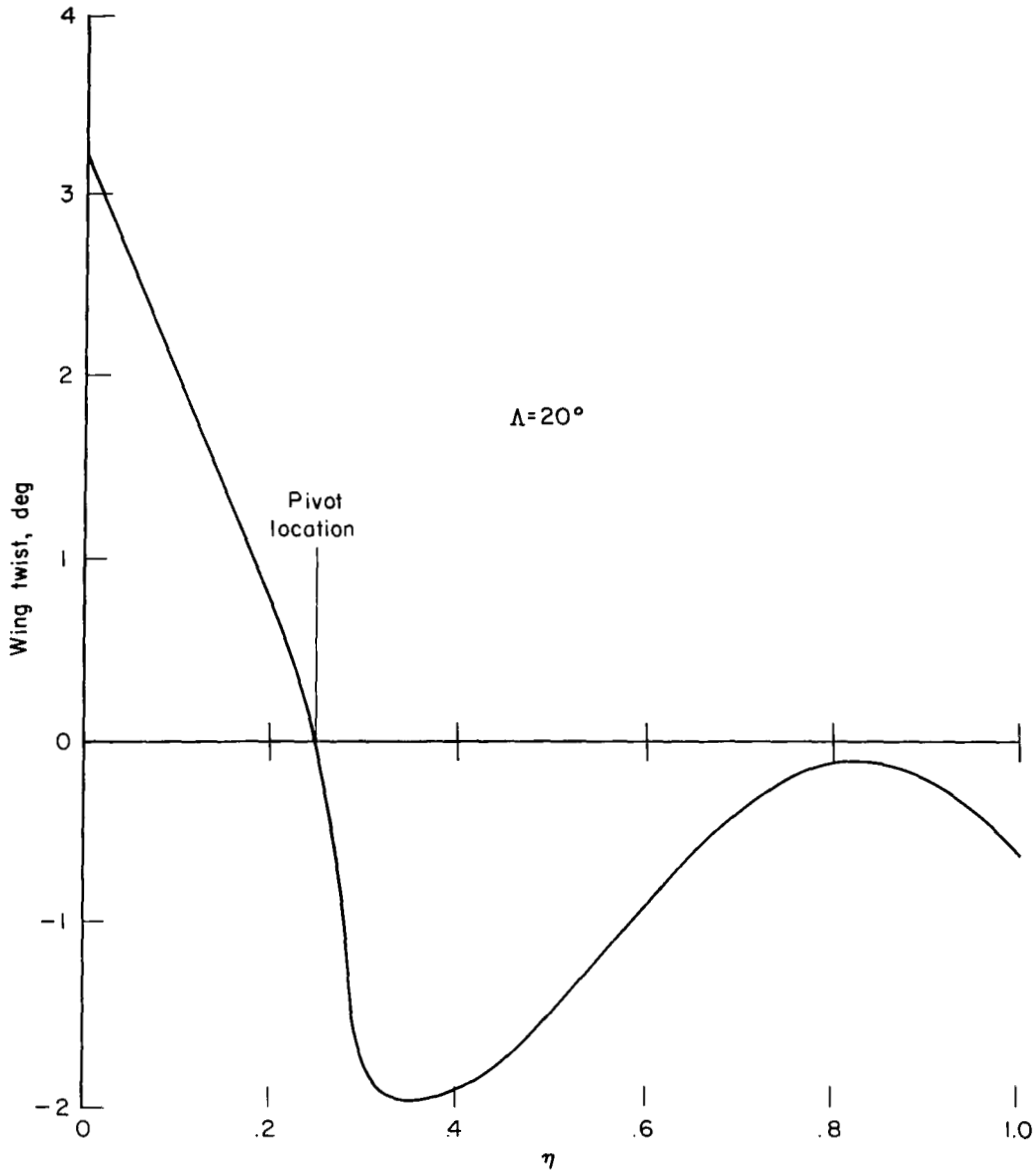

(e) Wing twist.

Figure 2.- Concluded.

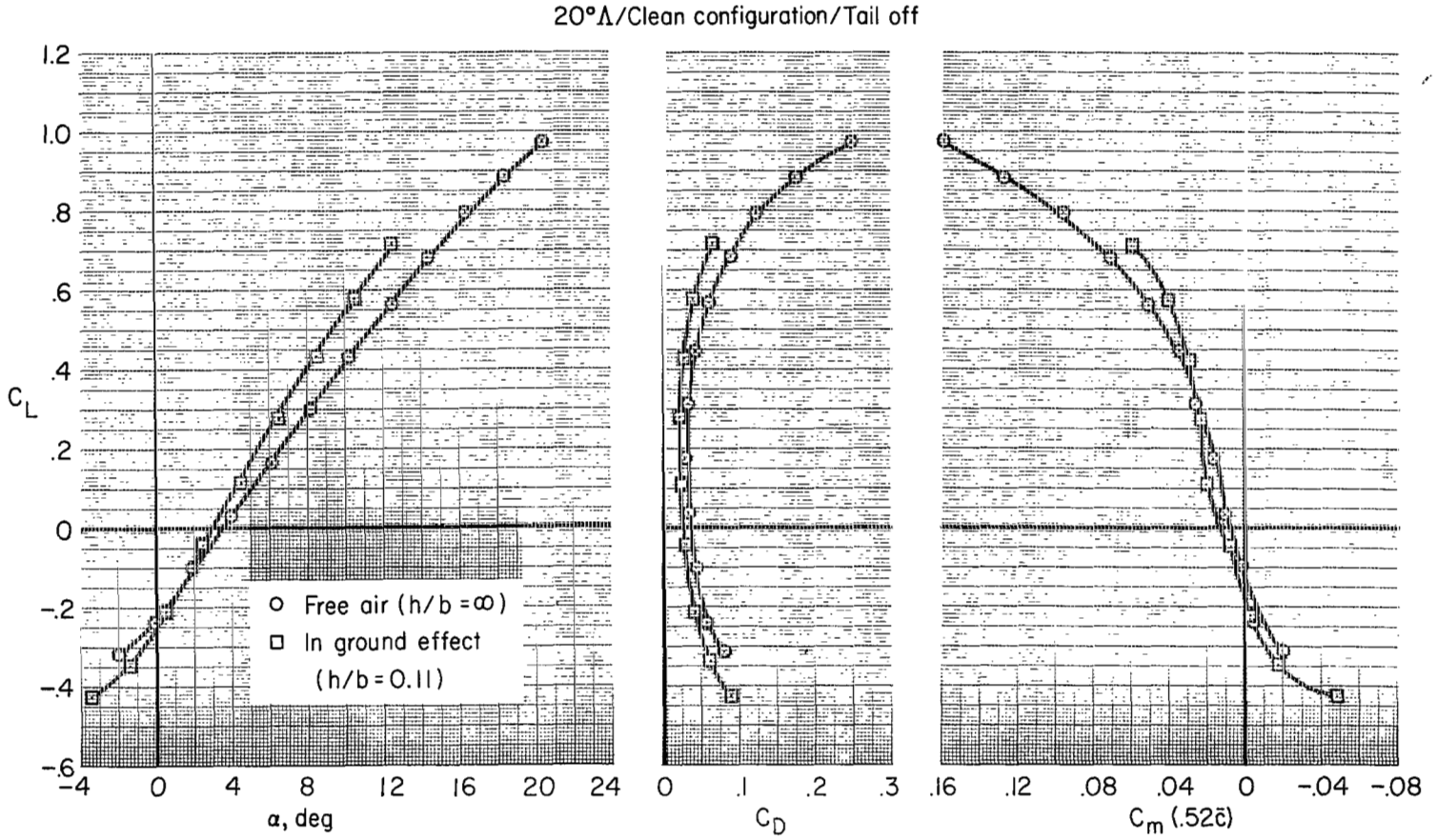

Figure 3.- Effect of ground proximity on the longitudinal characteristics of the 20° wing sweep, clean configuration, with tail off.

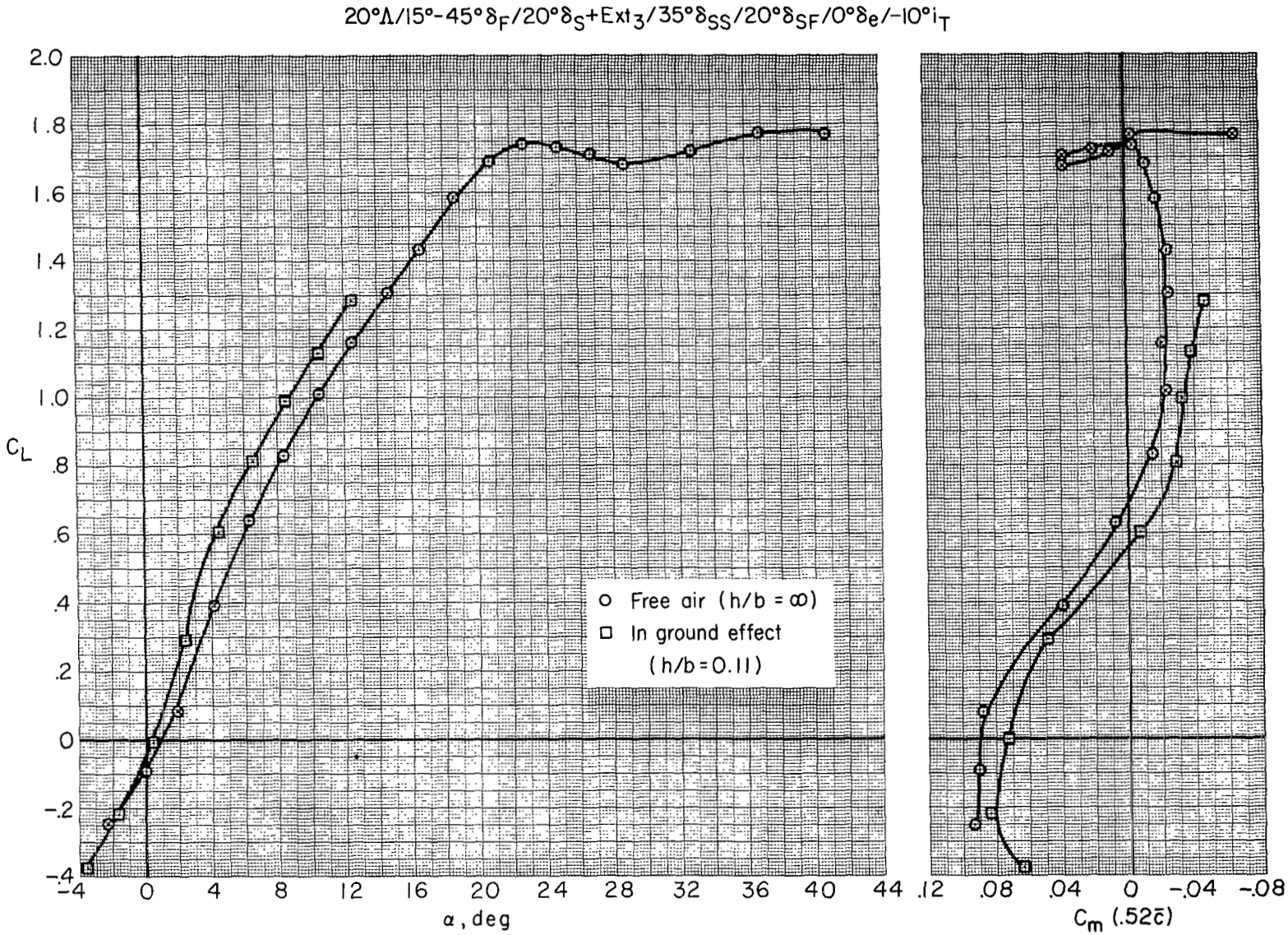

(a) C_L vs. α and C_m

Figure 4.- Effect of ground proximity on the longitudinal characteristics of the take-off configuration.

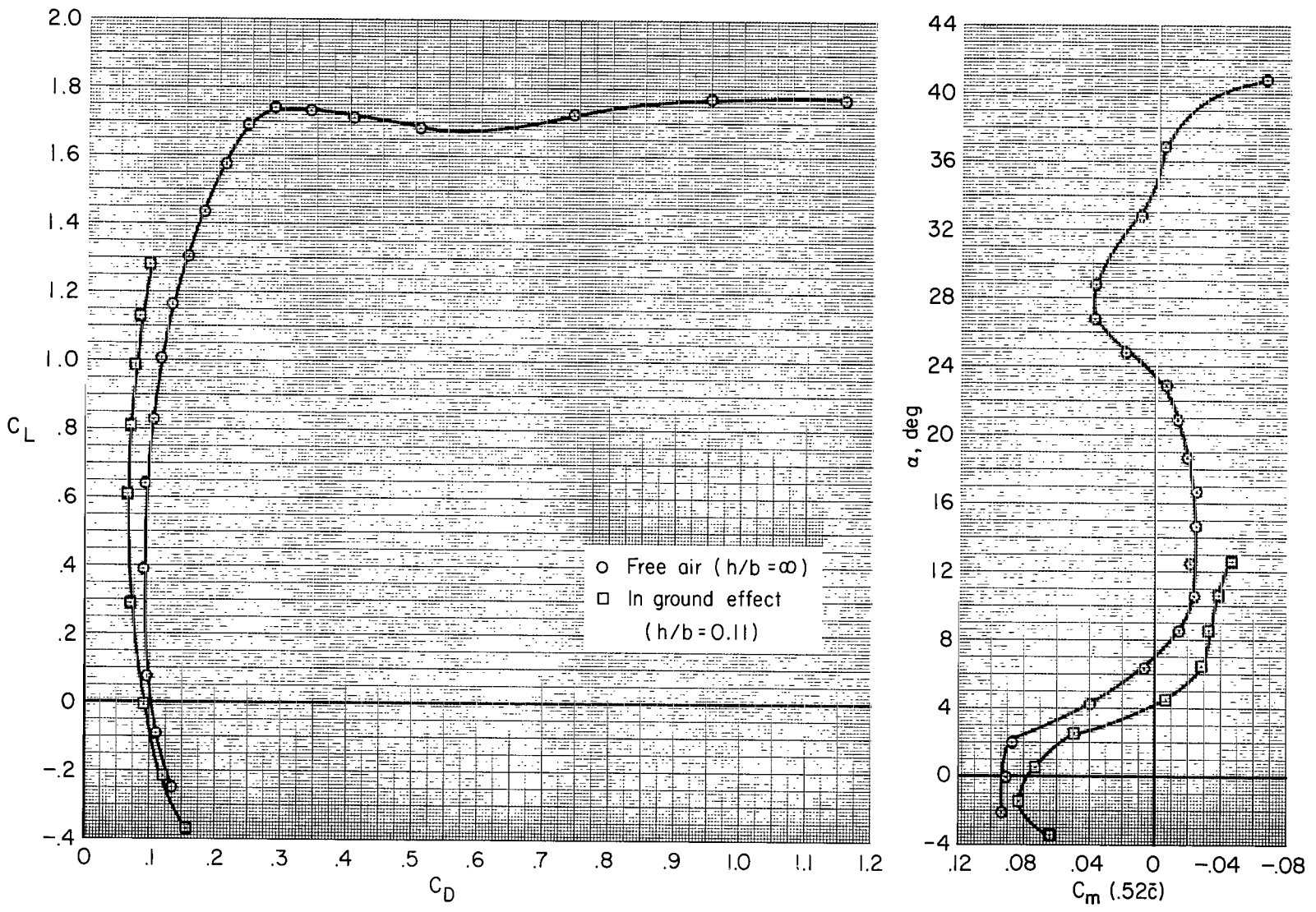

(b) C_L vs. C_D, α vs. C_m

Figure 4.- Concluded.

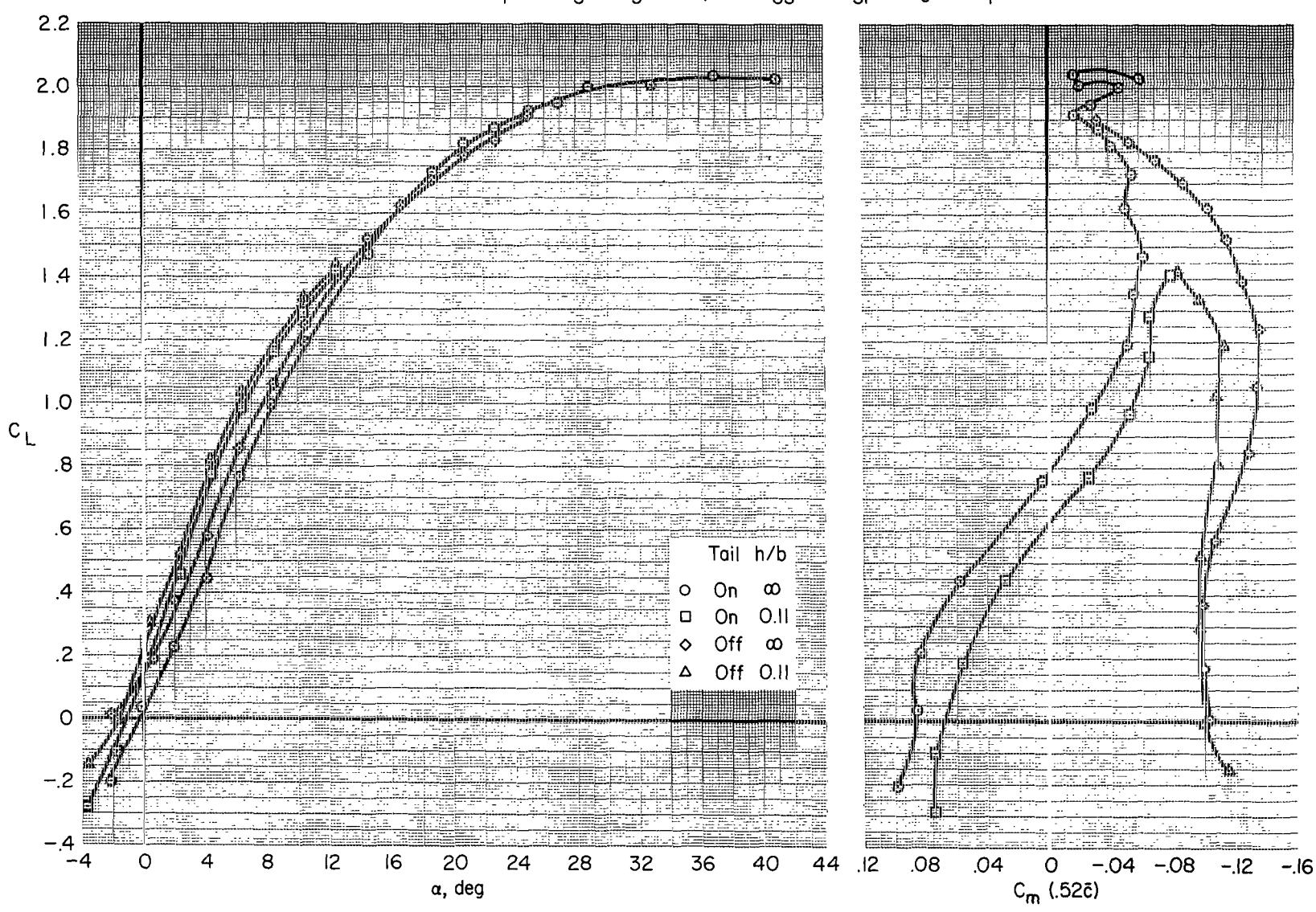

(a) C_L vs. α and C_m

Figure 5.- Effect of ground proximity on the aerodynamics of the landing configuration, both horizontal tail on and off.

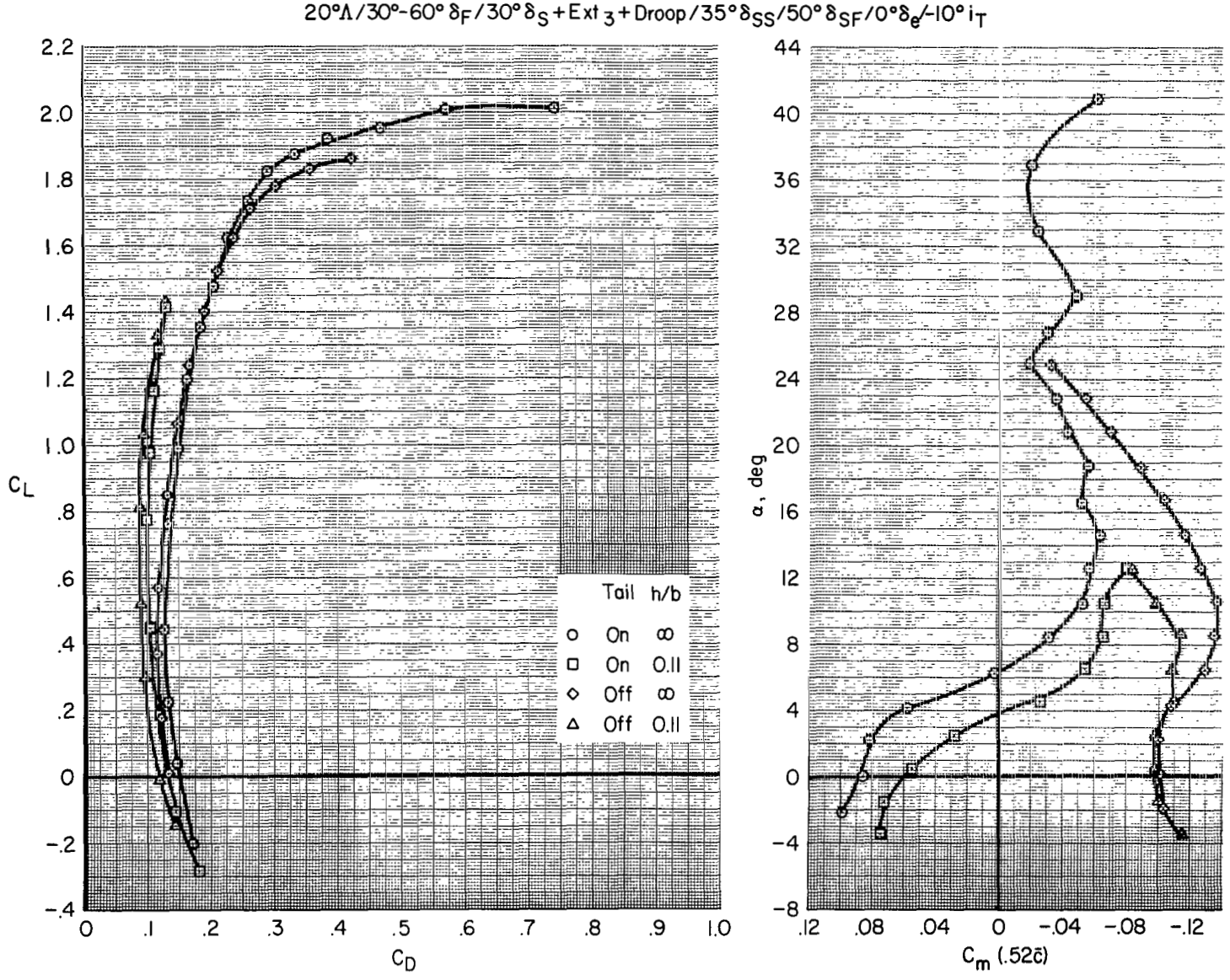

(b) C_L vs. C_D, α vs. C_m

Figure 5.- Concluded.

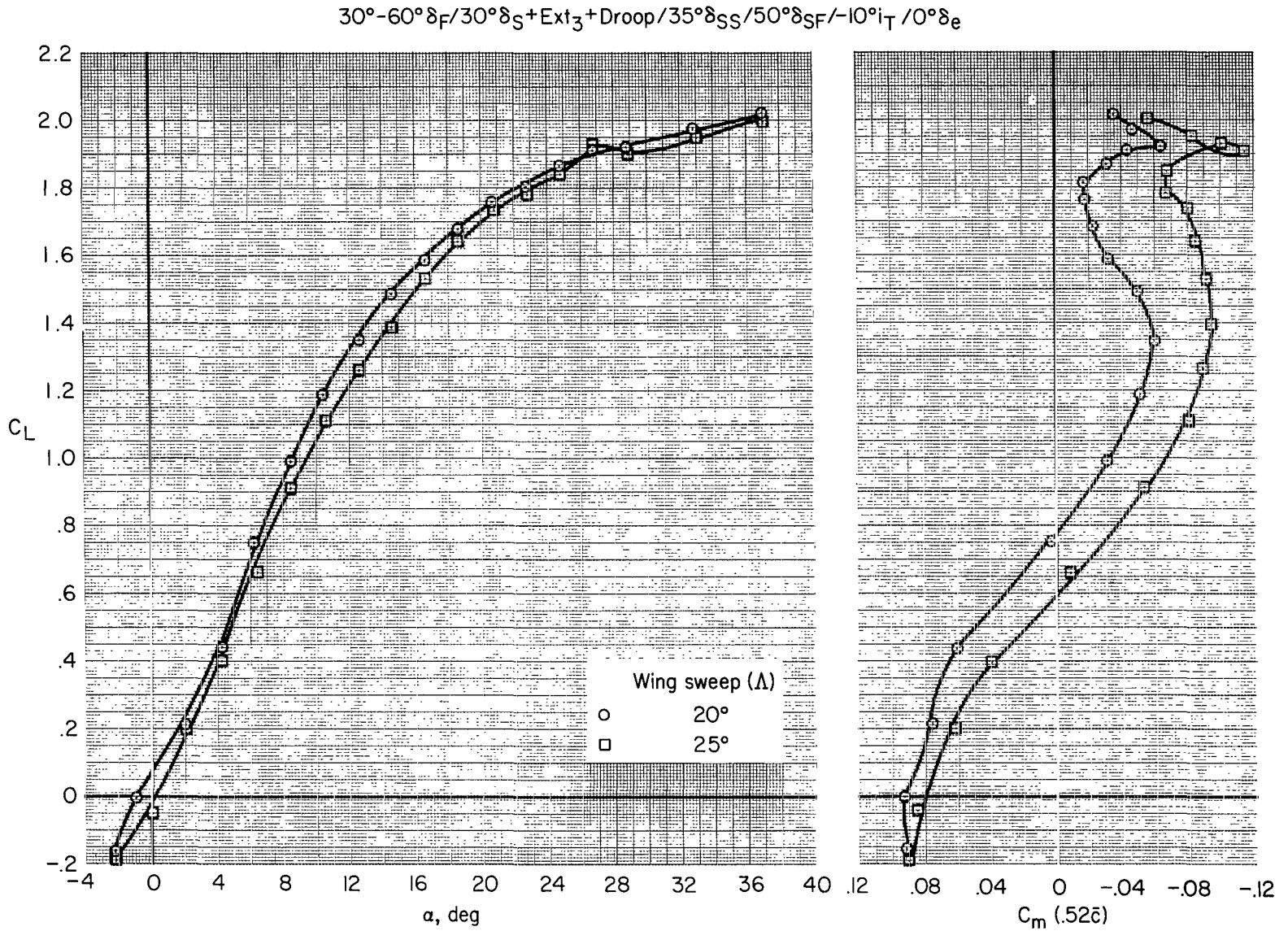

(a) C_L vs. α and C_m

Figure 6.- Effect of wing sweep on the longitudinal characteristics of the optimized landing configuration.

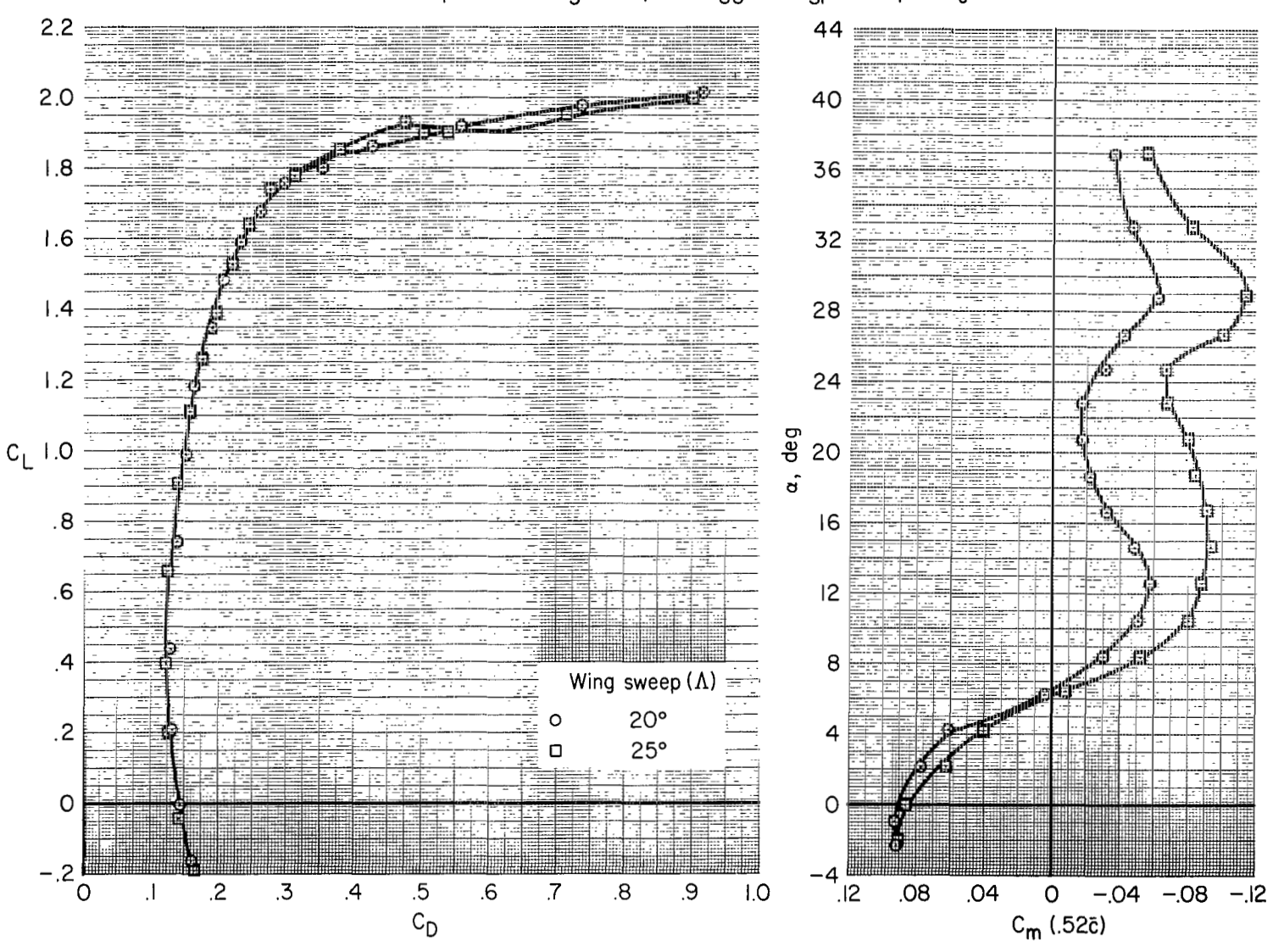

(b) C_L vs. C_D, α vs. C_m

Figure 6.- Concluded.

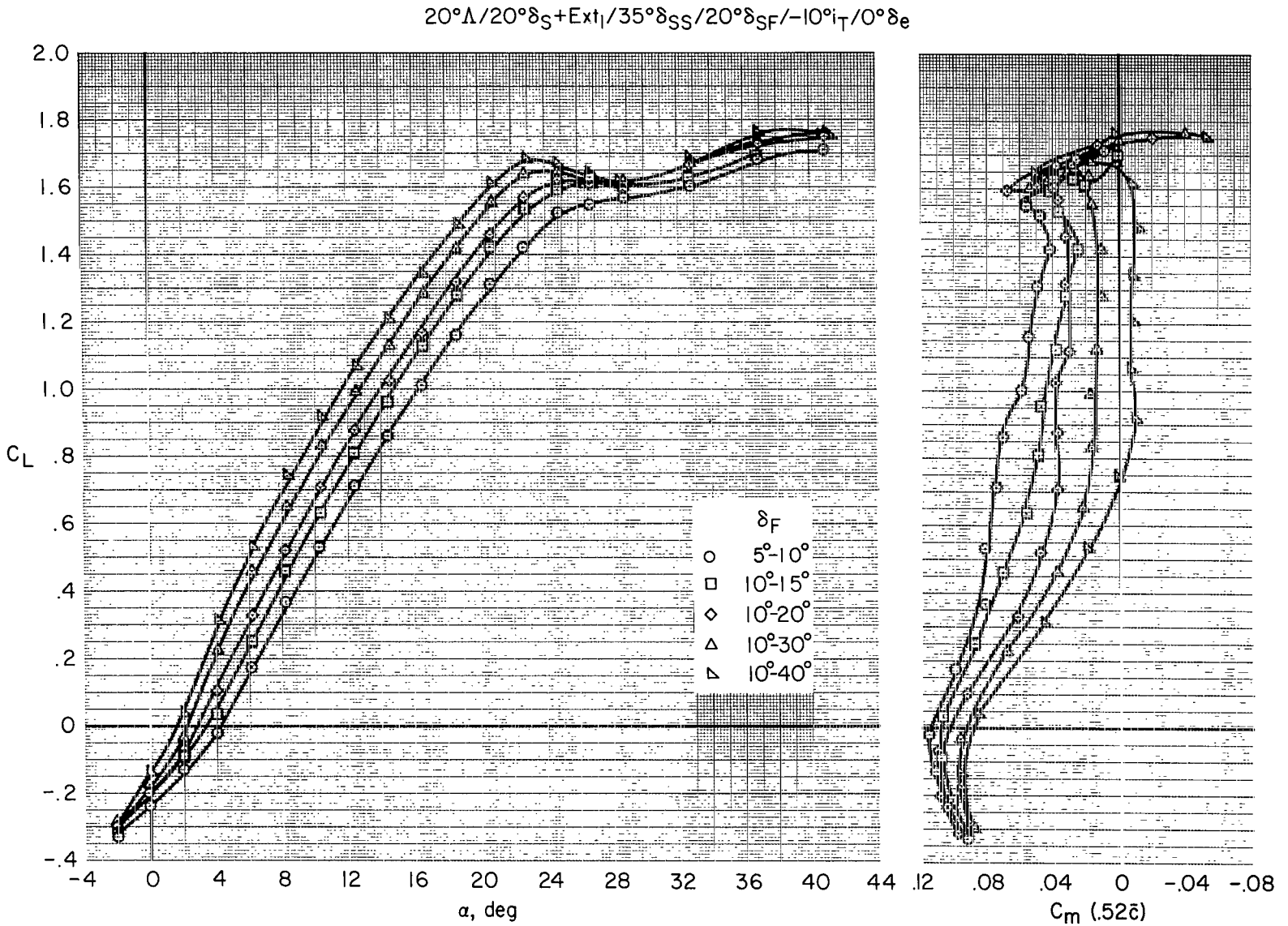

(a) C_L vs. α and C_m for small flap deflections.

Figure 7.- Longitudinal characteristics of trailing-edge flap deflection on take-off configuration, 20° wing sweep.

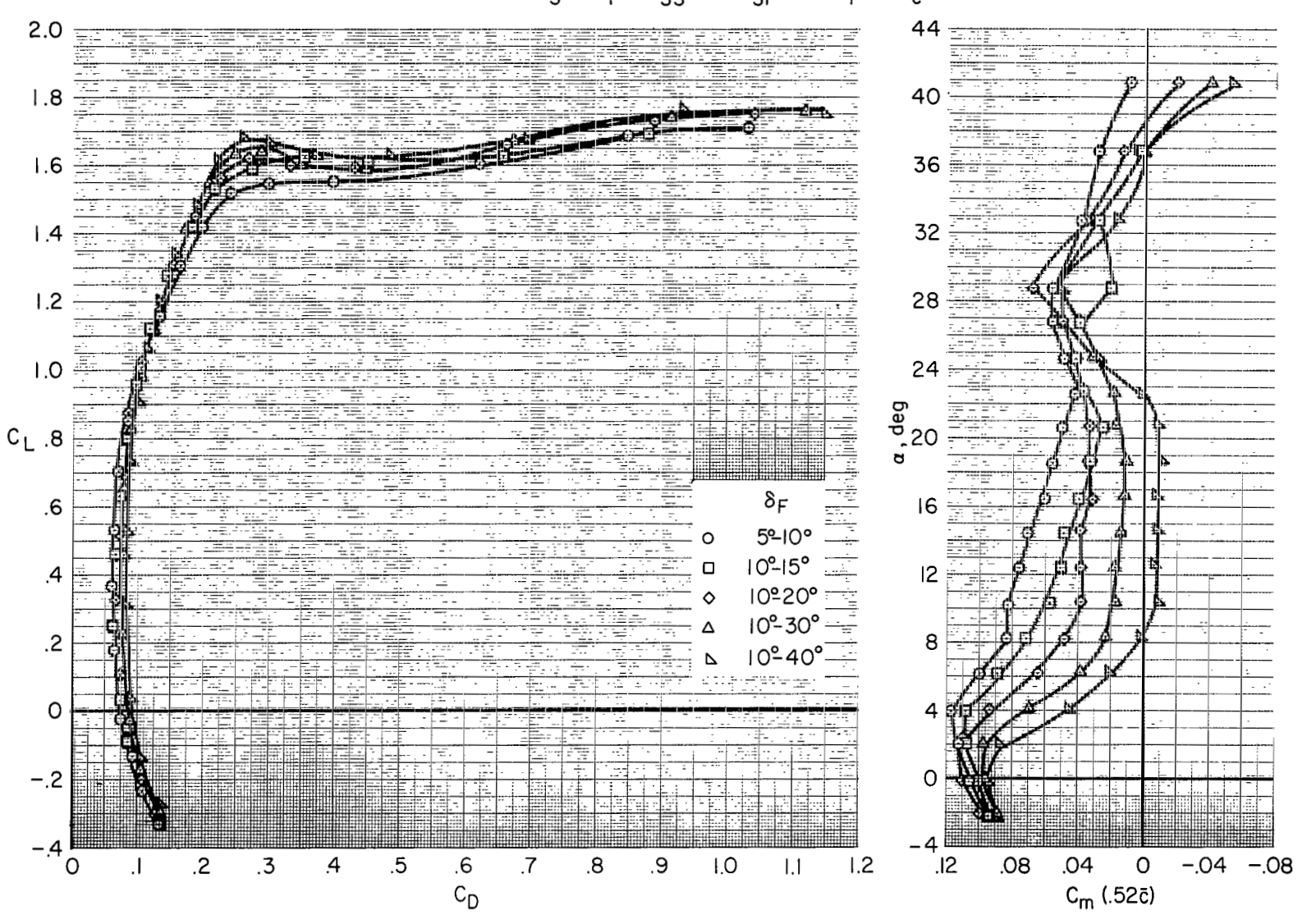

(b) C_L vs. C_D and α vs. C_m for small flap deflections.

Figure 7.- Continued.

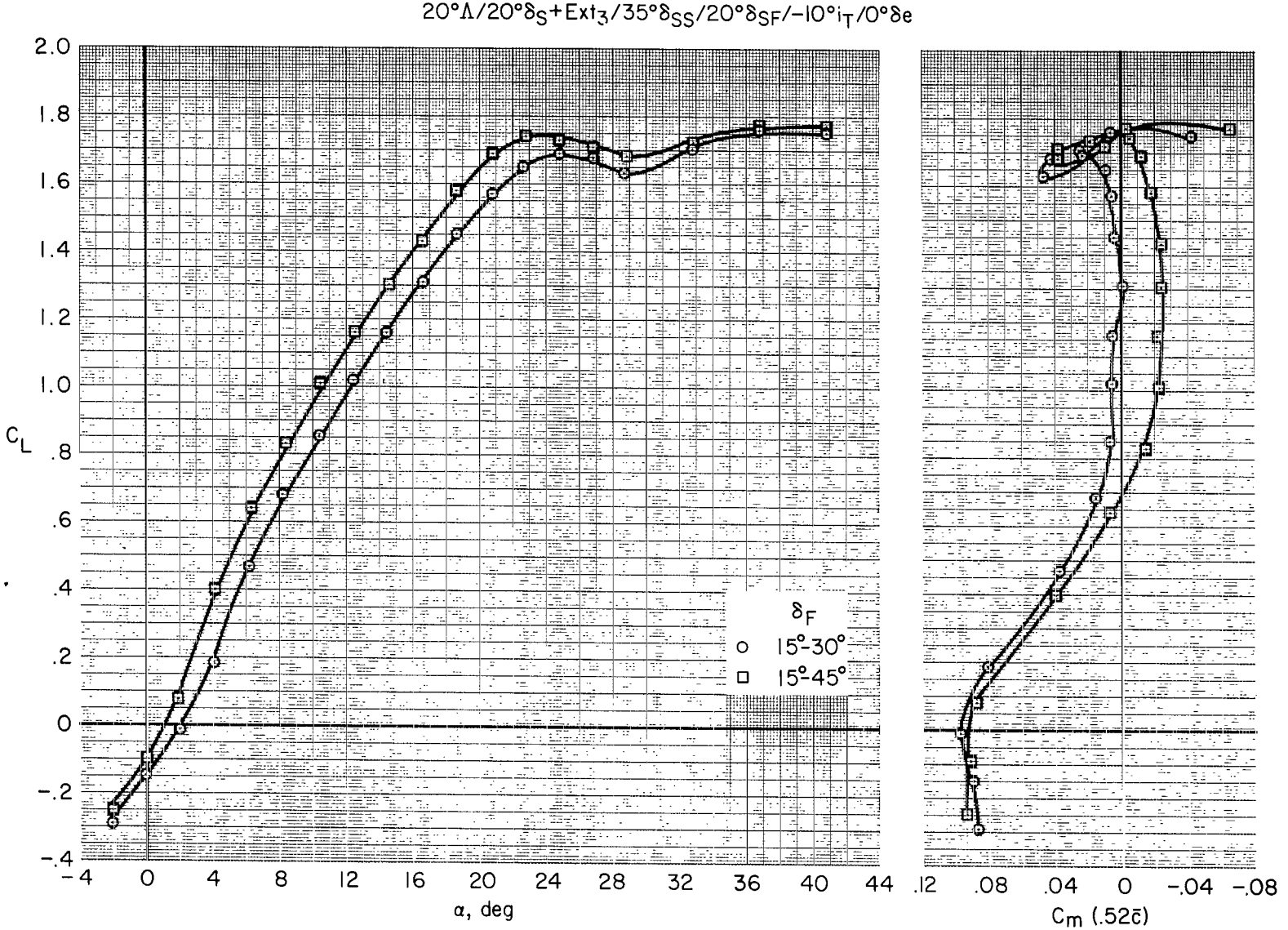

(c) C_L vs. α and C_m for an intermediate range of flap deflections.

Figure 7.- Continued.

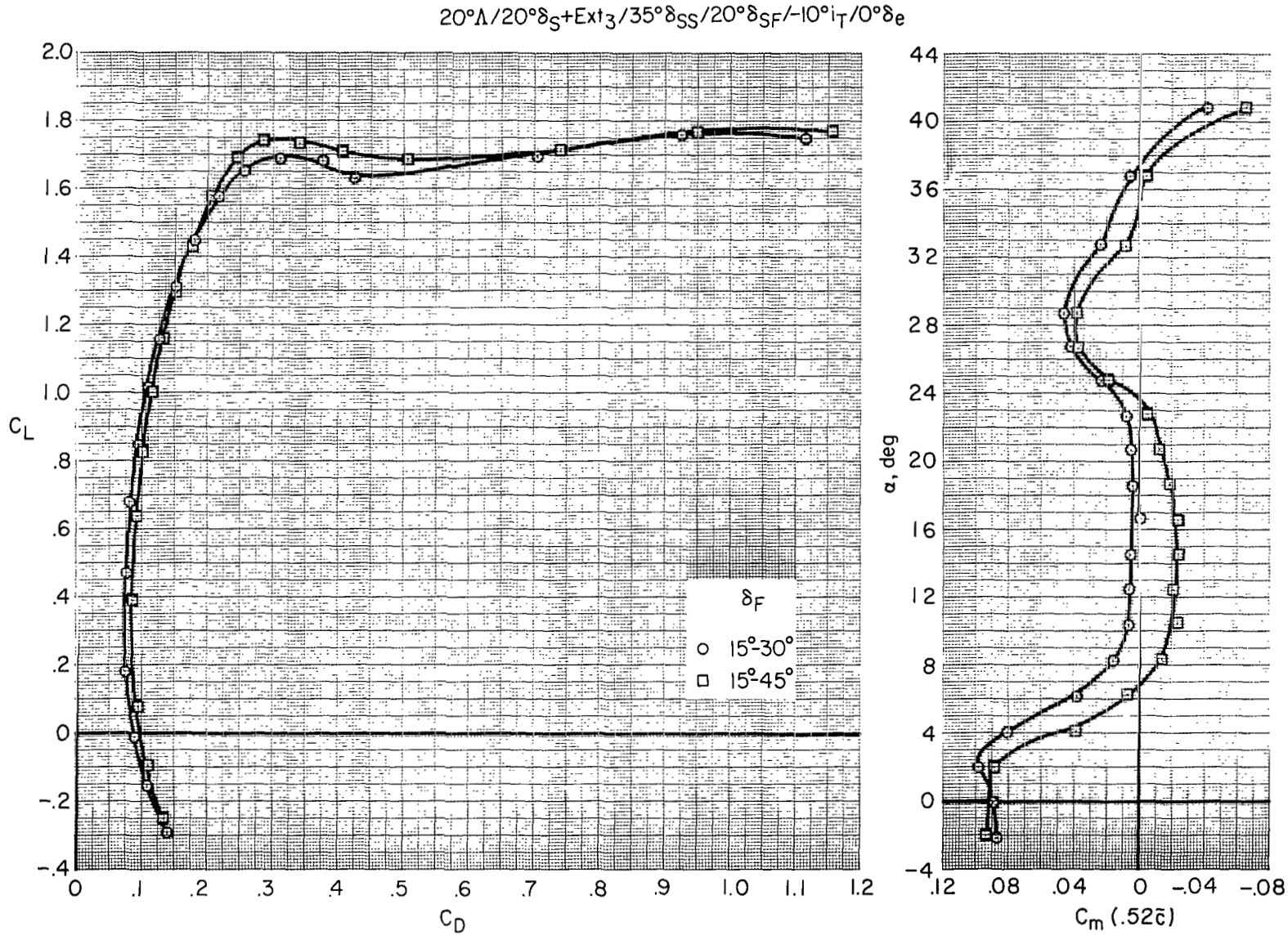

(d) C_L vs. C_D and α vs. C_m for an intermediate range of flap deflections.

Figure 7.- Continued.

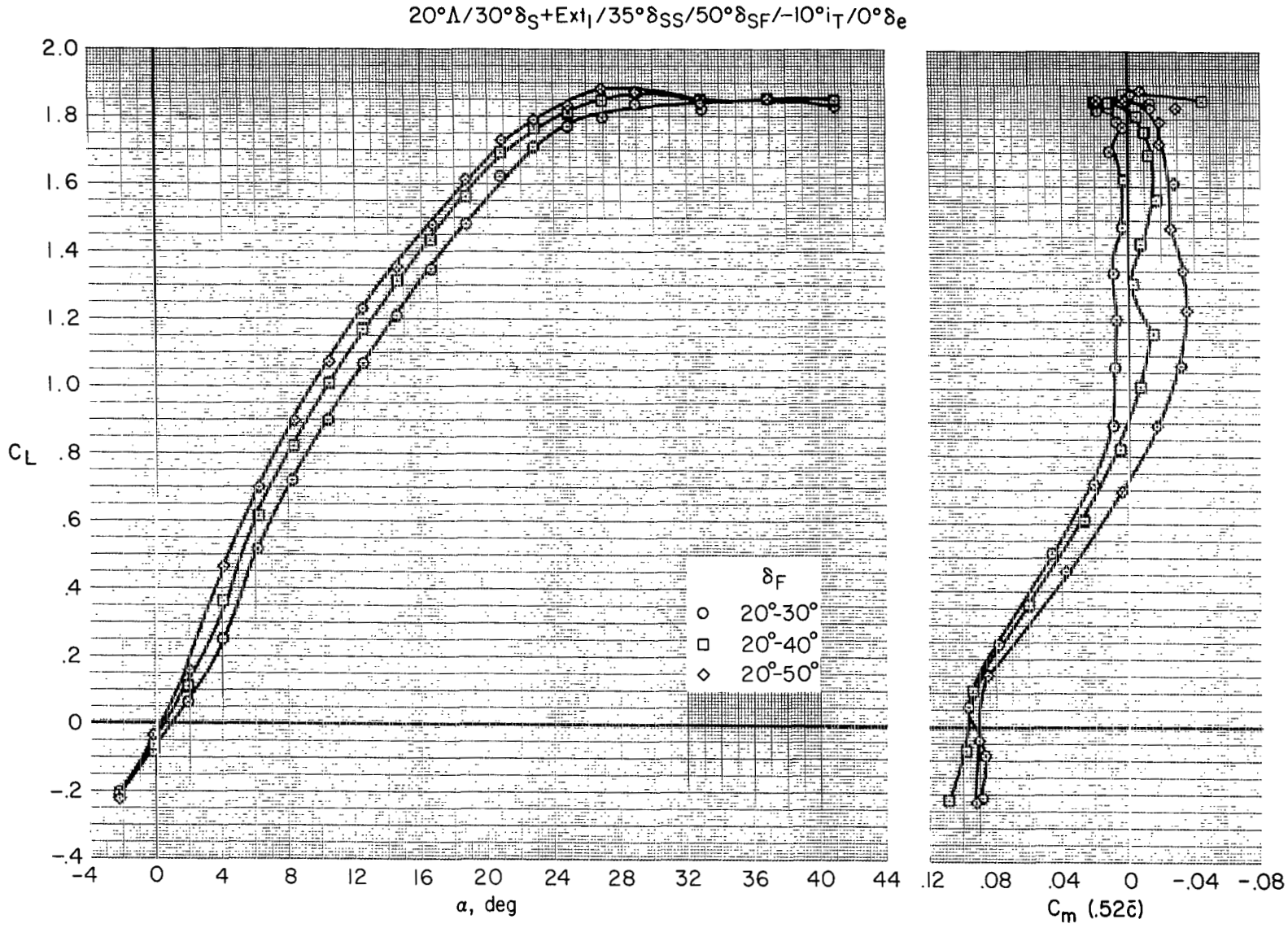

(e) C_L vs. α and C_m for the high range of flap deflections.

Figure 7.- Continued.

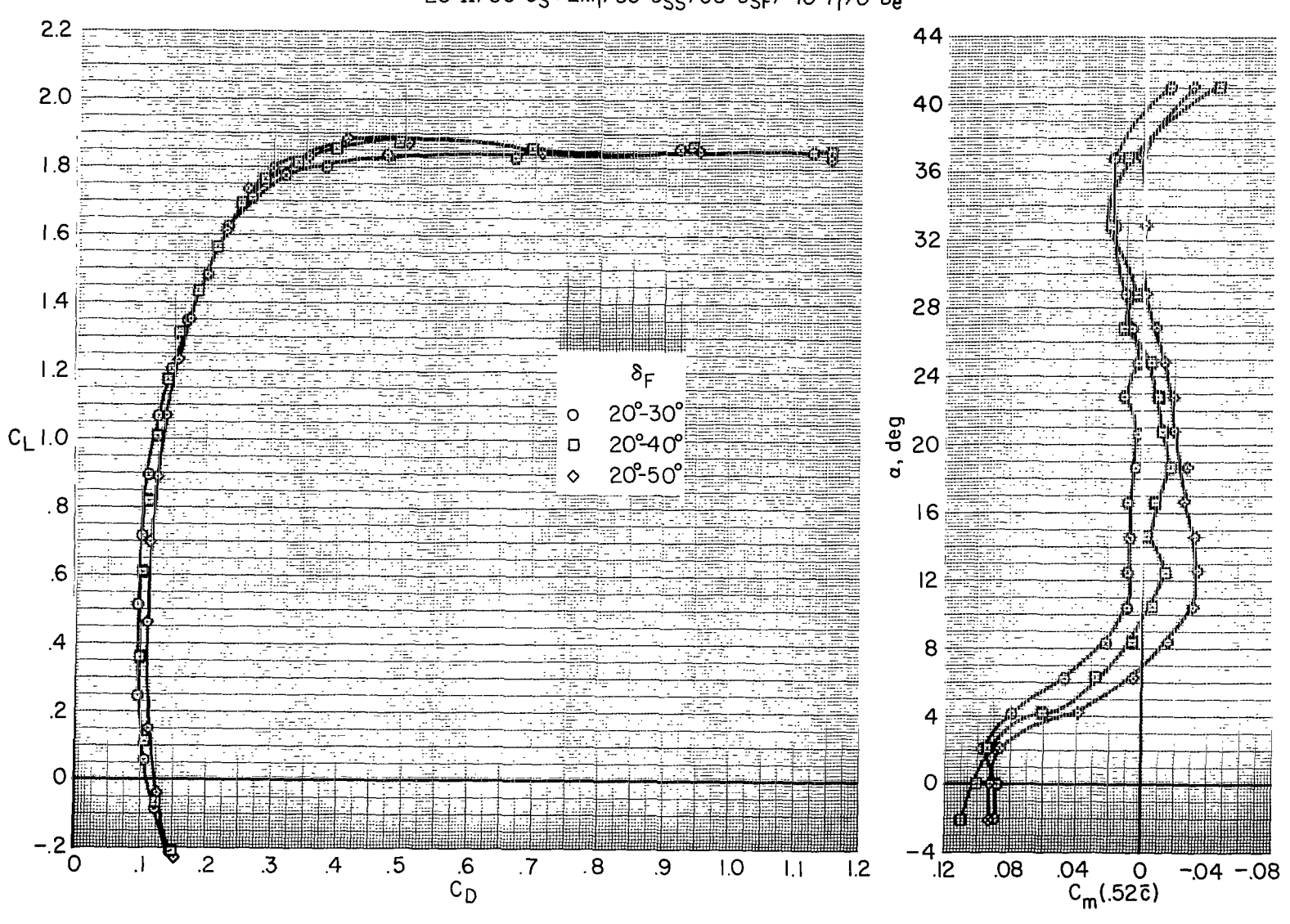

(f) C_L vs. C_D and α vs. C_m for the high range of flap deflections.

Figure 7.- Continued.

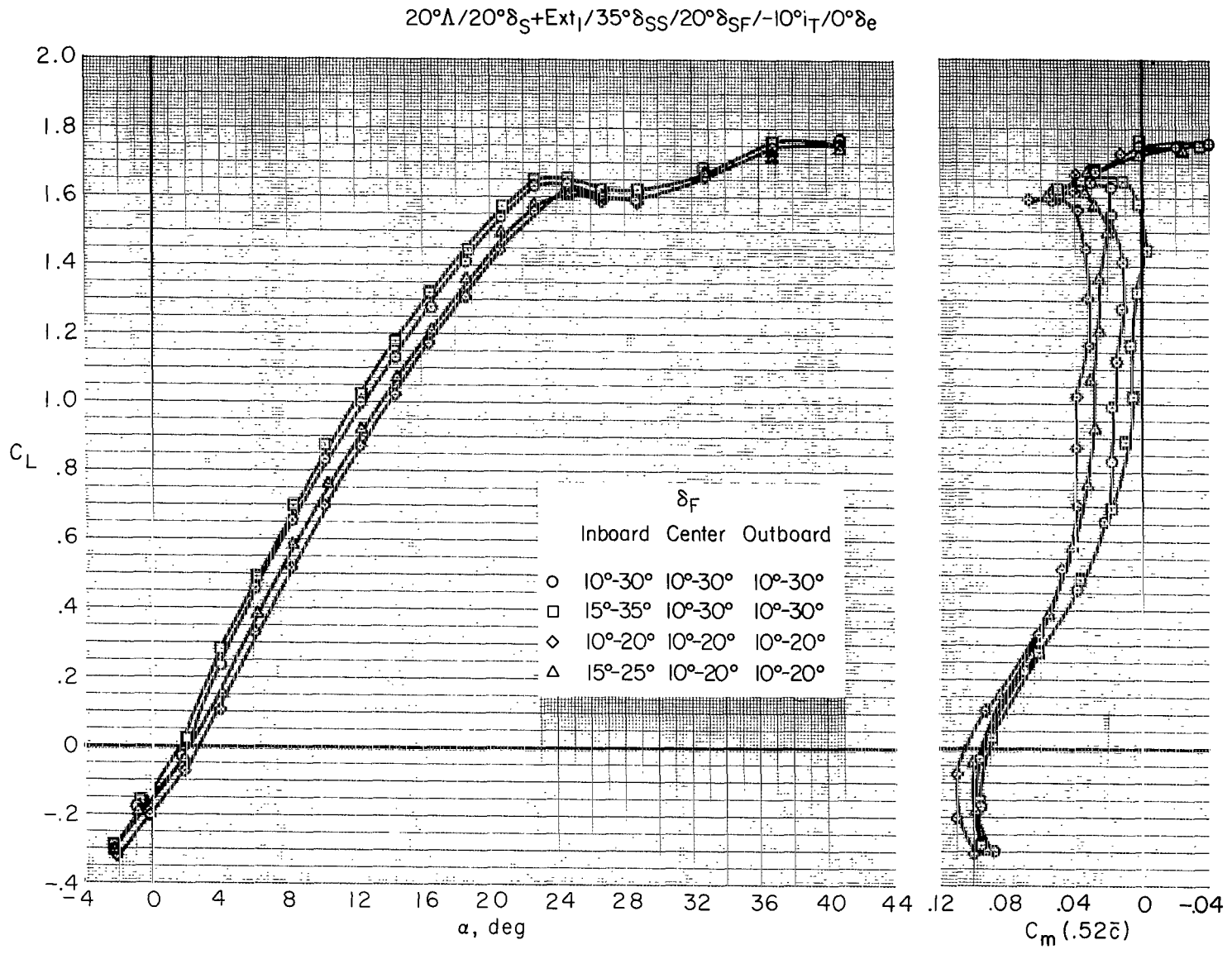

(g) C_L vs. α and C_m for various combinations of spanwise flap-segment deflections.

Figure 7.- Continued.

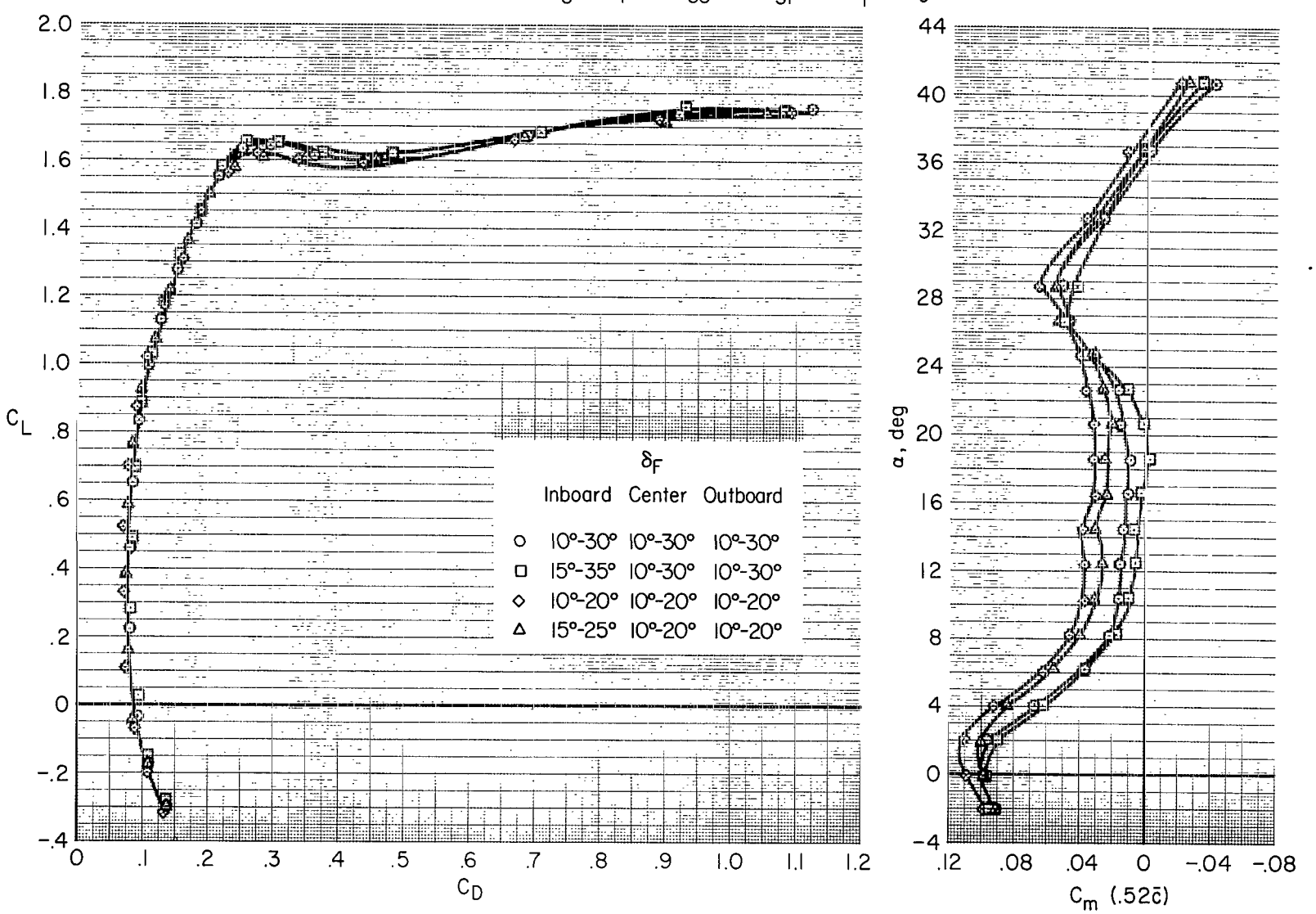

(h) C_L vs. C_D and α vs. C_m for various combinations of spanwise flap-segment deflections.

Figure 7.- Concluded.

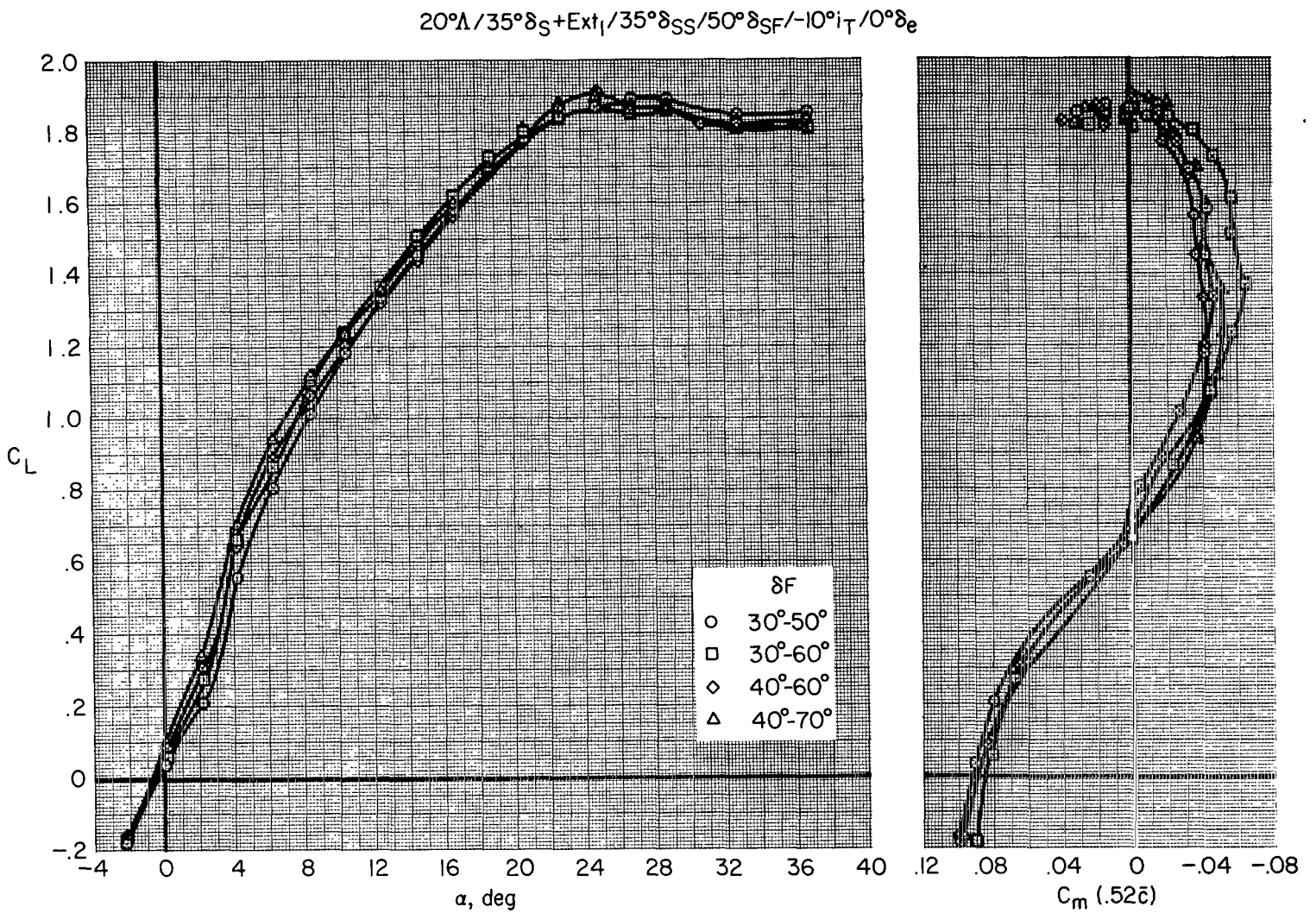

(a) C_L vs. α and C_m

Figure 8.- Longitudinal characteristics of trailing-edge flap deflection; landing configuration.

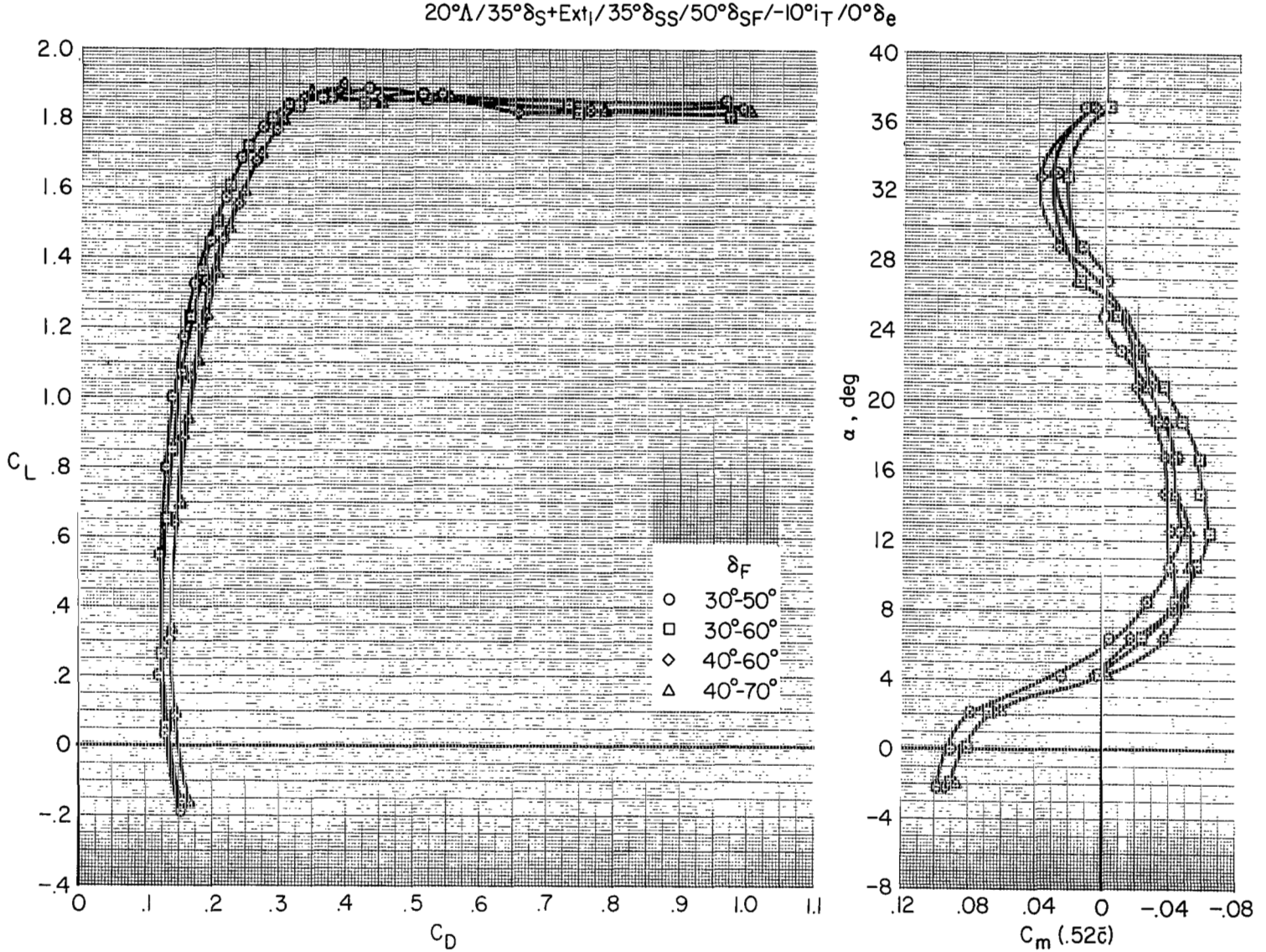

(b) C_L vs. C_D, α vs. C_m

Figure 8.- Concluded.

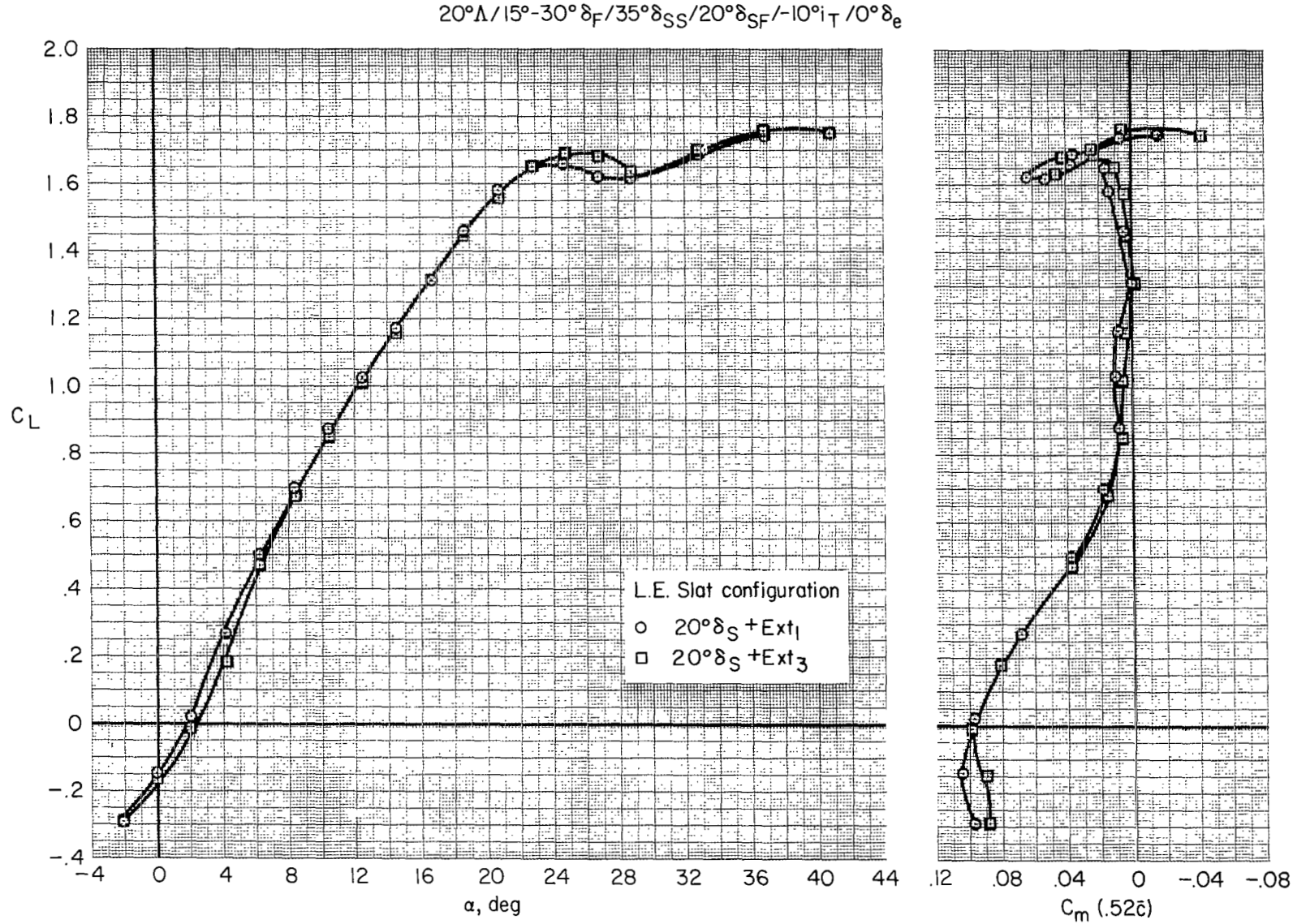

(a) Extended chord slat, C_L vs. α and C_m.

Figure 9.- Longitudinal characteristics of the take-off configuration with various leading-edge slat settings.

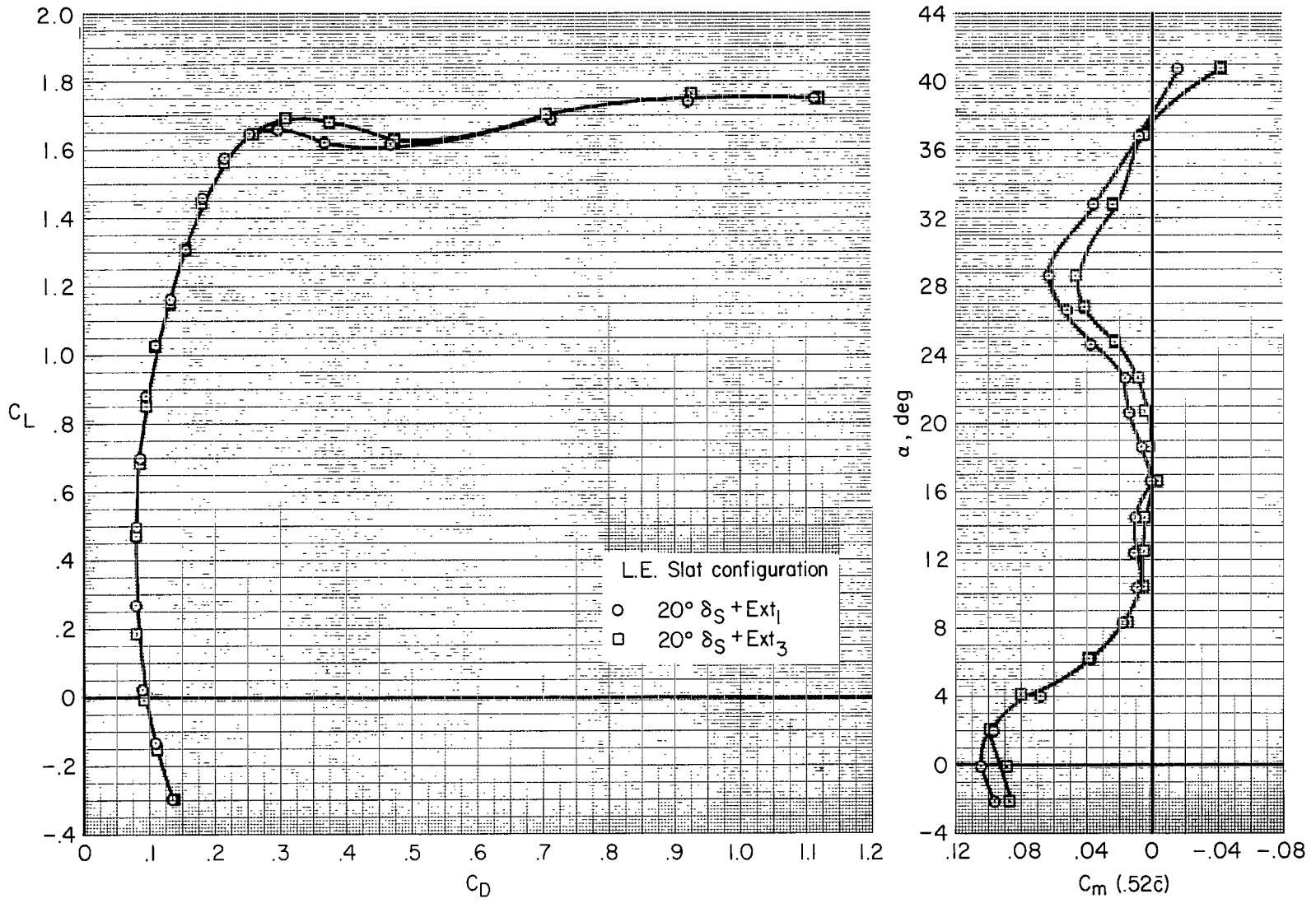

(b) Extended chord slat; C_L vs. C_D, α vs. C_m.

Figure 9.- Continued.

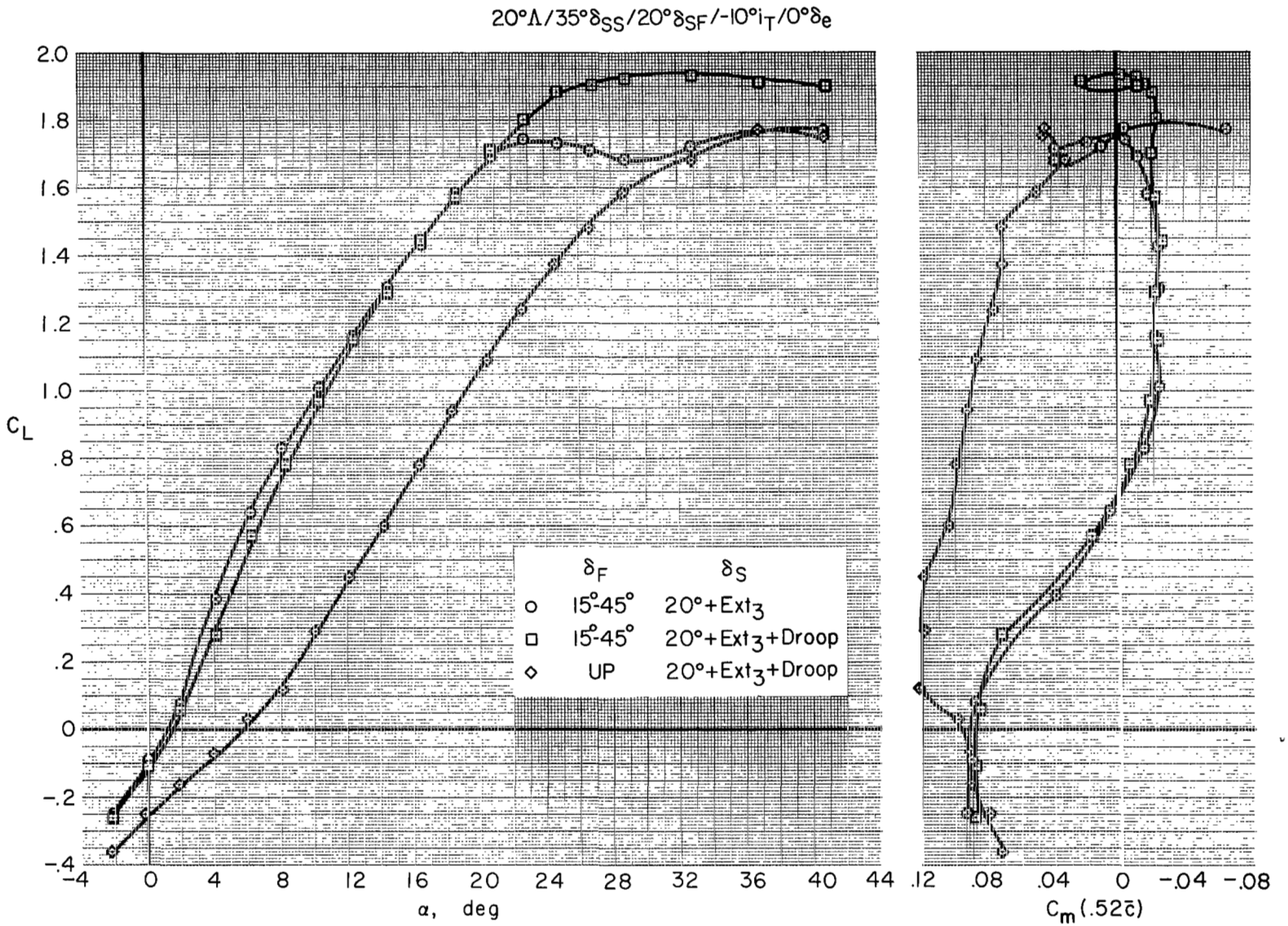

(c) Effect of slat drooped leading-edge with trailing-edge flaps both deflected and up, C_L vs. α and C_m.

Figure 9.- Continued.

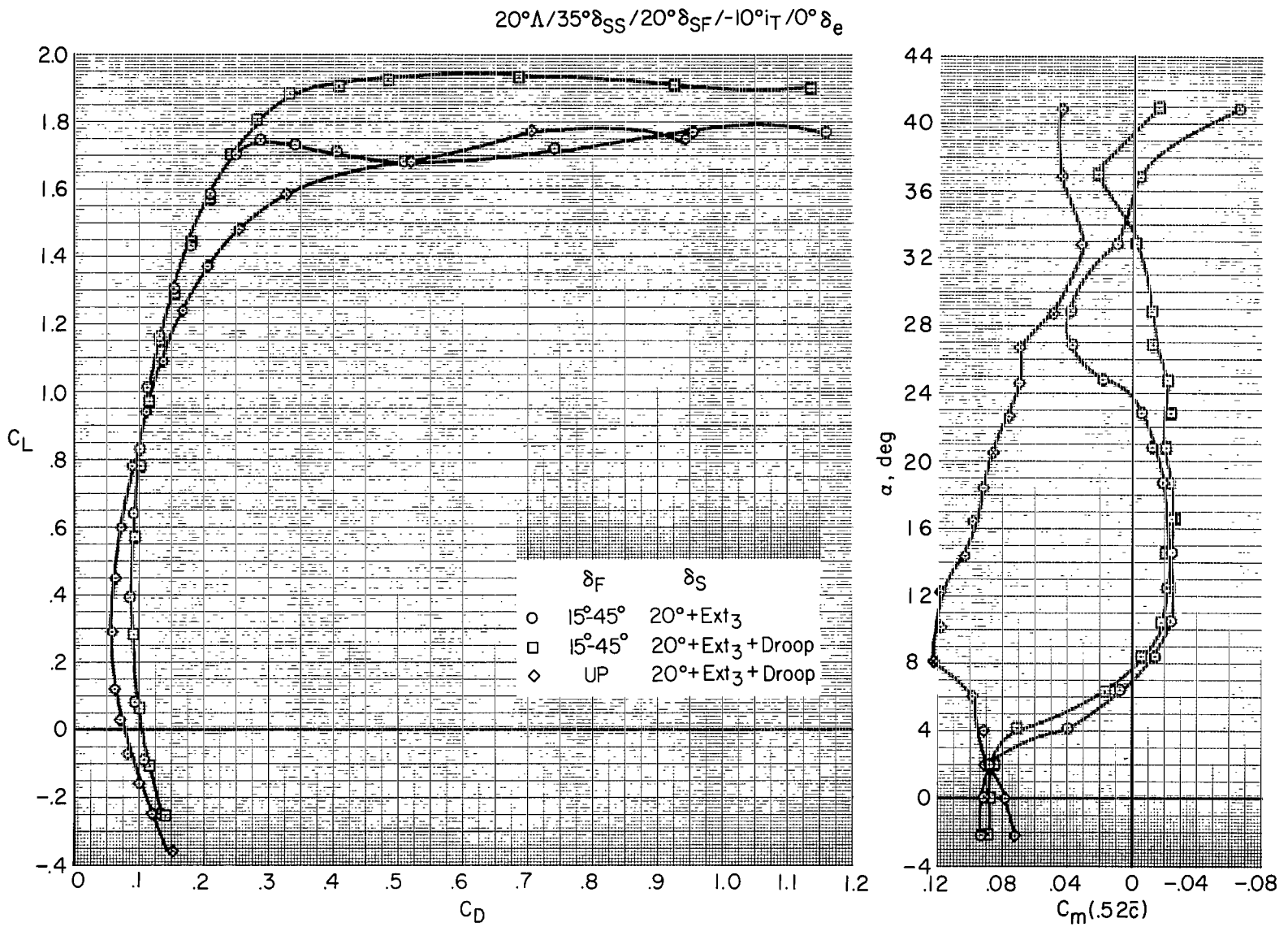

(d) Effect of slat drooped leading edge; C_L vs. C_D, α vs. C_m.

Figure 9.- Concluded.

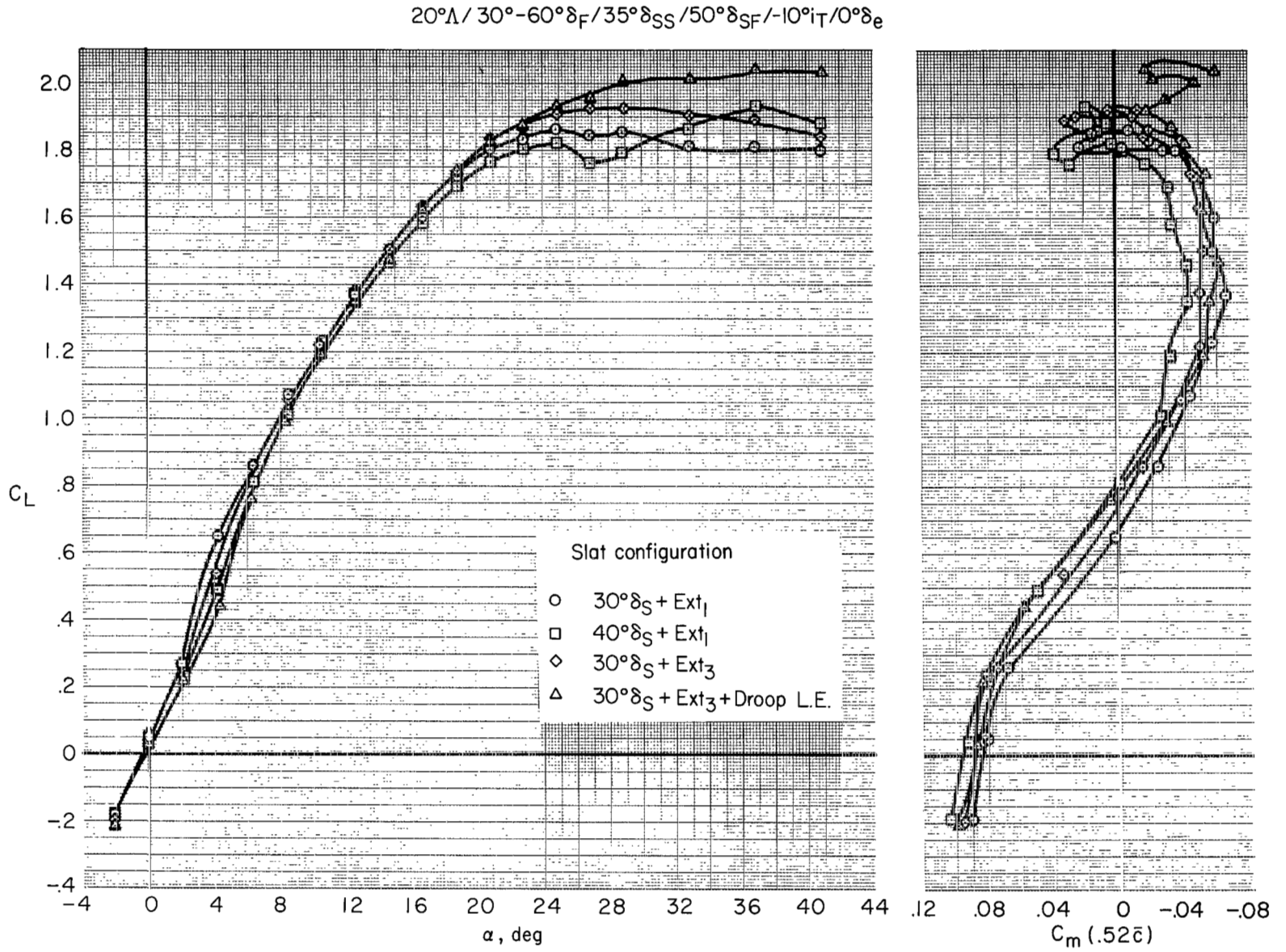

(a) C_L vs. α and C_m

Figure 10.- Longitudinal characteristics of the landing configuration with various leading-edge slat settings.

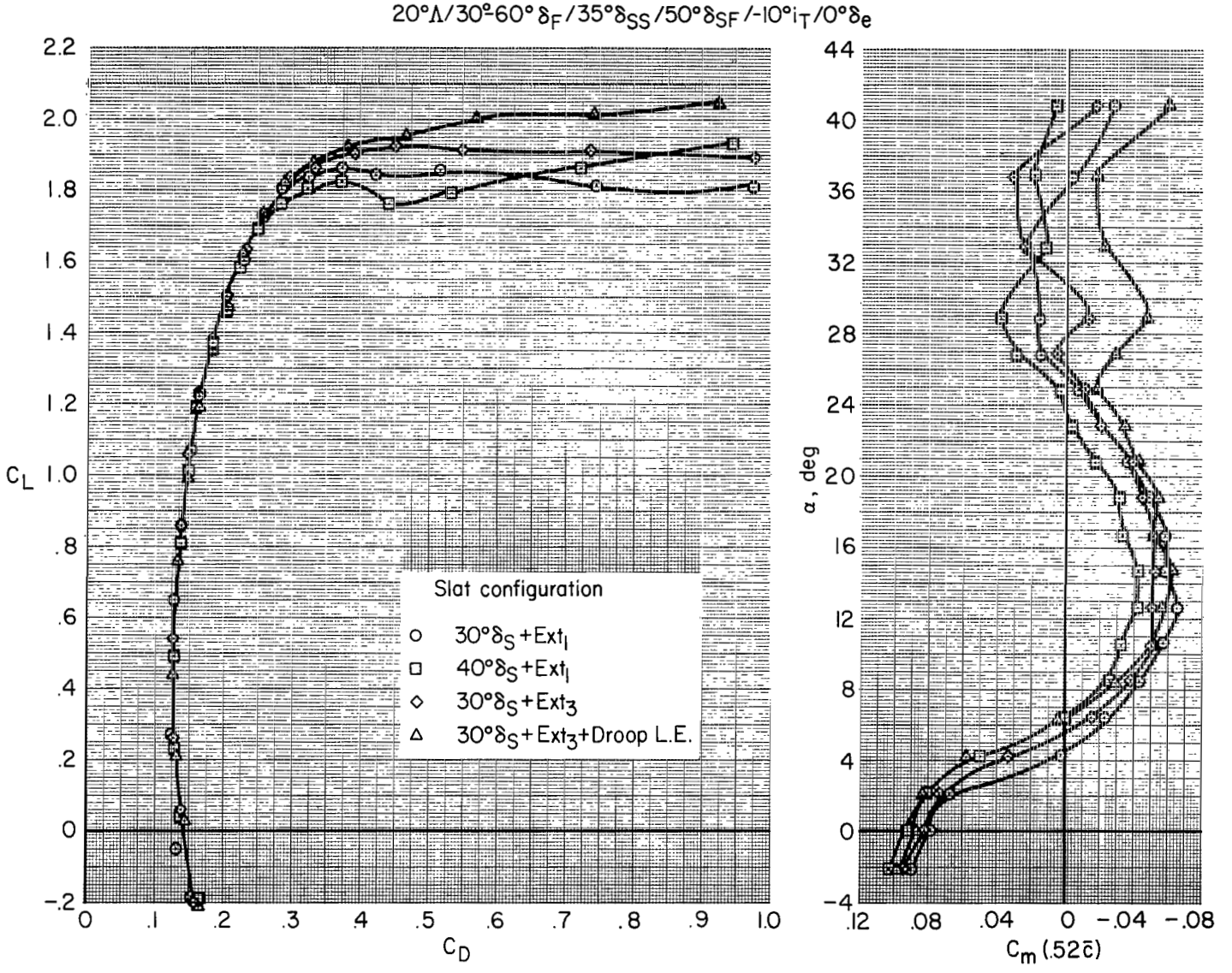

(b) C_L vs. C_D, α vs. C_m

Figure 10.- Concluded.

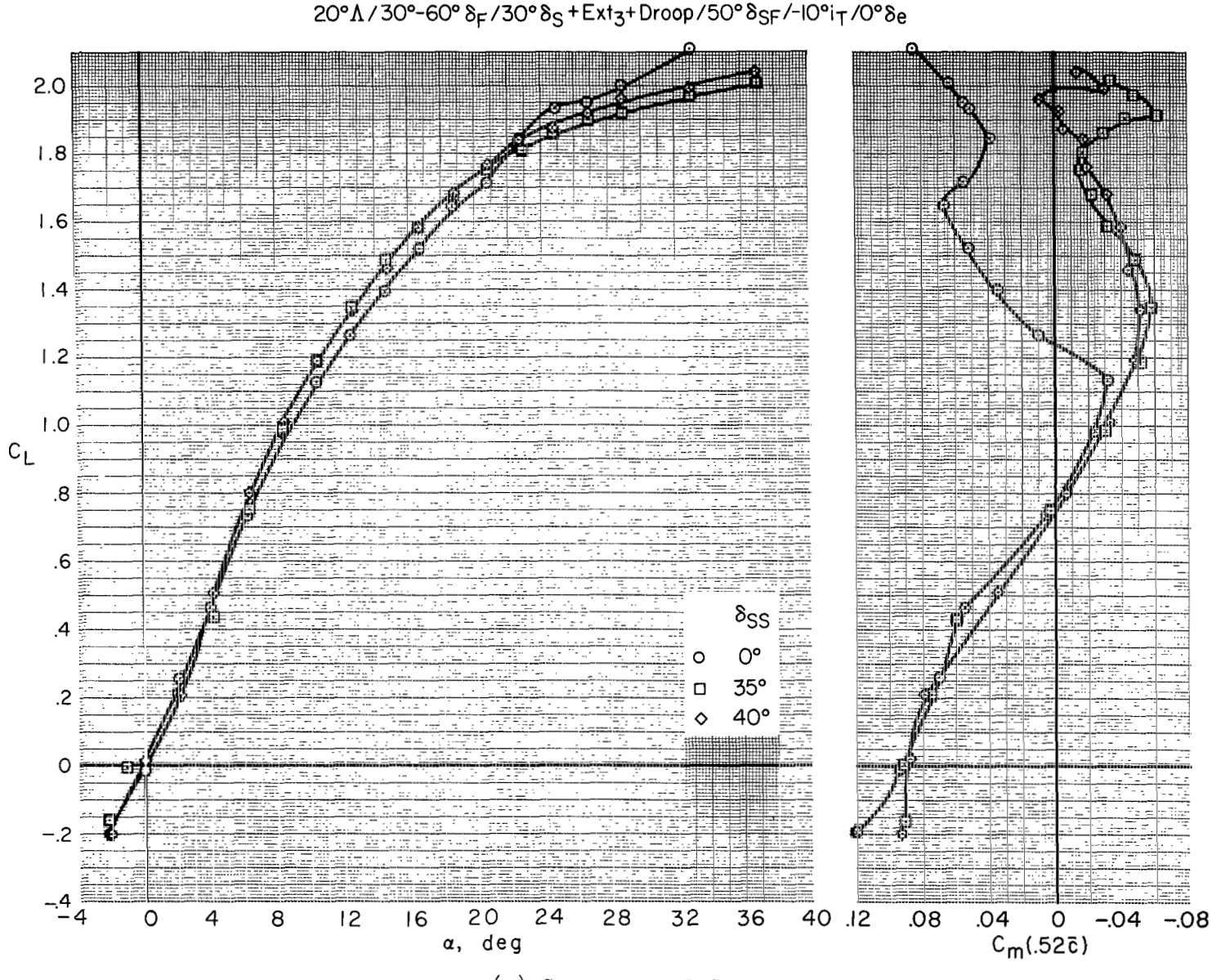

(a) C_L vs. α and C_m

Figure 11.- Effects of strake leading-edge slat deflection; landing configuration.

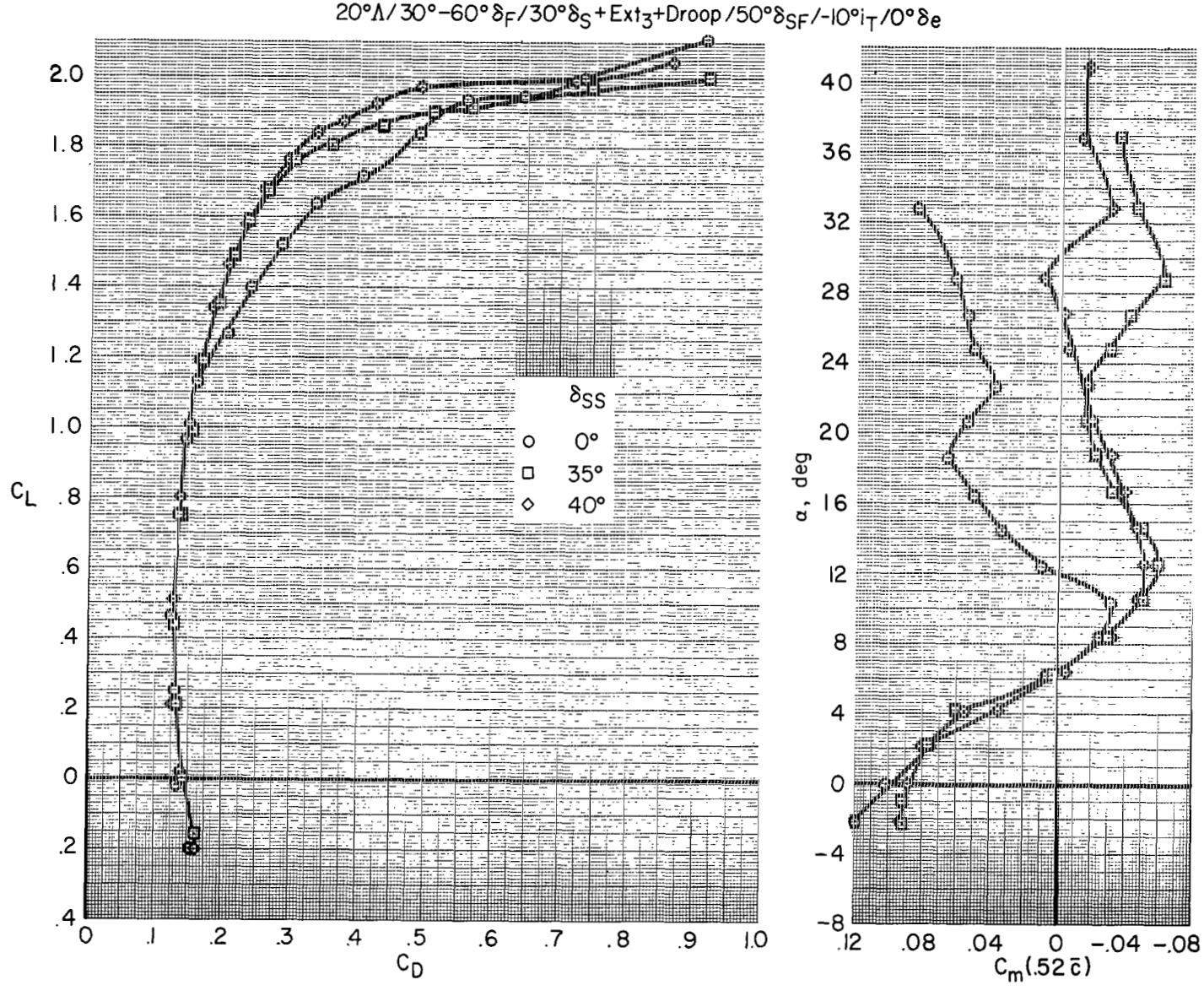

(b) C_L vs. C_D, α vs. C_m

Figure 11.- Concluded.

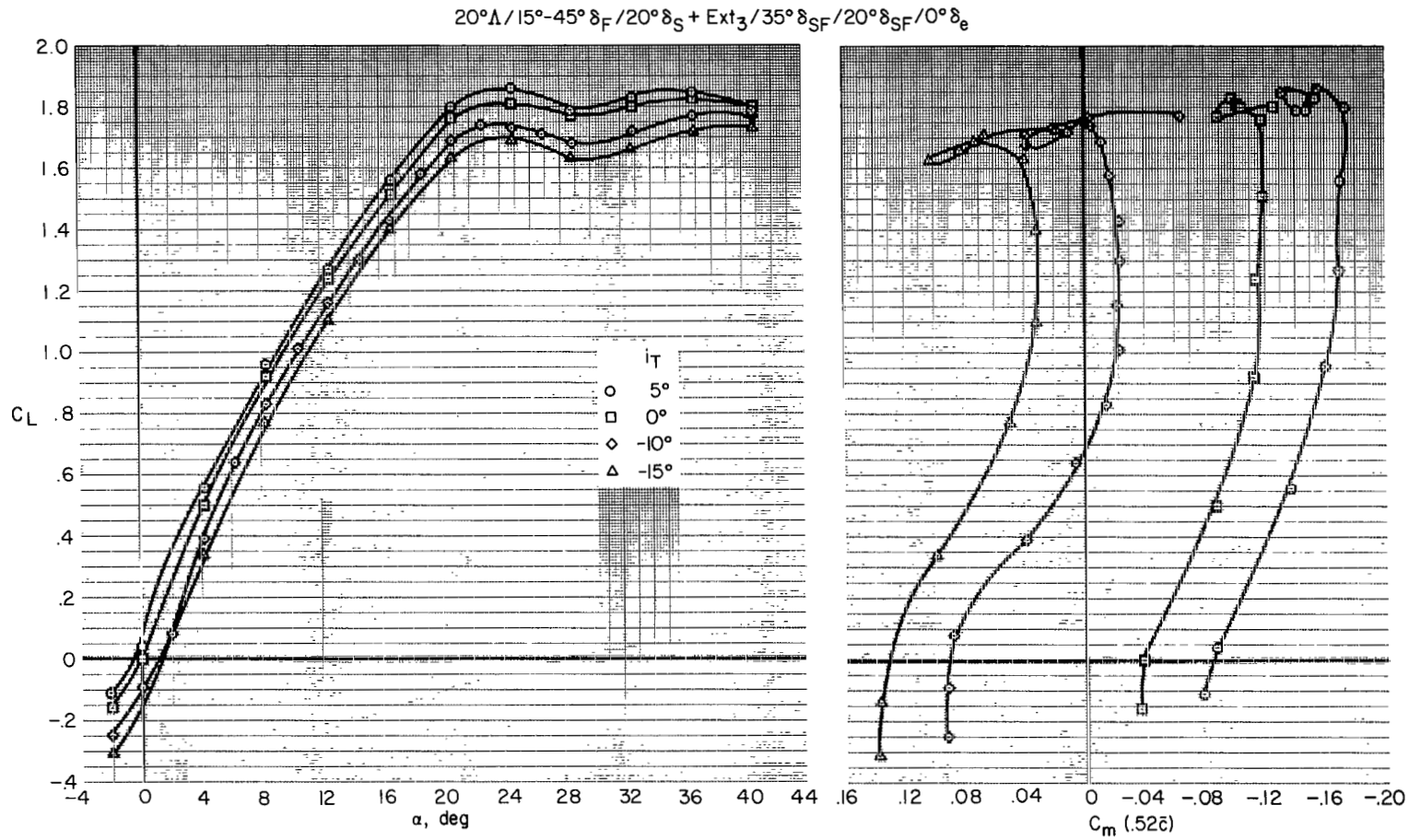

(a) Effect of horizontal-tail incidence, C_L vs. α and C_m.

Figure 12.- Effects of horizontal-tail incidence and elevator deflection on the longitudinal characteristics of the optimized take-off configuration.

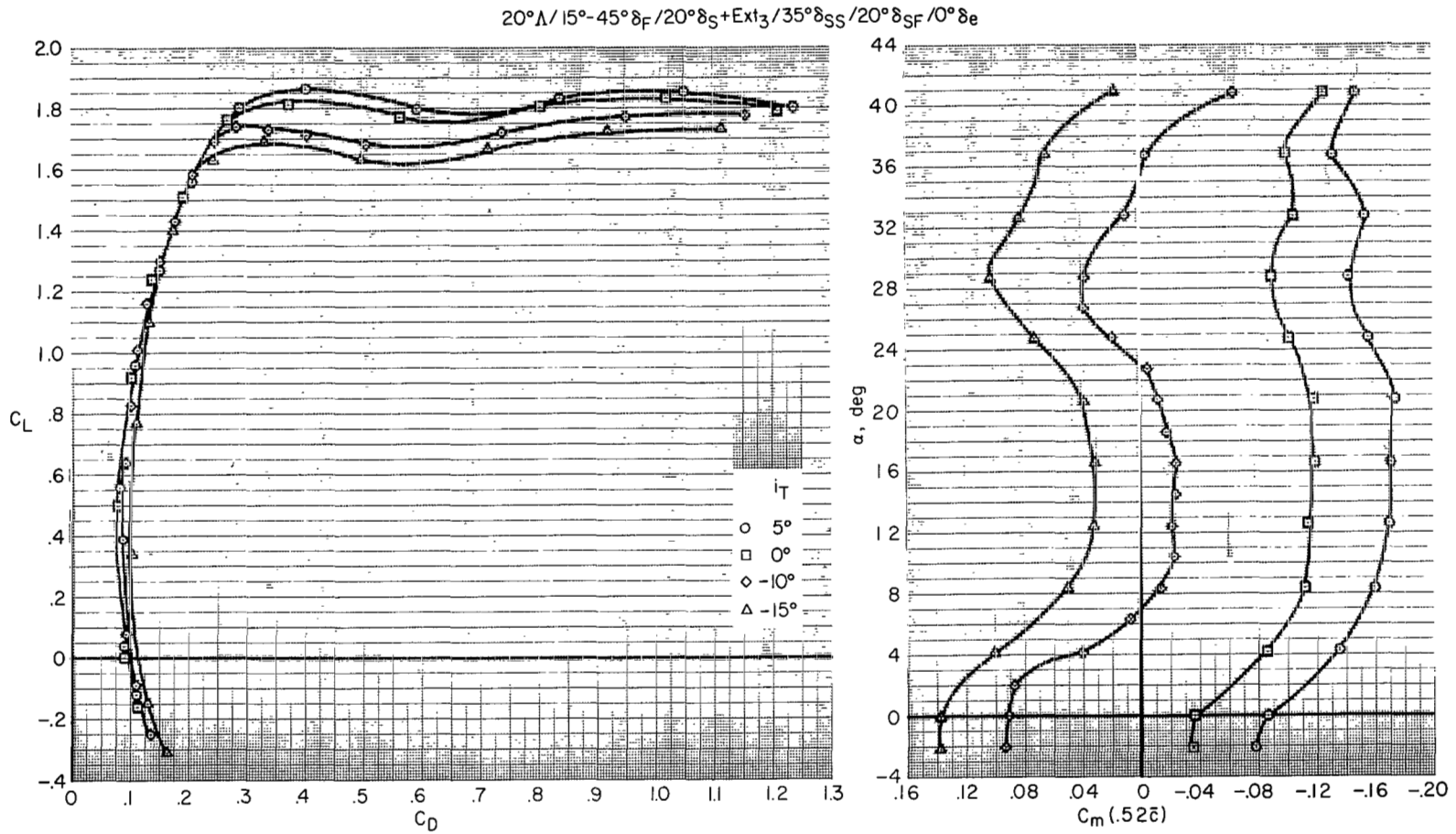

(b) Effect of horizontal-tail incidence; C_L vs. C_D, α vs. C_m.

Figure 12.- Continued.

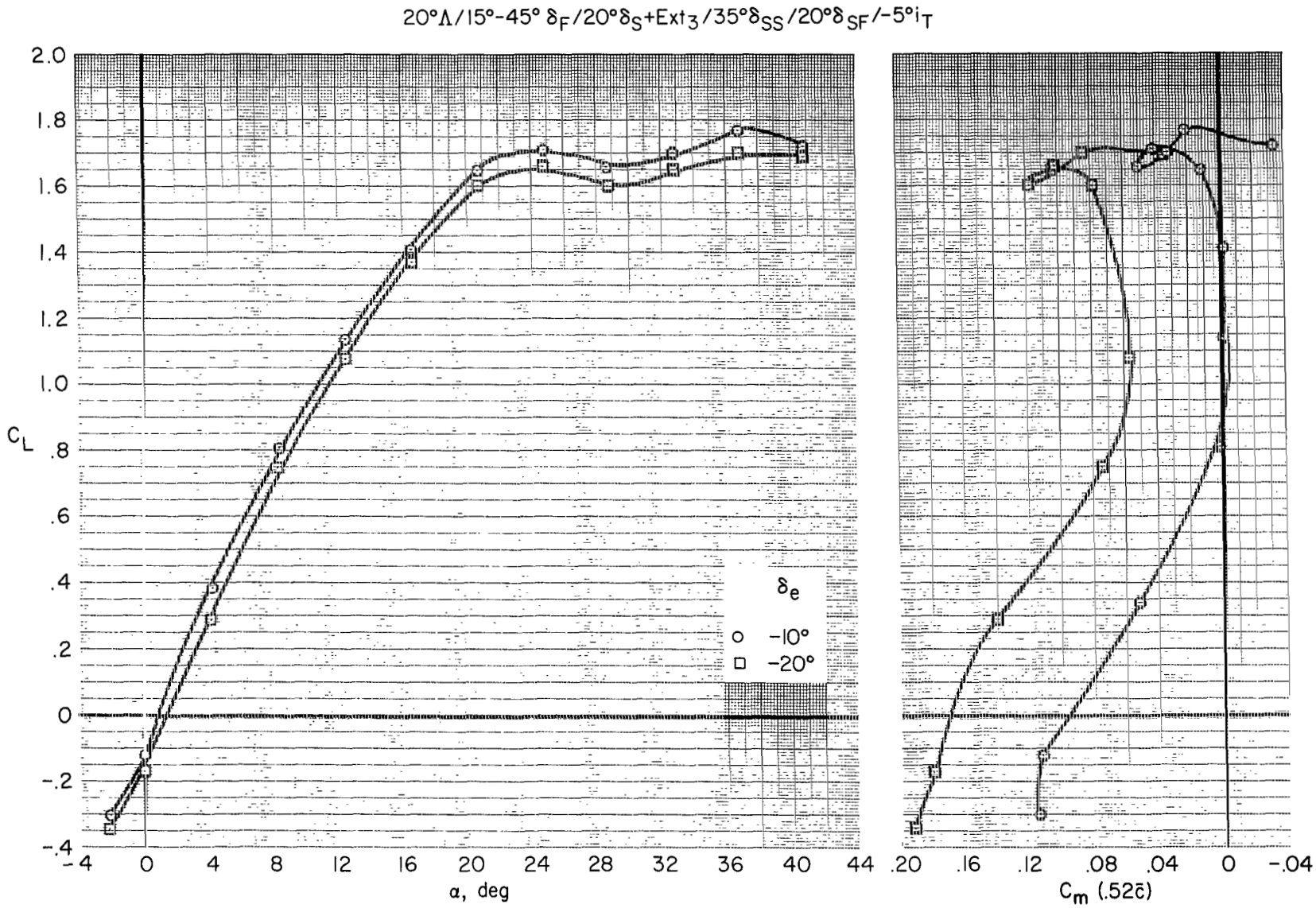

(c) Effect of elevator deflection, C_L vs. α and C_m.

Figure 12.- Continued.

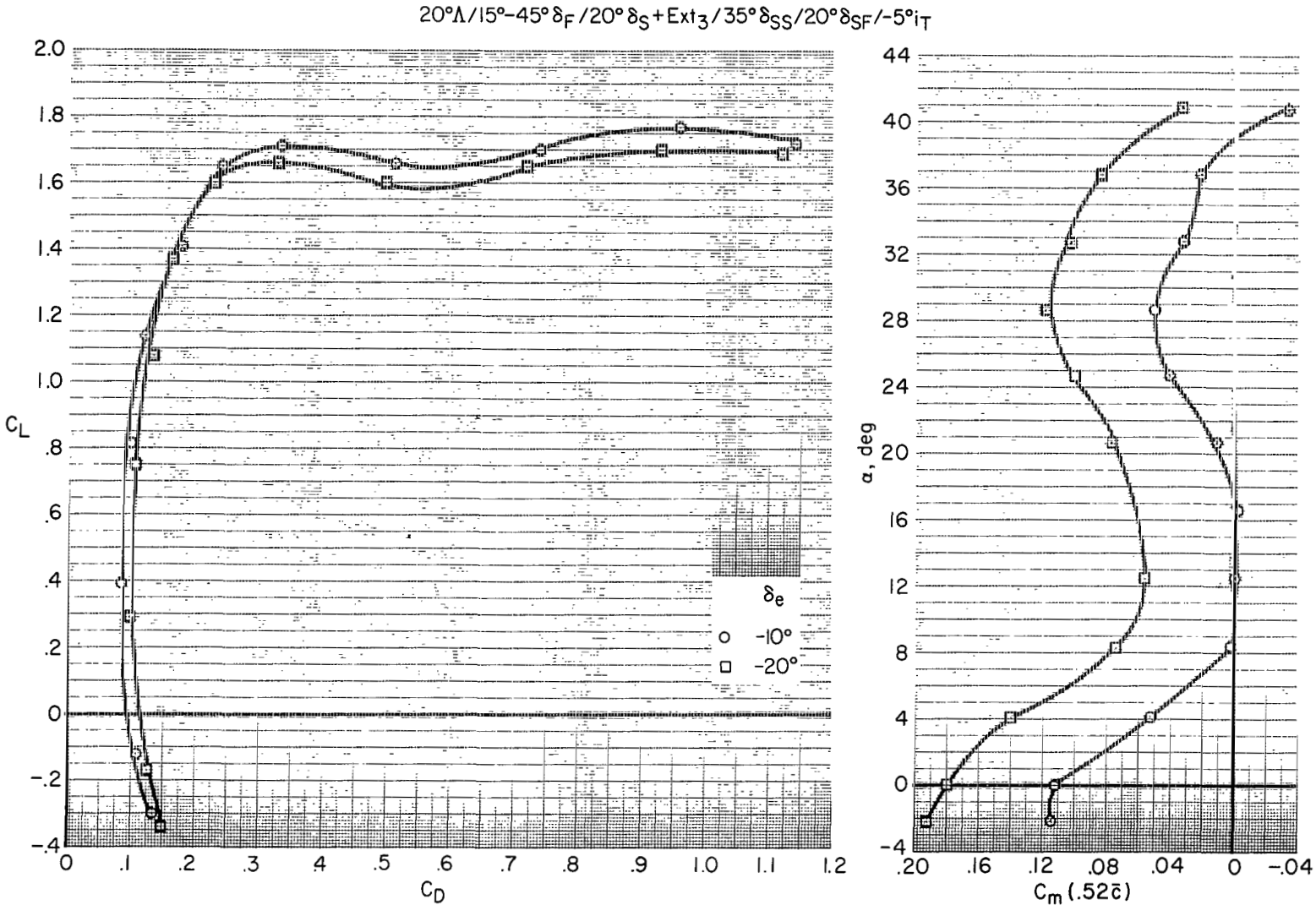

(d) Effect of elevator deflection; C_L vs. C_D, α vs. C_m.

Figure 12.- Concluded.

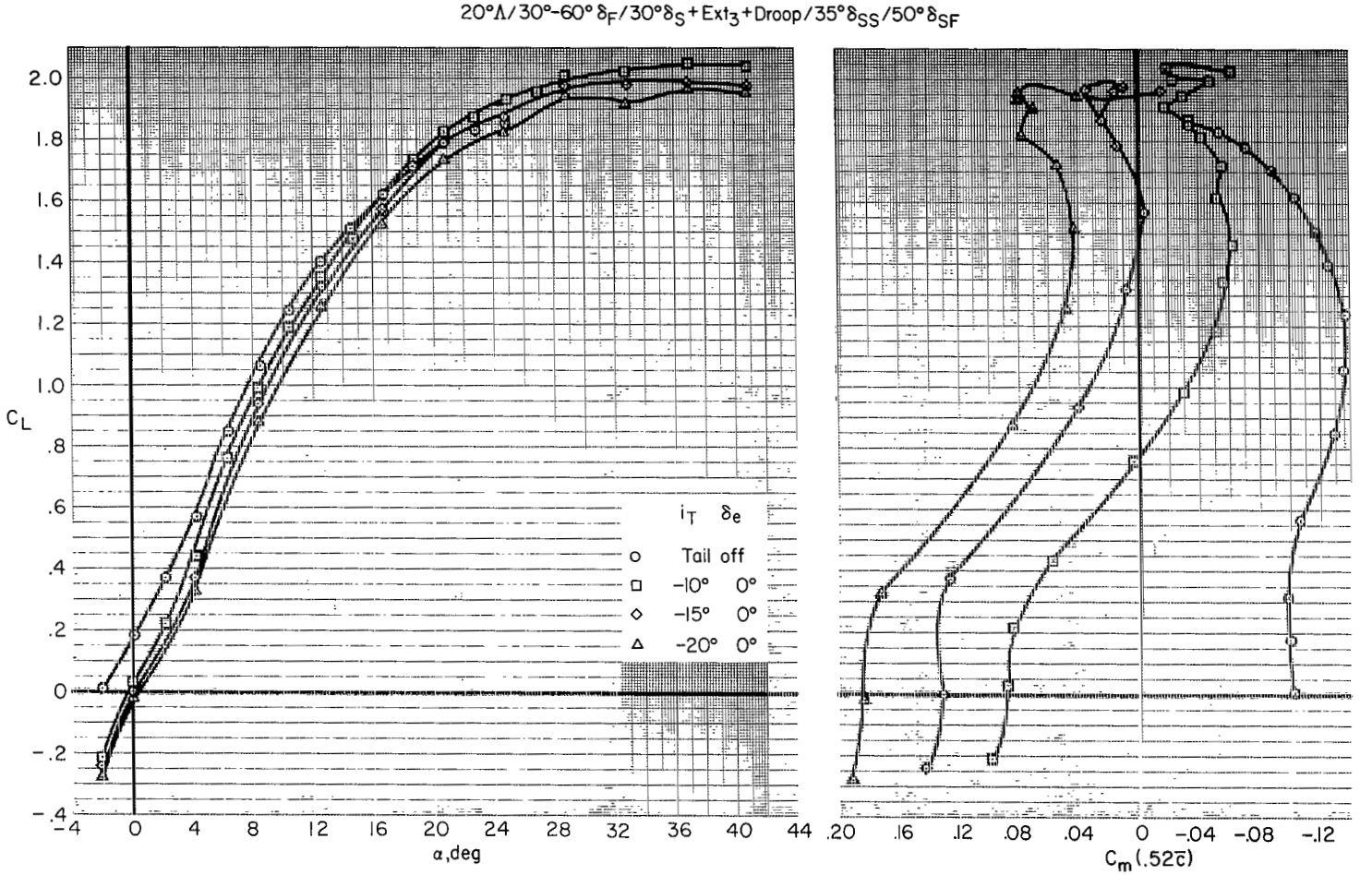

(a) Horizontal-tail incidence, C_L vs. α and C_m.

Figure 13.- Effects of horizontal-tail incidence and elevator deflection on the longitudinal characteristics of the optimized landing configuration.

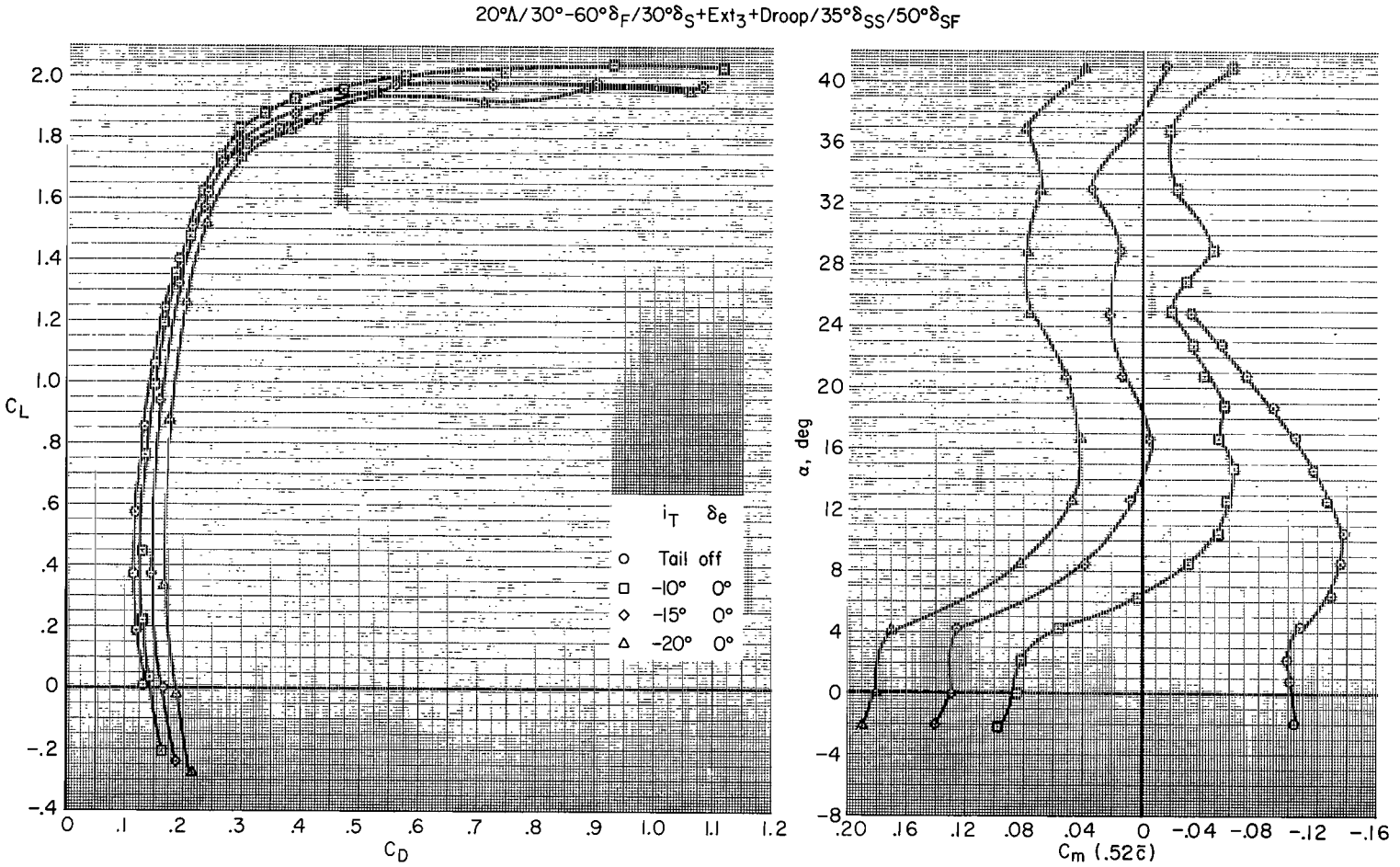

(b) Horizontal-tail incidence; C_L vs. C_D, α vs. C_m.

Figure 13.- Continued.

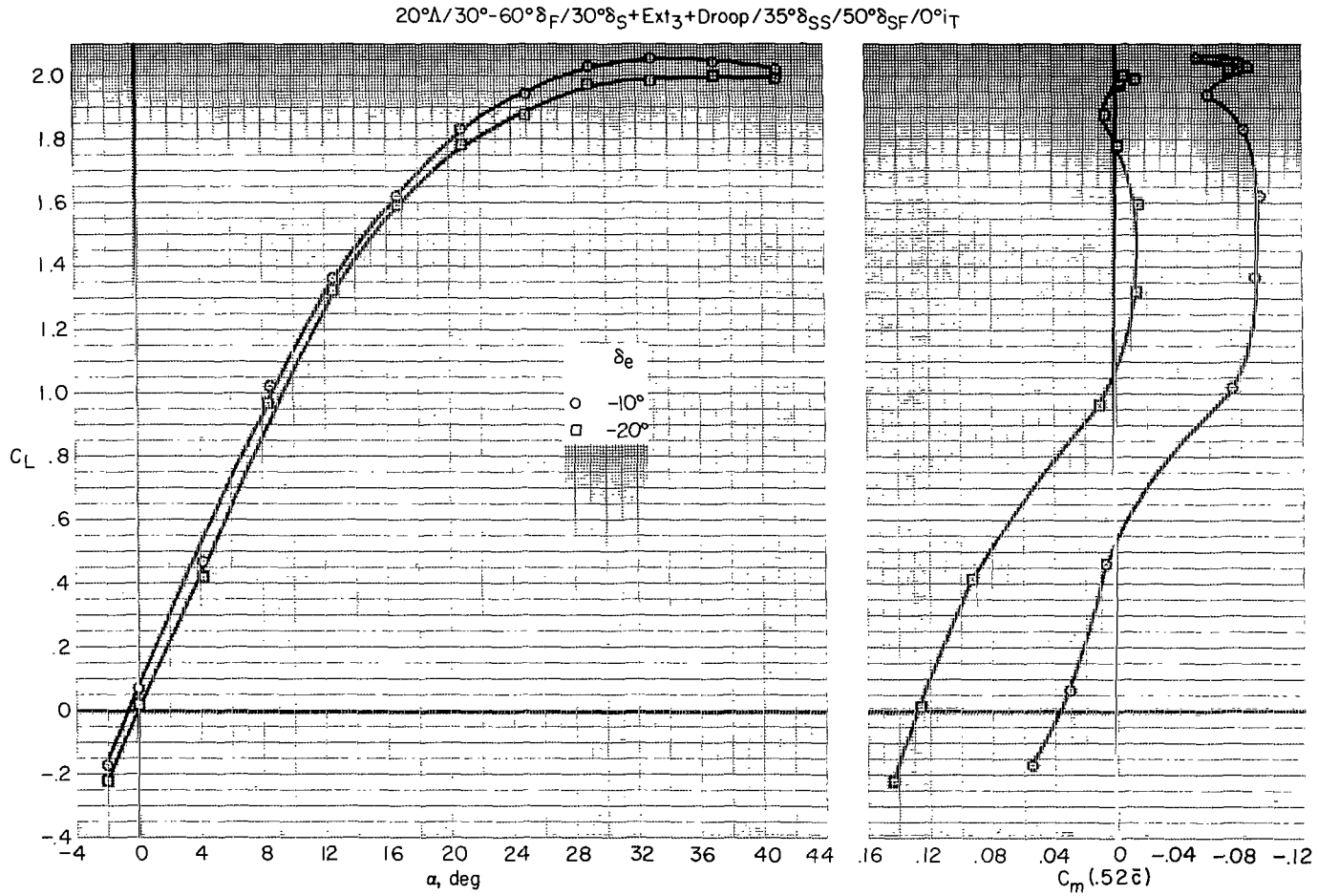

(c) Elevator deflection, C_L vs. α and C_m.

Figure 13.- Continued.

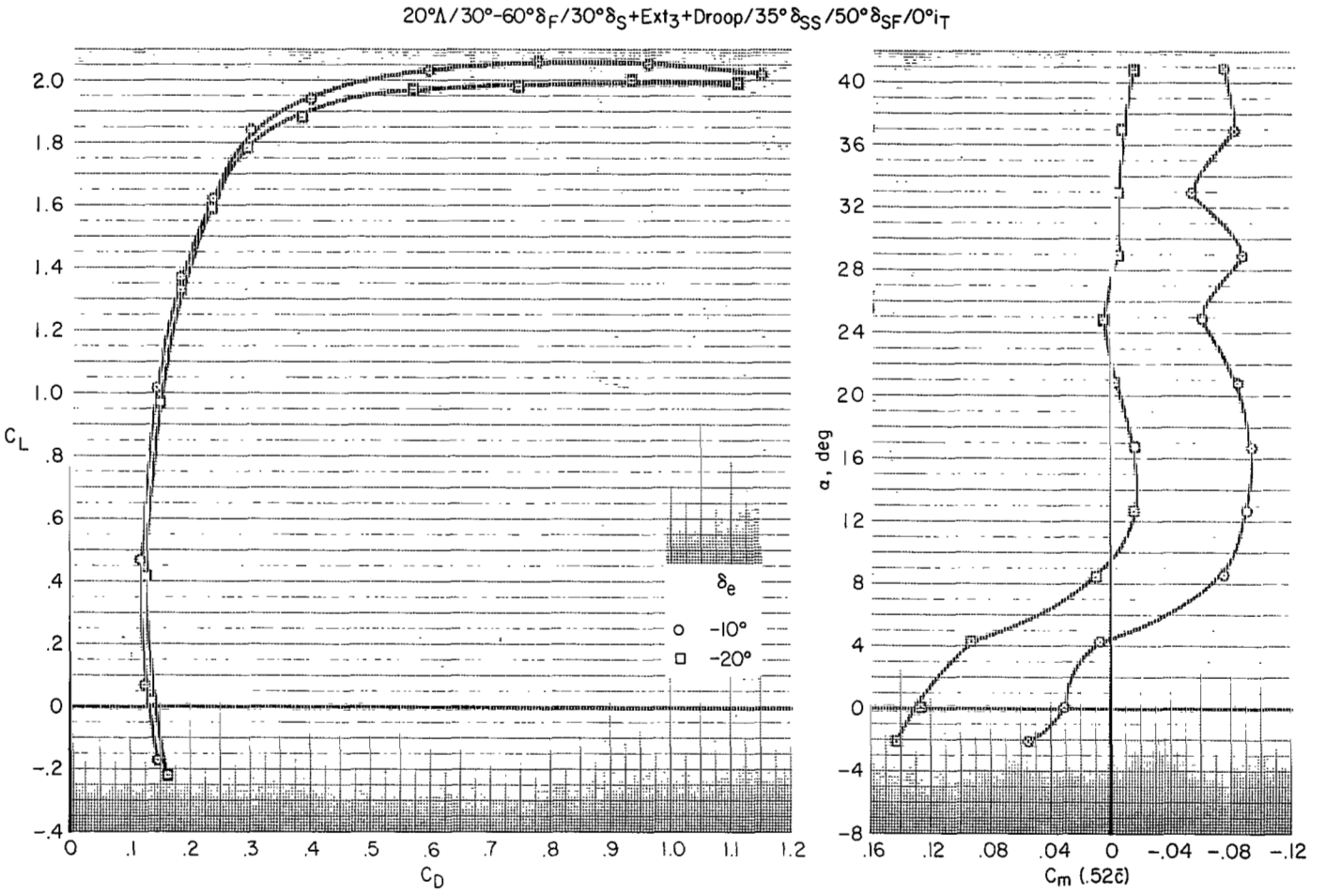

(d) Elevator deflection; C_L vs. C_D, α vs. C_m.

Figure 13.- Concluded.

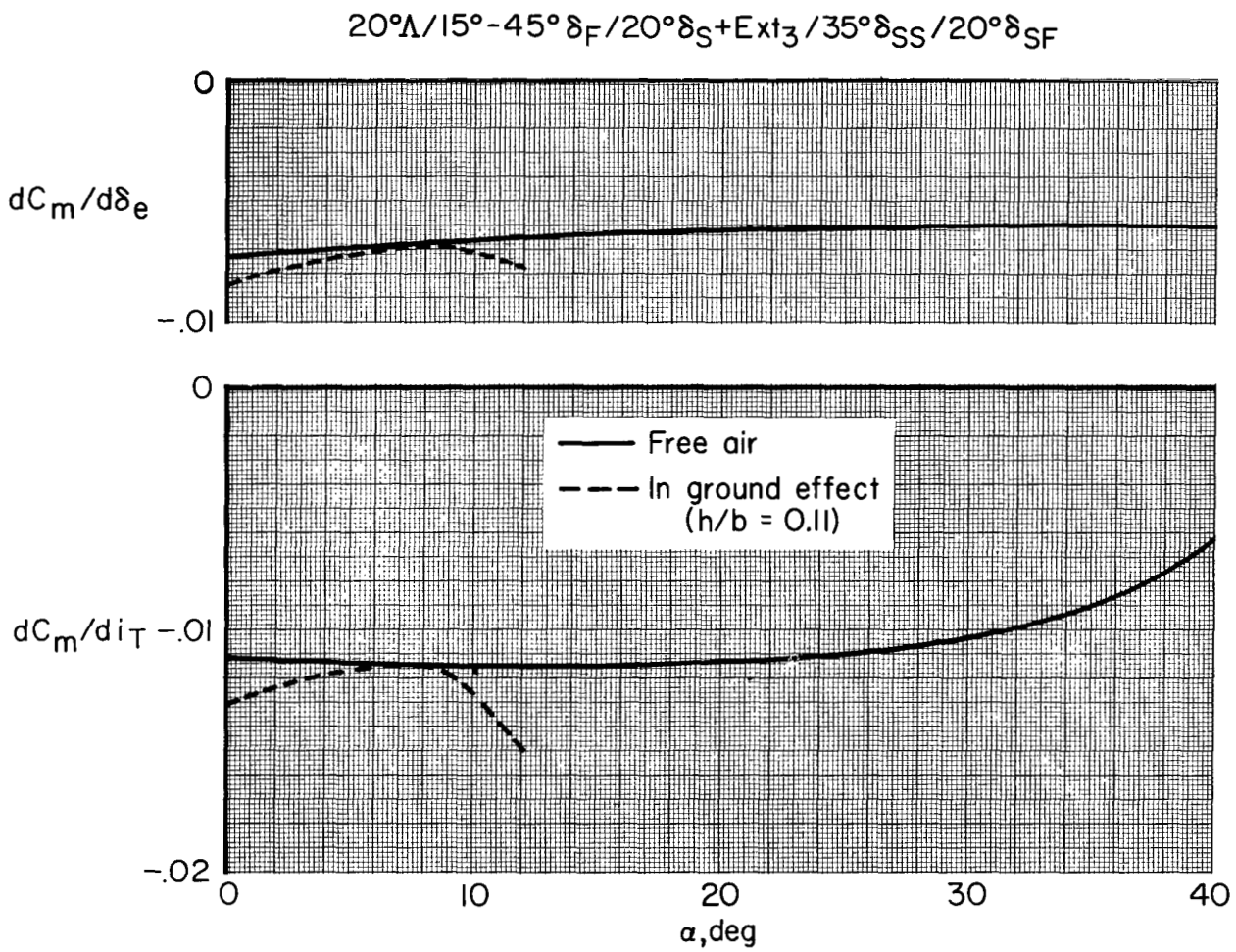

(a) Take-off configuration.

Figure 14.- Summary of longitudinal control power variations with angle of attack, both in and out of ground effect.

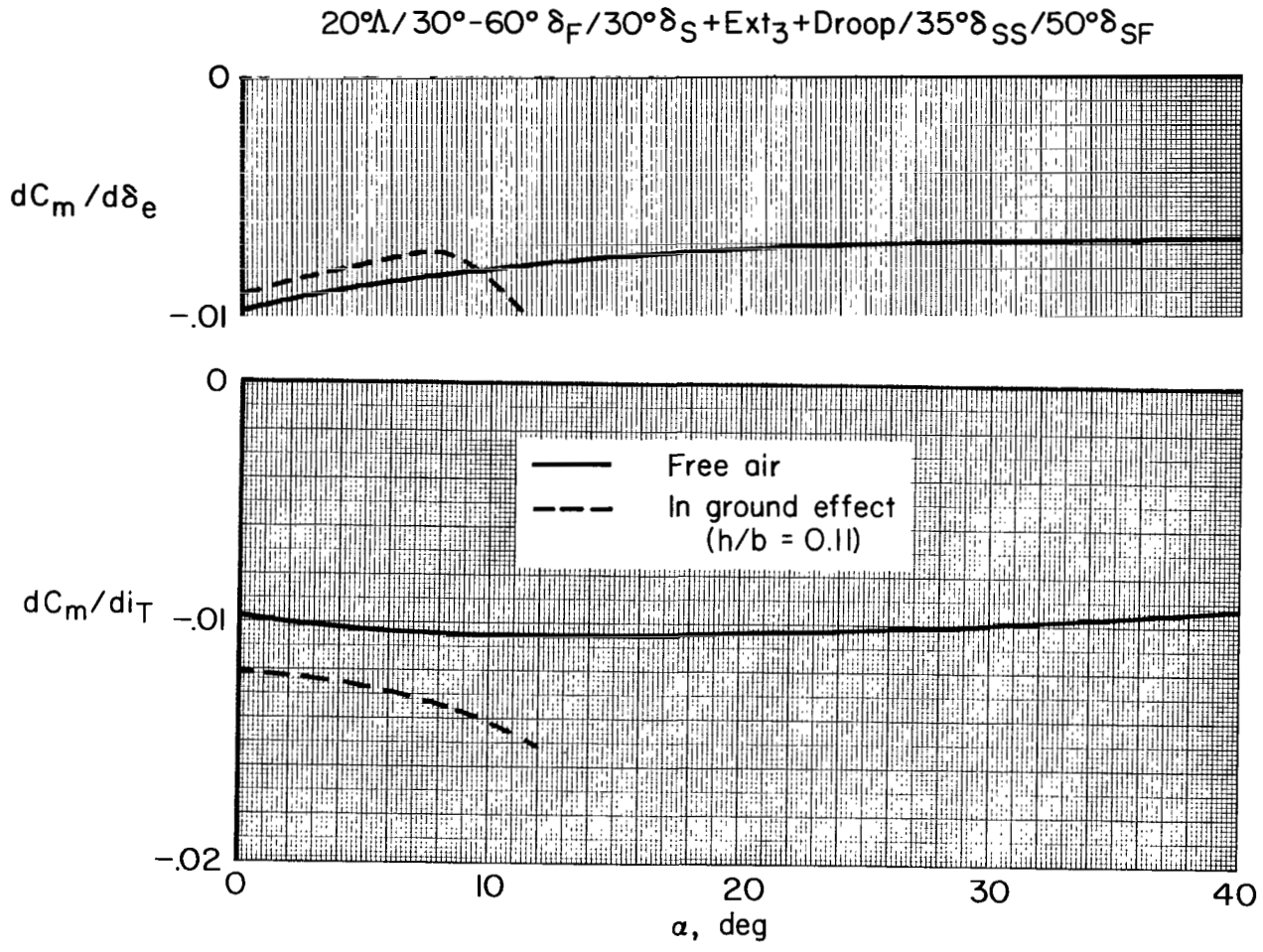

(b) Landing configuration.

Figure 14.- Concluded.

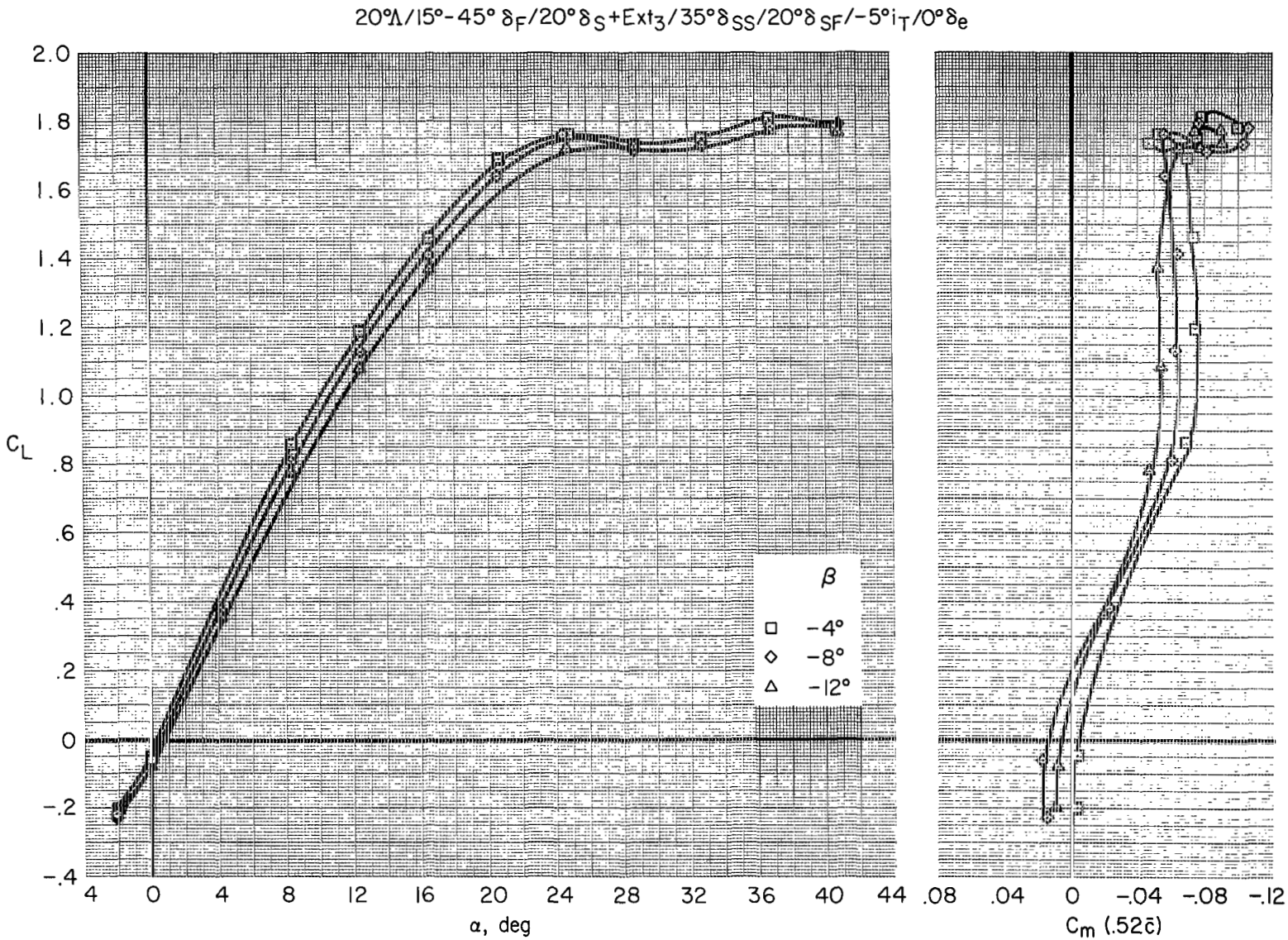

(a) Longitudinal characteristics, C_L vs. α and C_m.

Figure 15.- Characteristics of take-off configuration in sideslip.

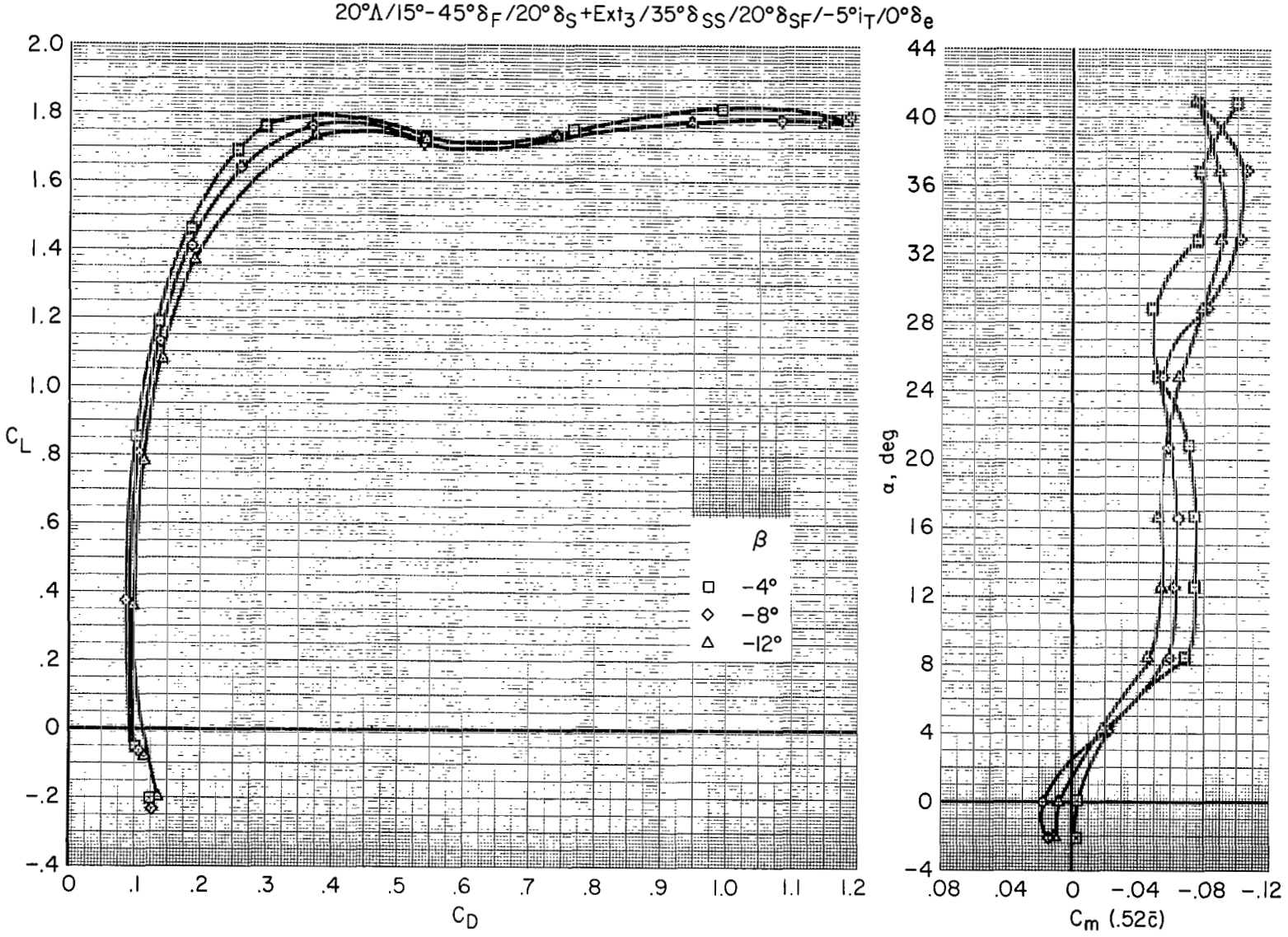

(b) Longitudinal characteristics; C_L vs. C_D, α vs. C_m.

Figure 15.- Continued.

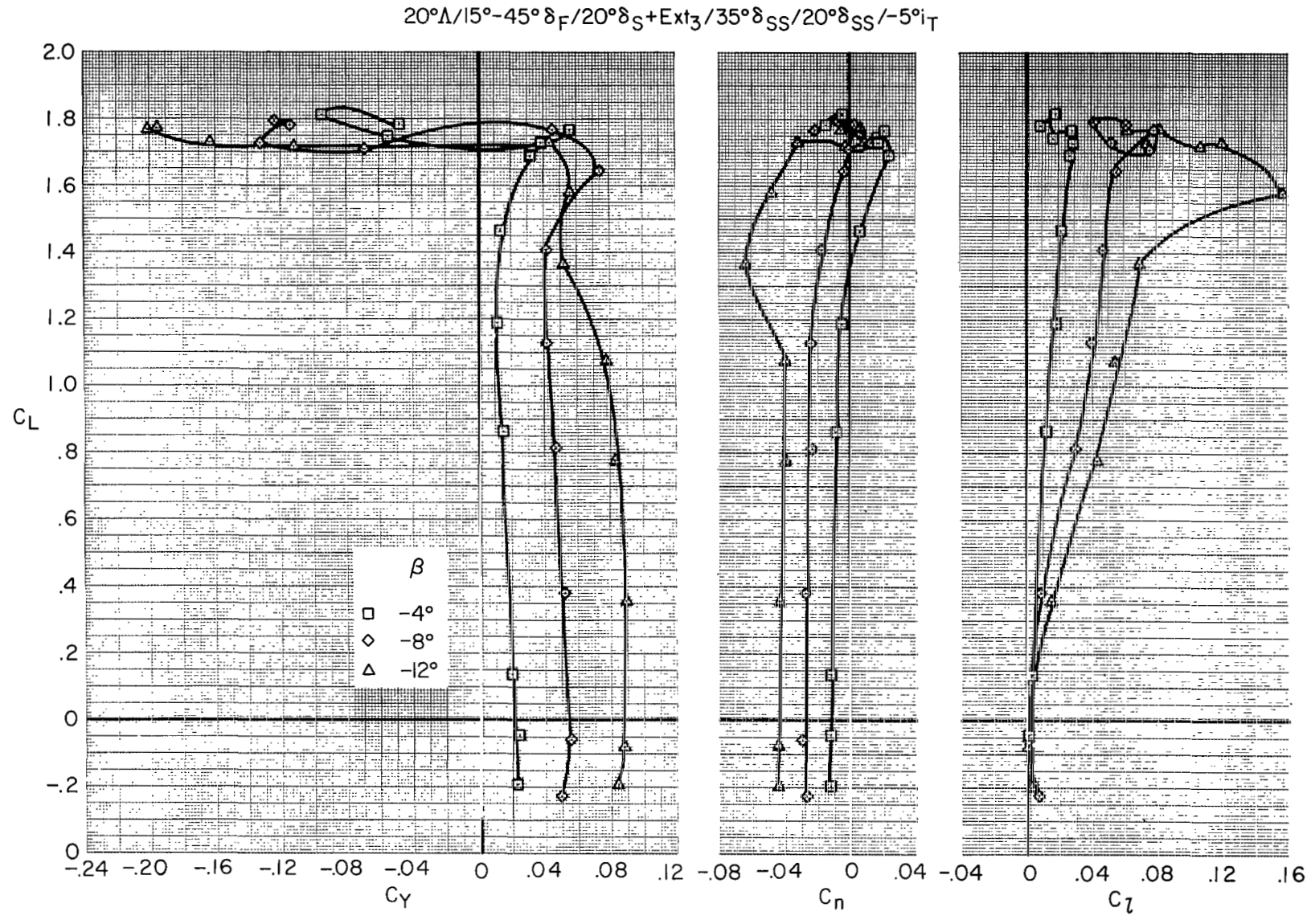

(c) Lateral-directional characteristics.

Figure 15.- Concluded.

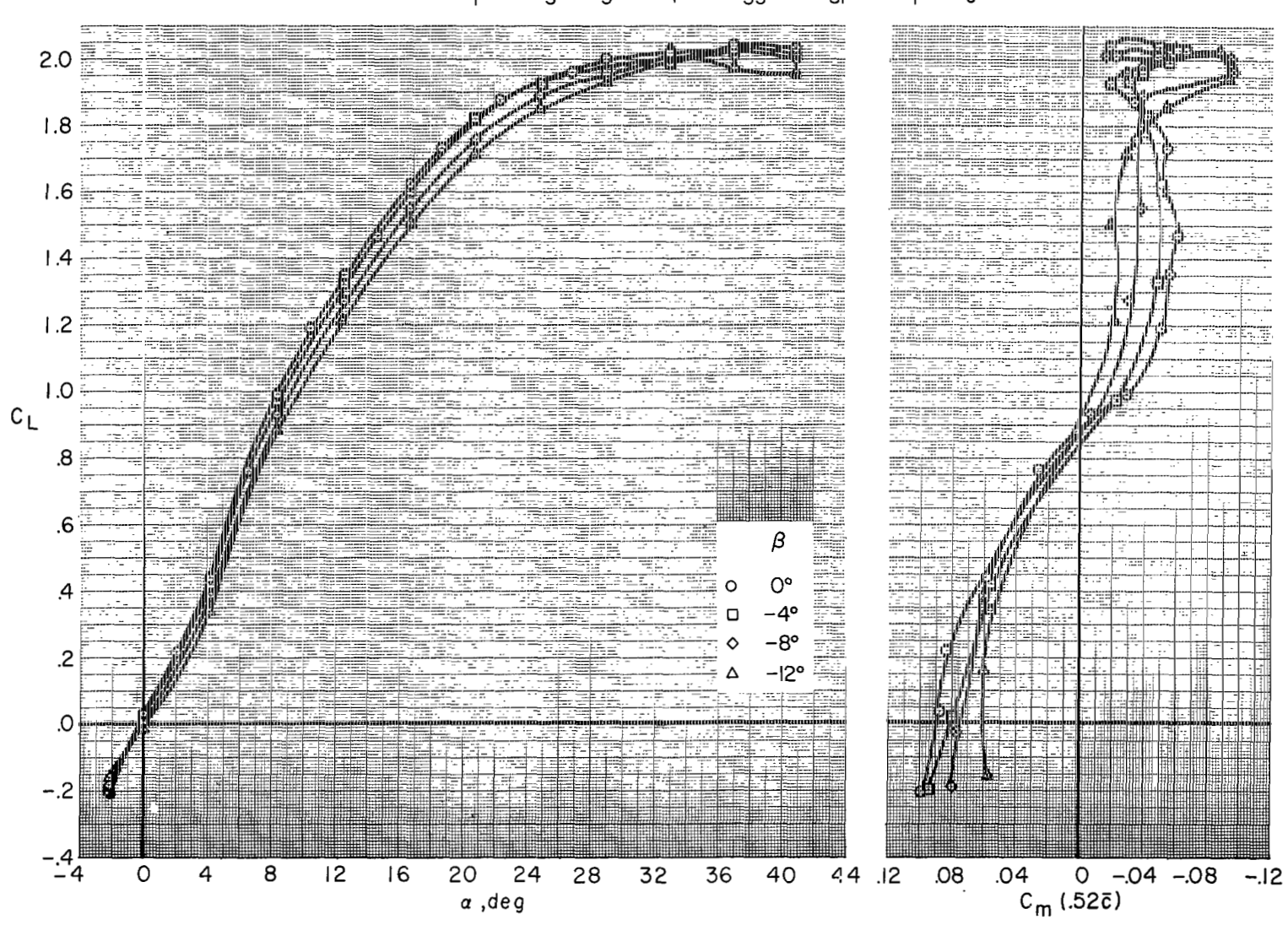

(a) Longitudinal characteristics, C_L vs. α and C_m.

Figure 16.- Characteristics of landing configuration in sideslip.

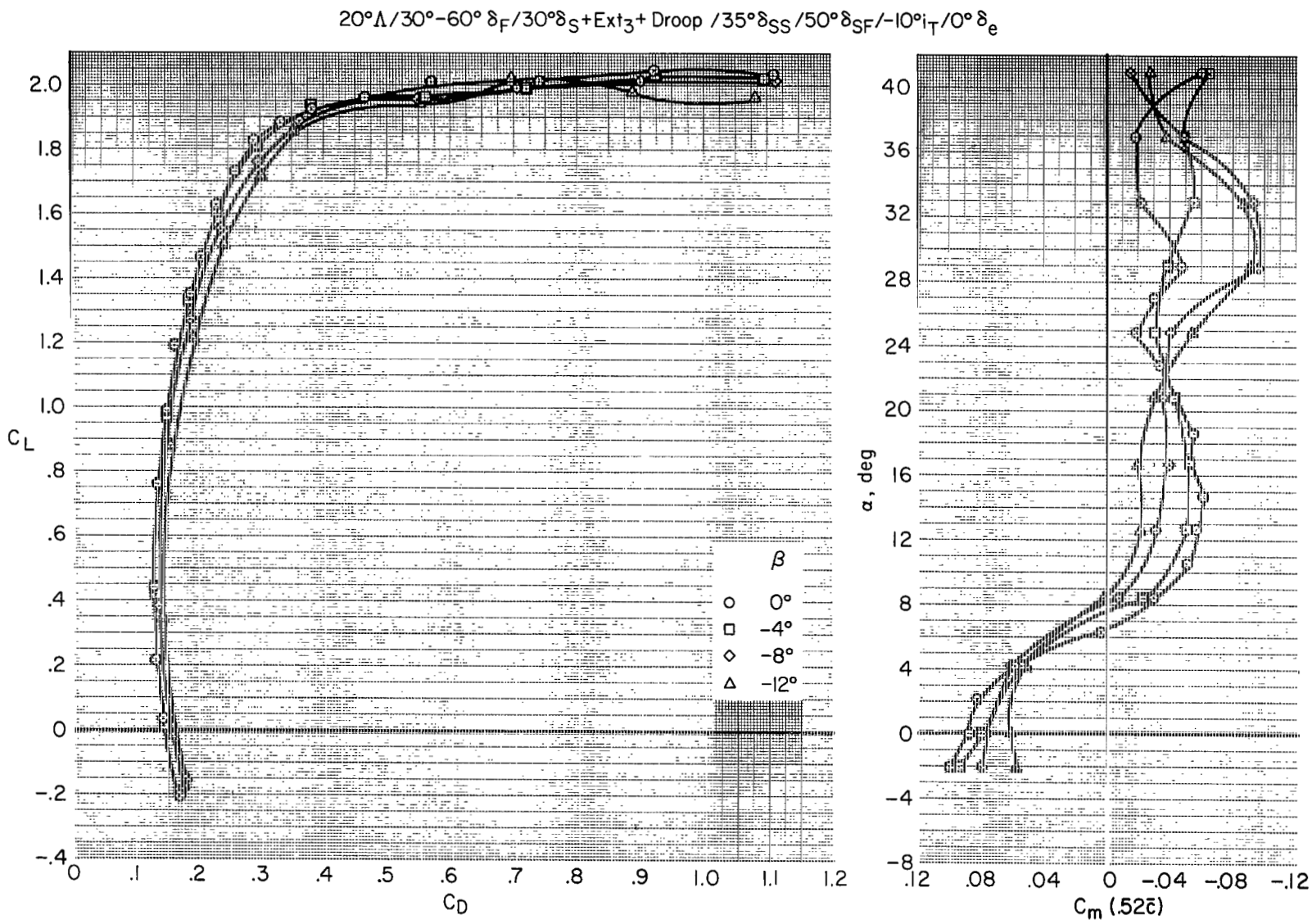

(b) Longitudinal characteristics; C_L vs. C_D, α vs. C_m.

Figure 16.- Continued.

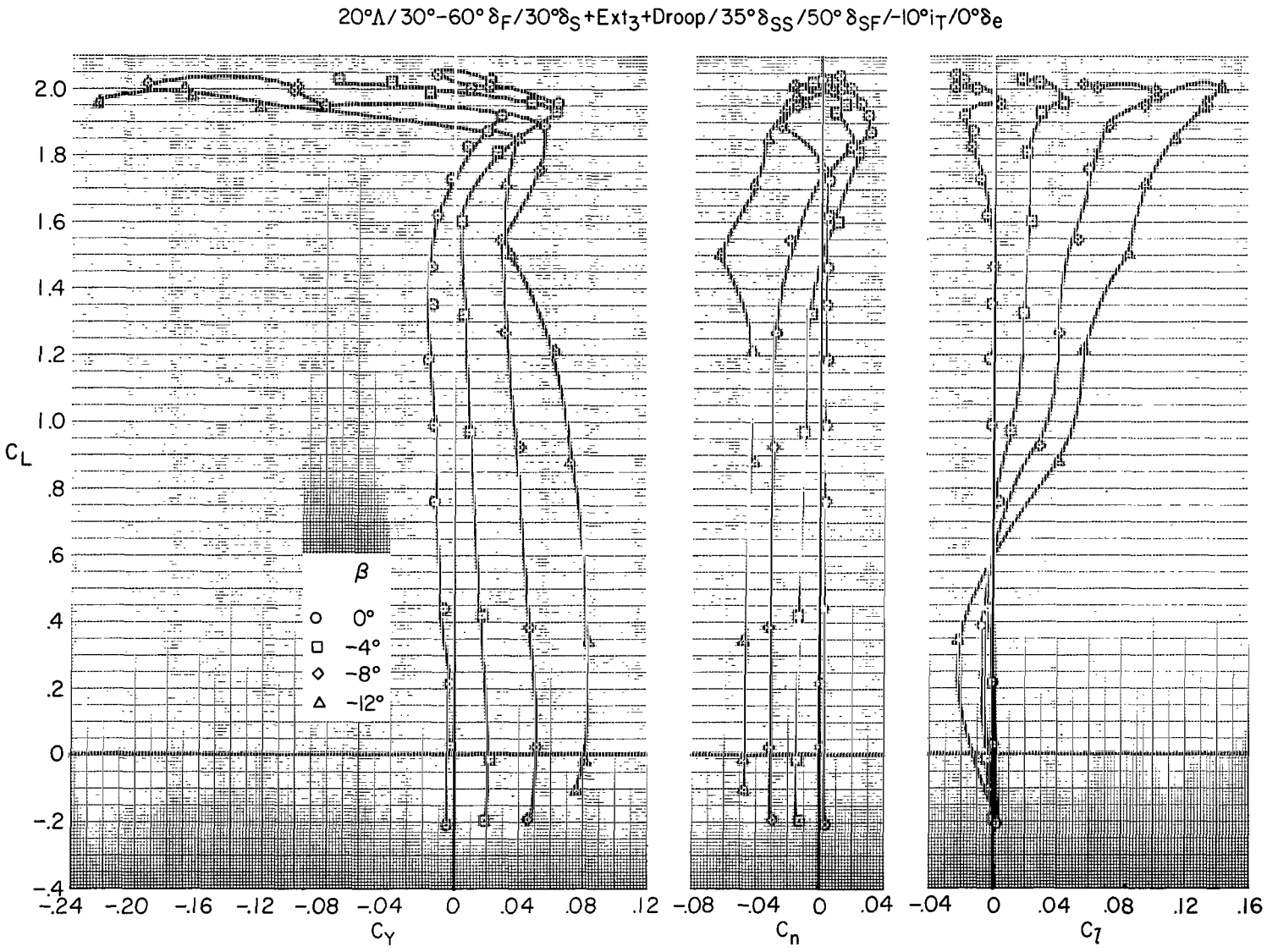

(c) Lateral-directional characteristics.

Figure 16.- Concluded.

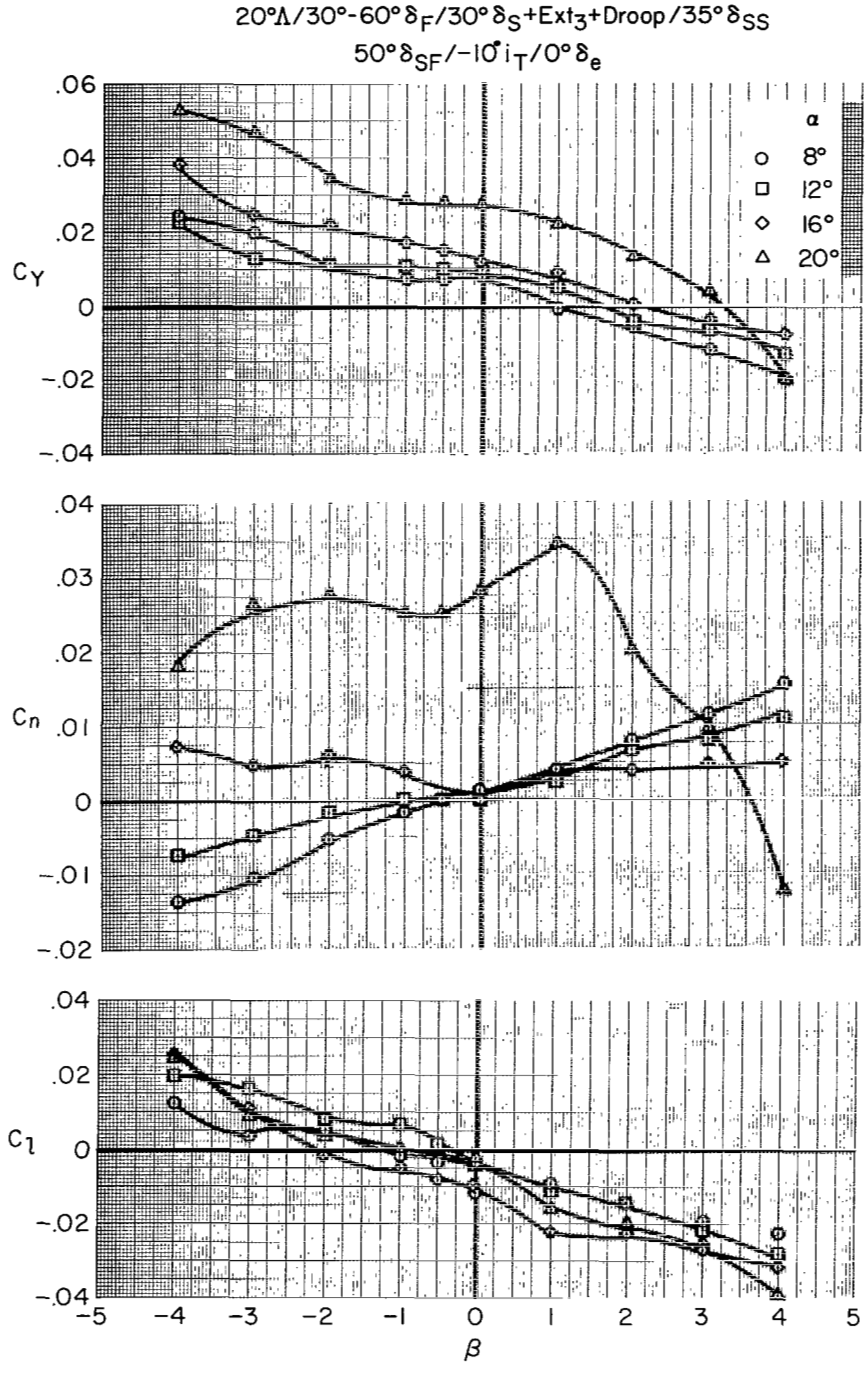

(a) $\delta_R = 0$

Figure 17.- Effects of rudder deflection and strake slats on the lateral-directional characteristics of the optimum landing configuration.

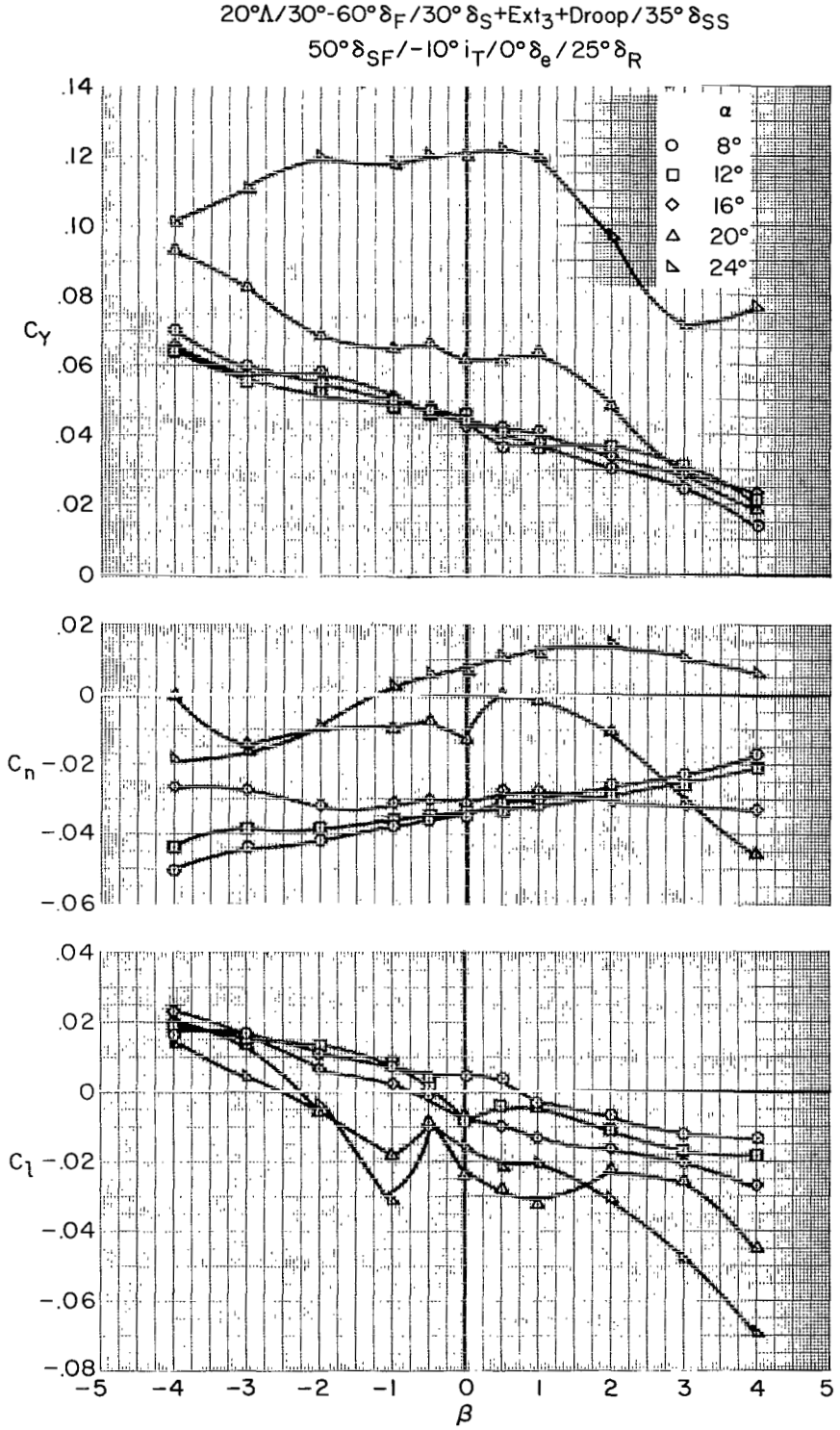

(b) $\delta_R = 25^\circ$

Figure 17.- Continued.

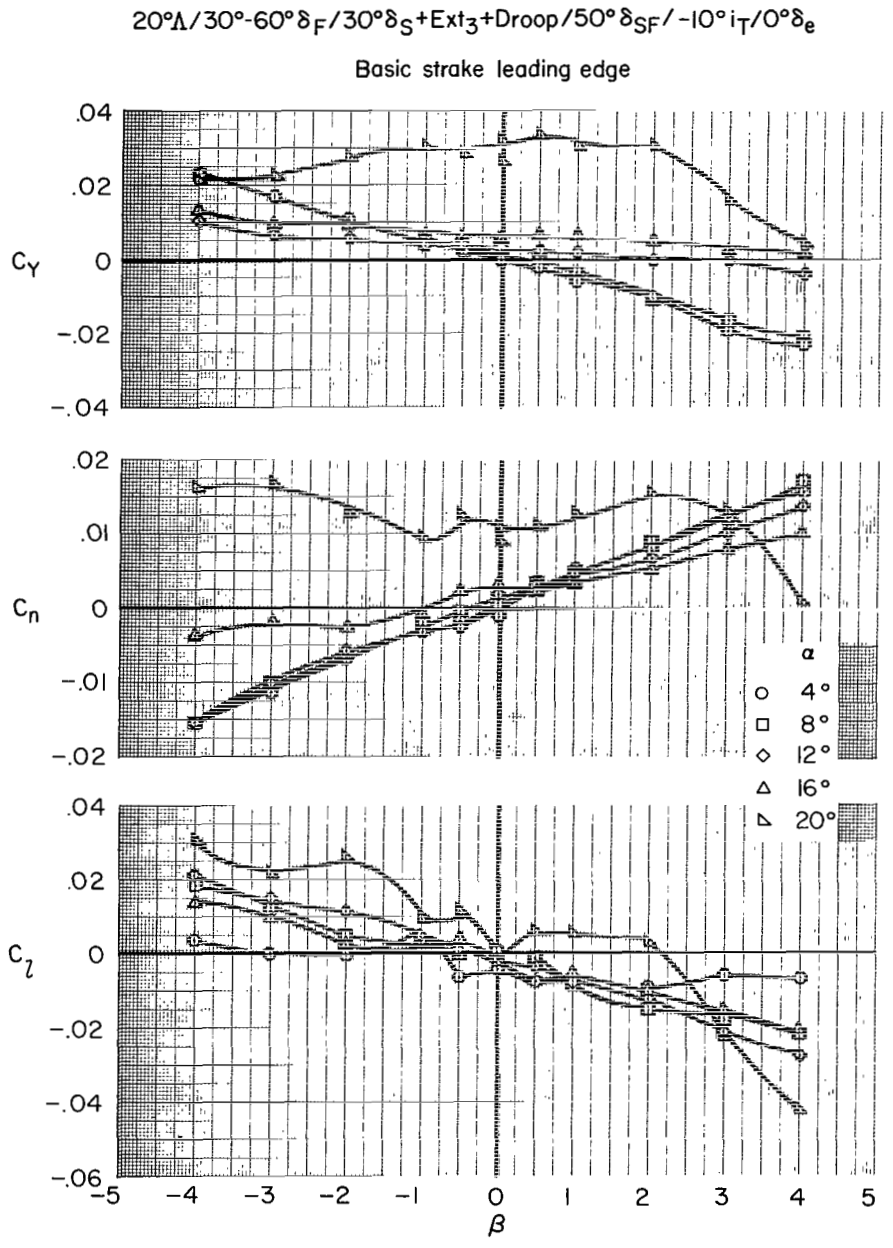

(c) Strake leading-edge slat removed, $\delta_R = 0$.

Figure 17.- Concluded.

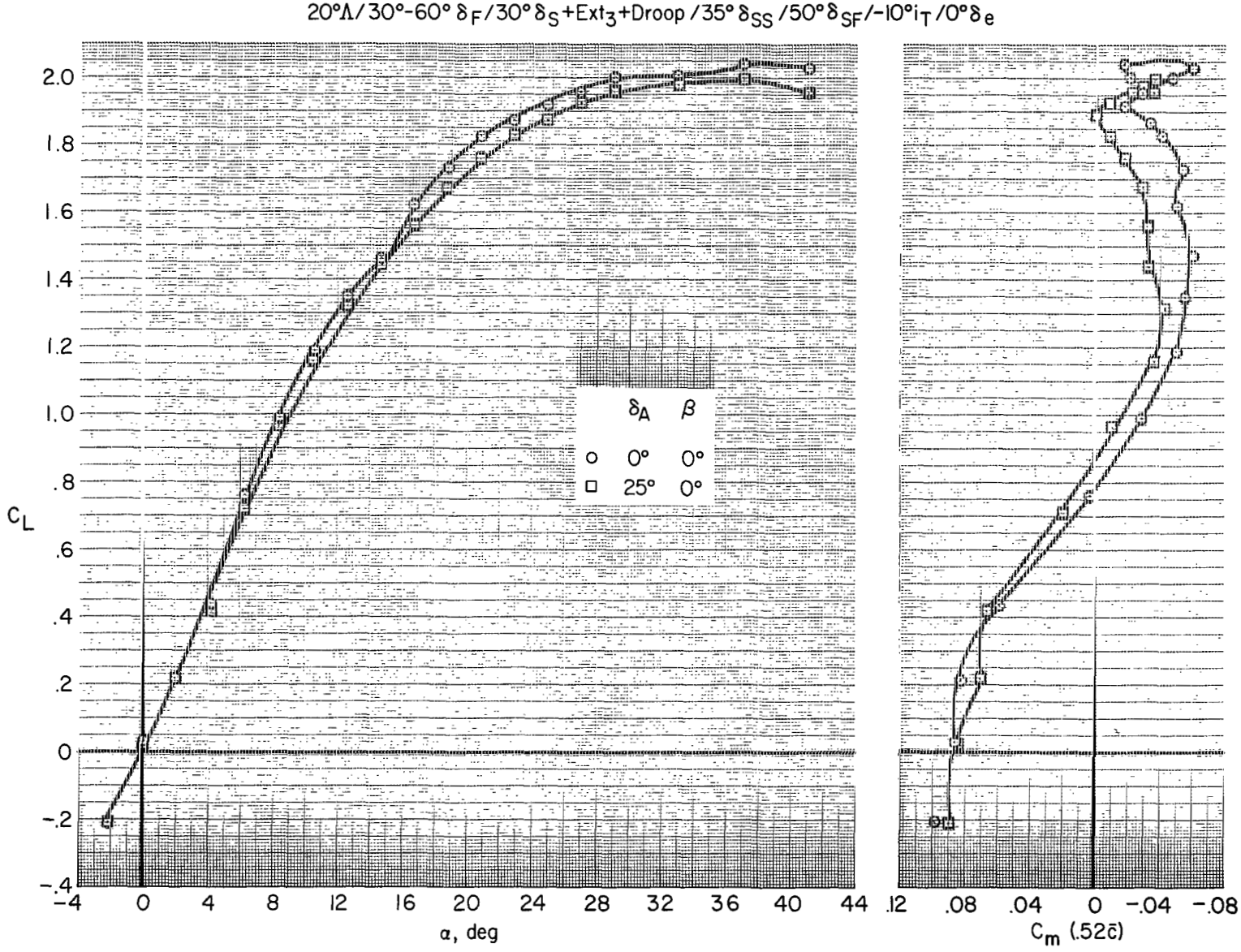

(a) Longitudinal characteristics, C_L vs. α and C_m.

Figure 18.- Effects of aileron deflection; landing configuration.

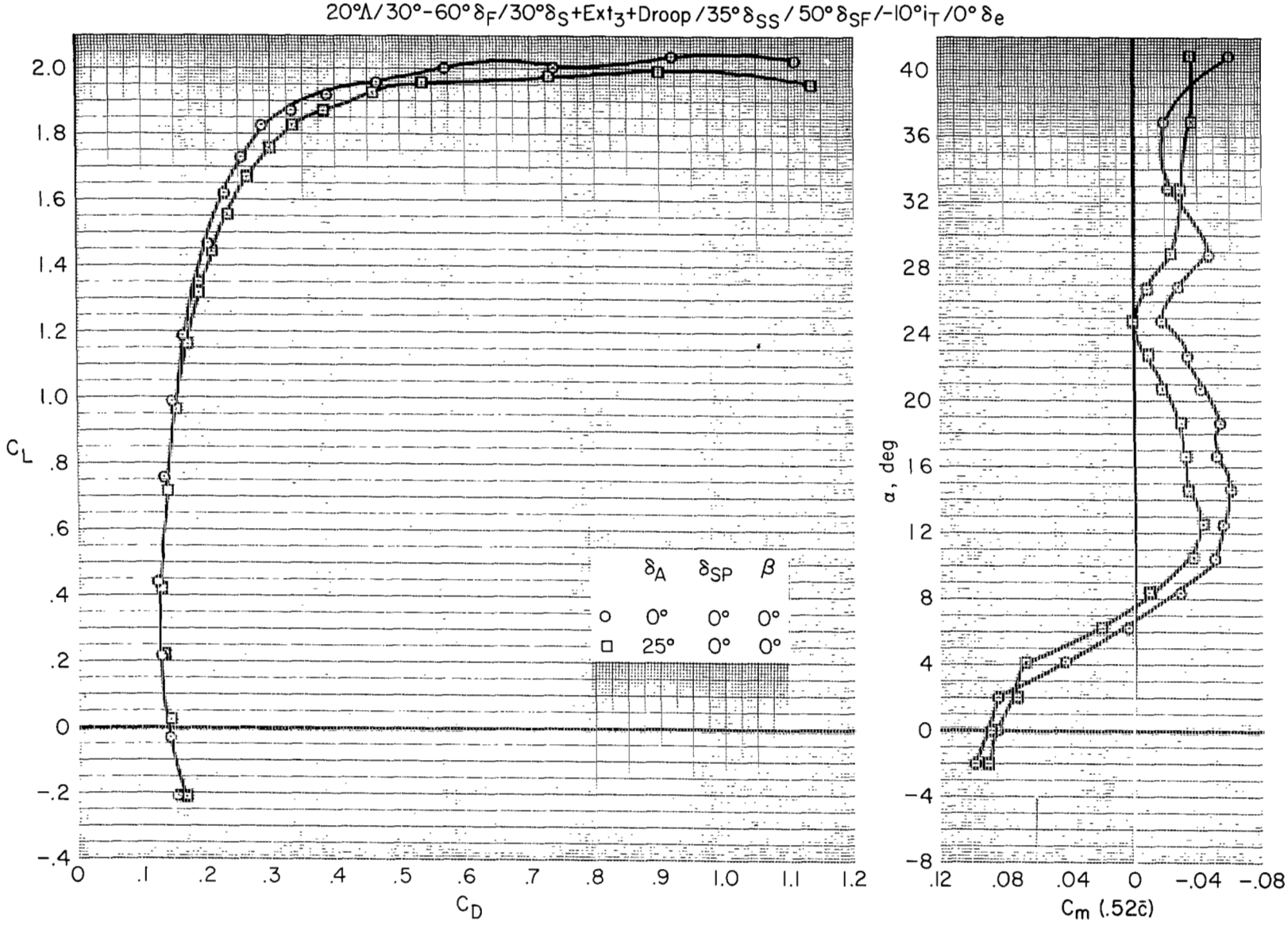

(b) Longitudinal characteristics; C_L vs. C_D, α vs. C_m.

Figure 18.- Continued.

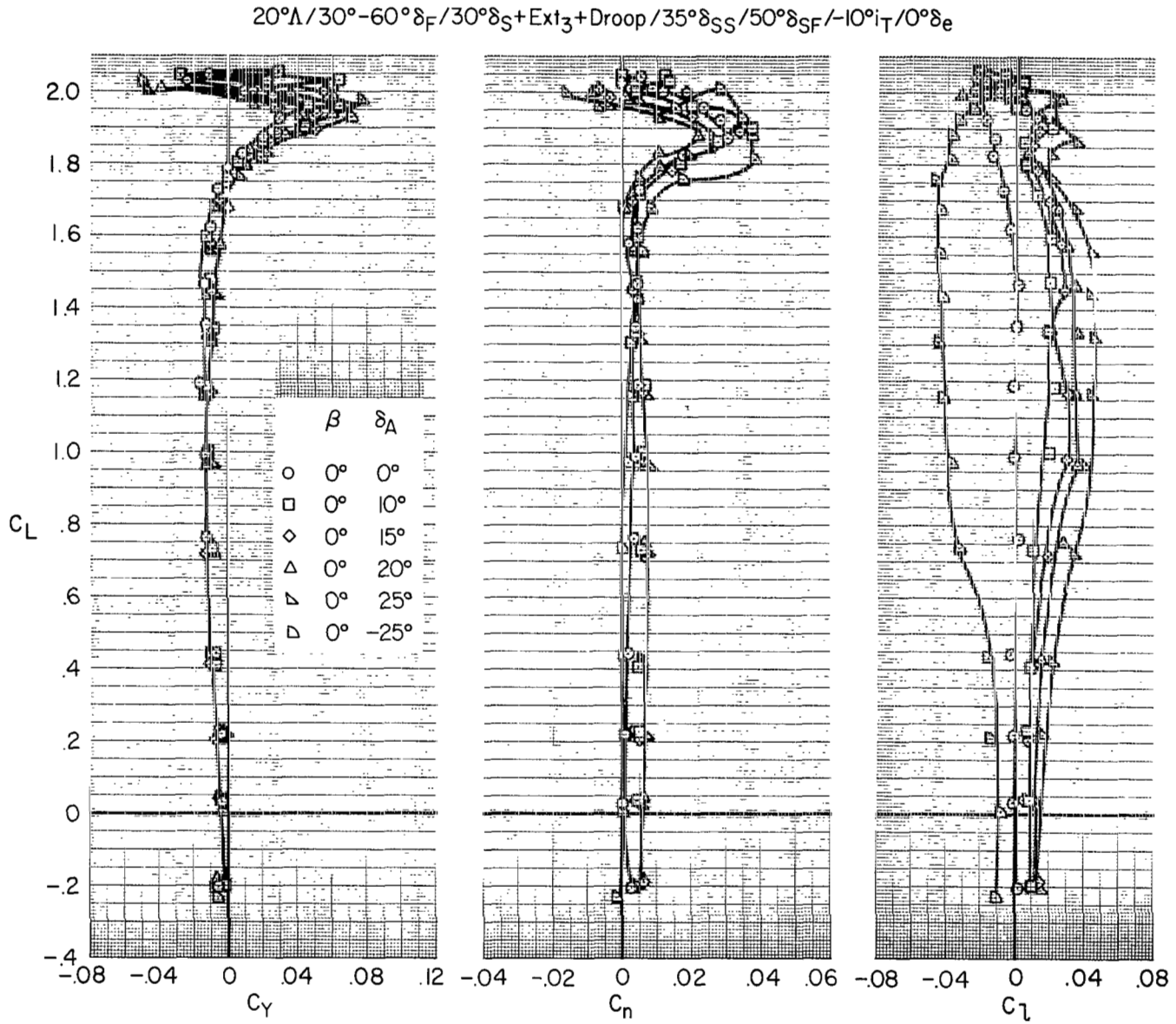

(c) Lateral-directional characteristics at zero sideslip.

Figure 18.- Continued.

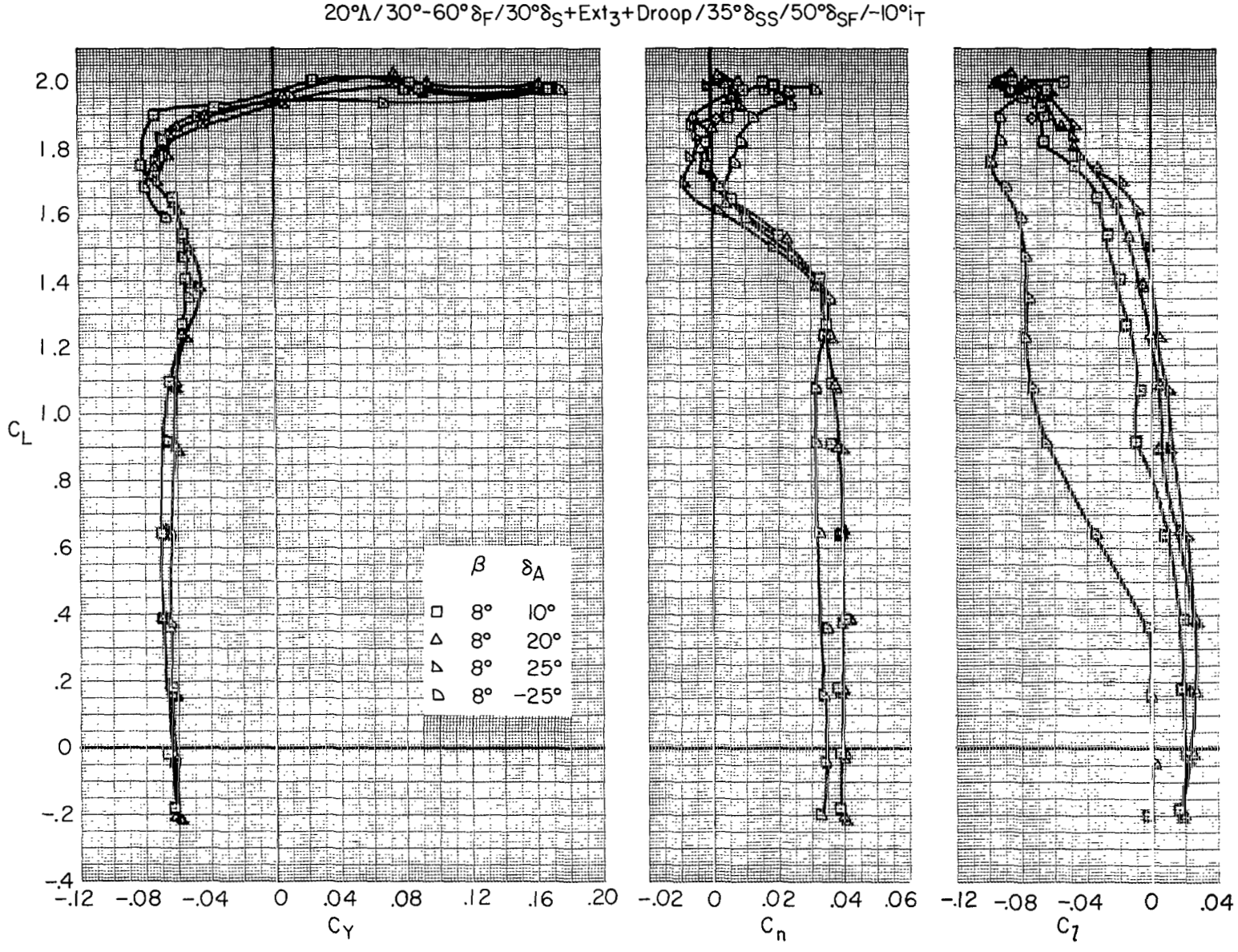

(d) Lateral-directional characteristics at 8° sideslip.

Figure 18.- Concluded.

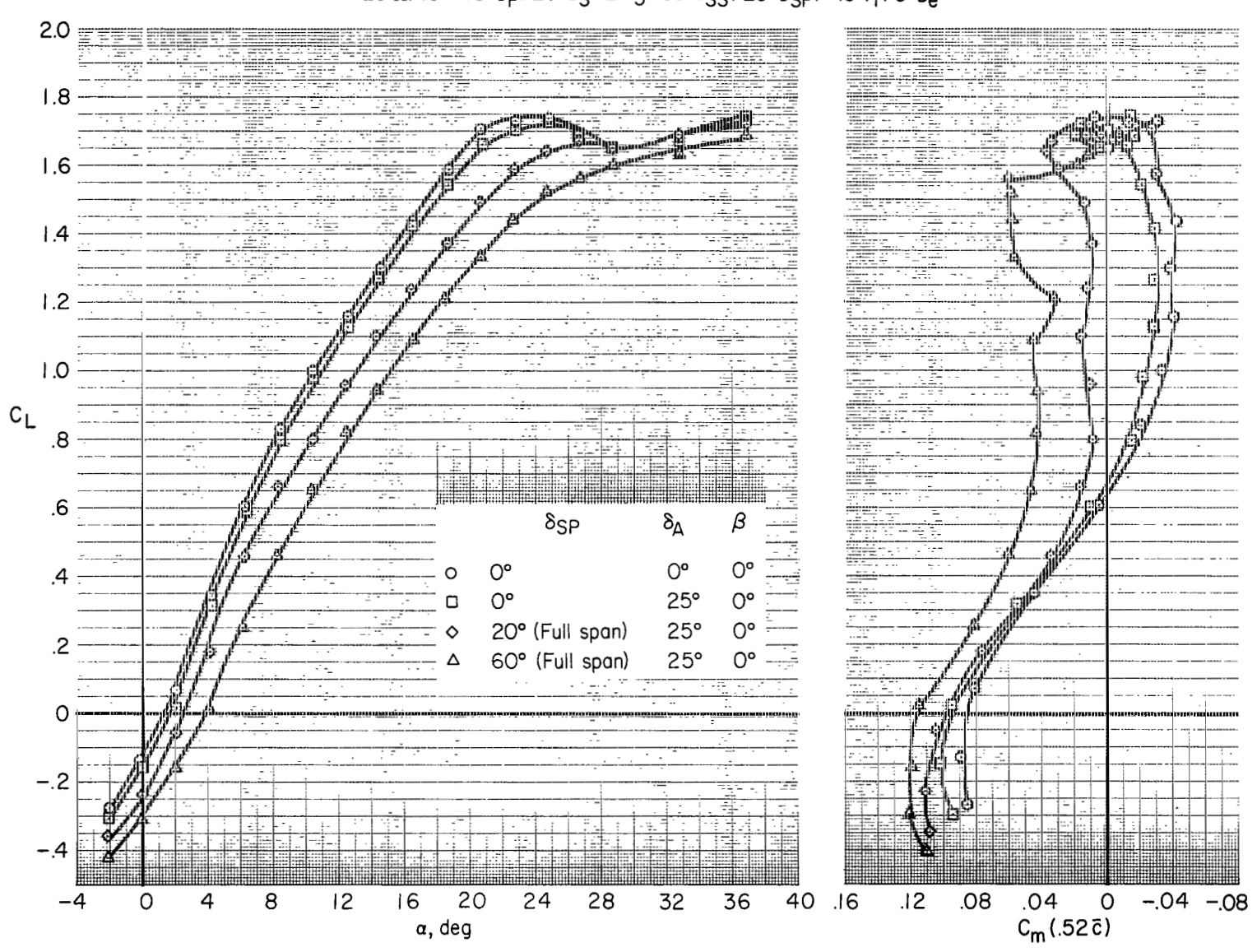

(a) Longitudinal characteristics, C_L vs. α and C_m.

Figure 19.- Effect of spoilers for lateral control, take-off configuration zero sideslip.

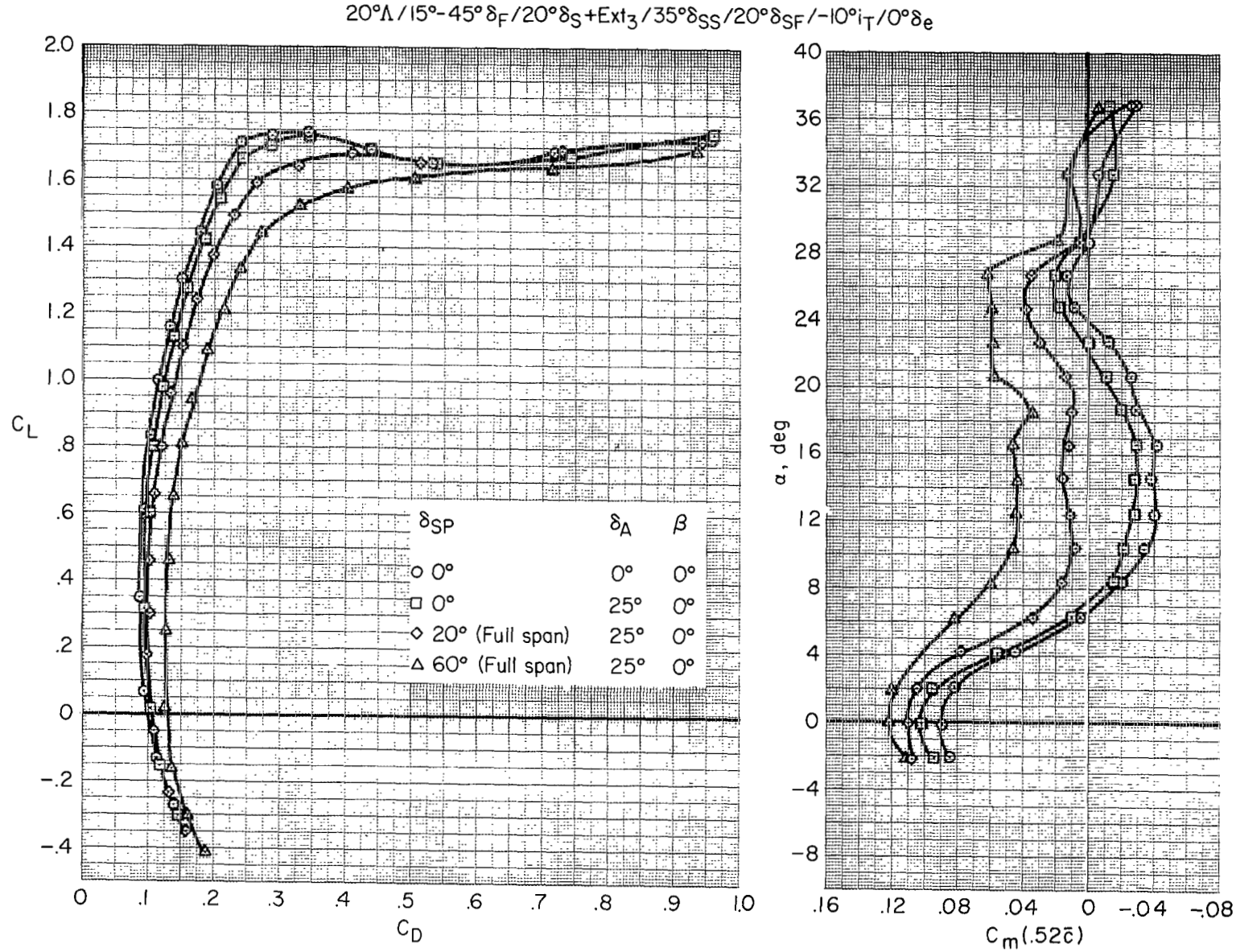

(b) Longitudinal characteristics; C_L vs. C_D, α vs. C_m.

Figure 19.- Continued.

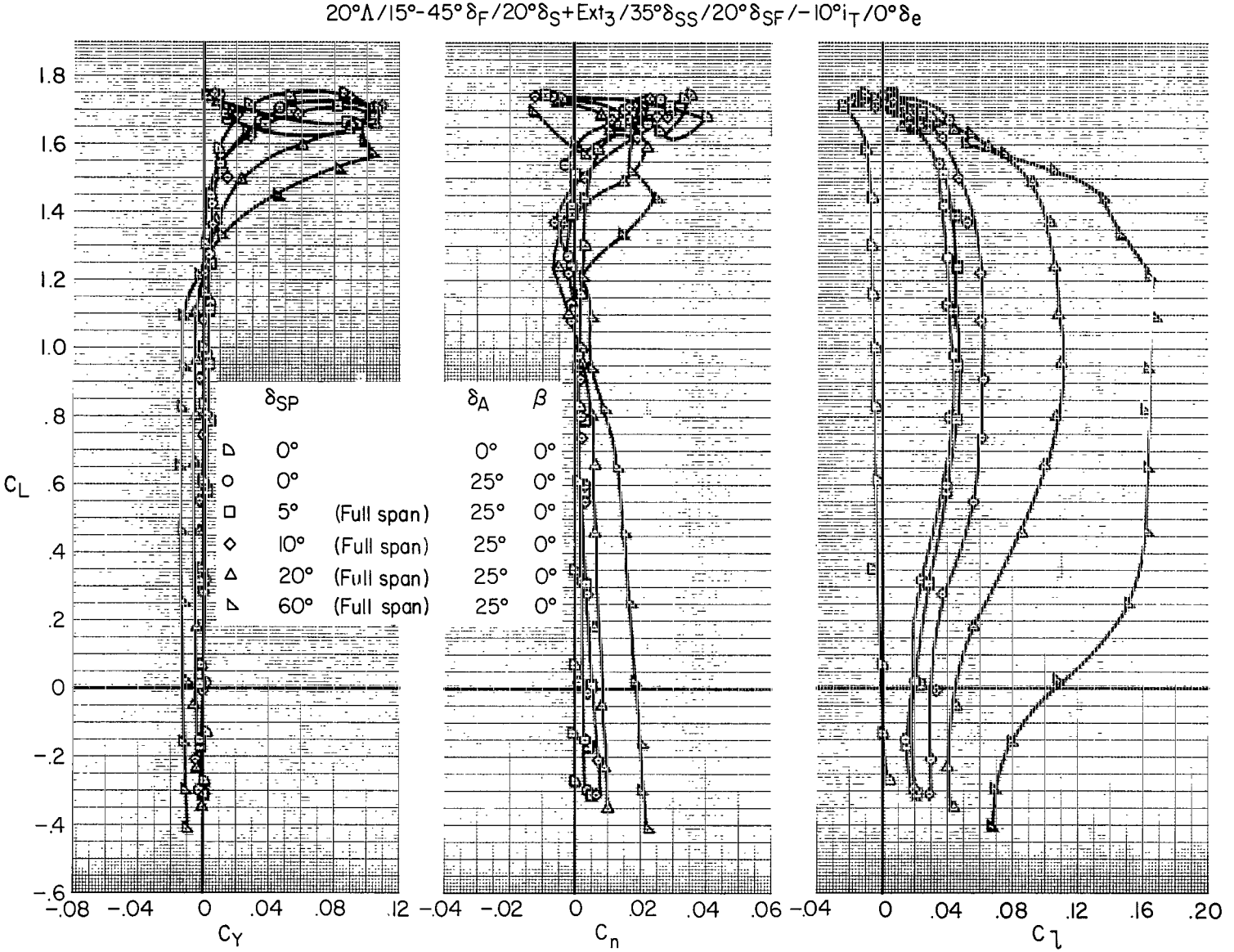

(c) Lateral-directional characteristics.

Figure 19.- Concluded.

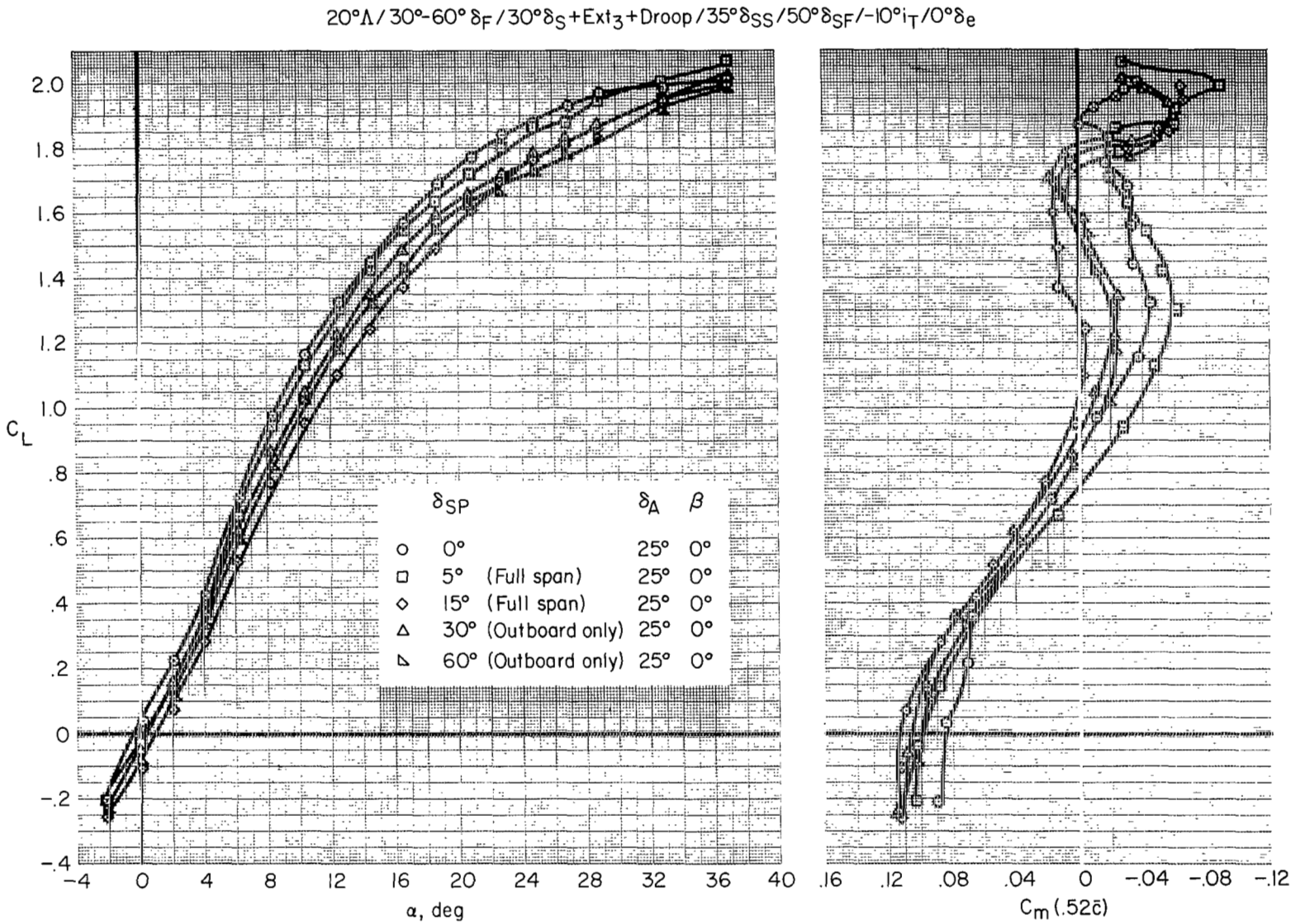

(a) Longitudinal characteristics, C_L vs. α and C_m.

Figure 20.- Effects of spoiler deflection, with 25° positive aileron, zero sideslip, landing configuration.

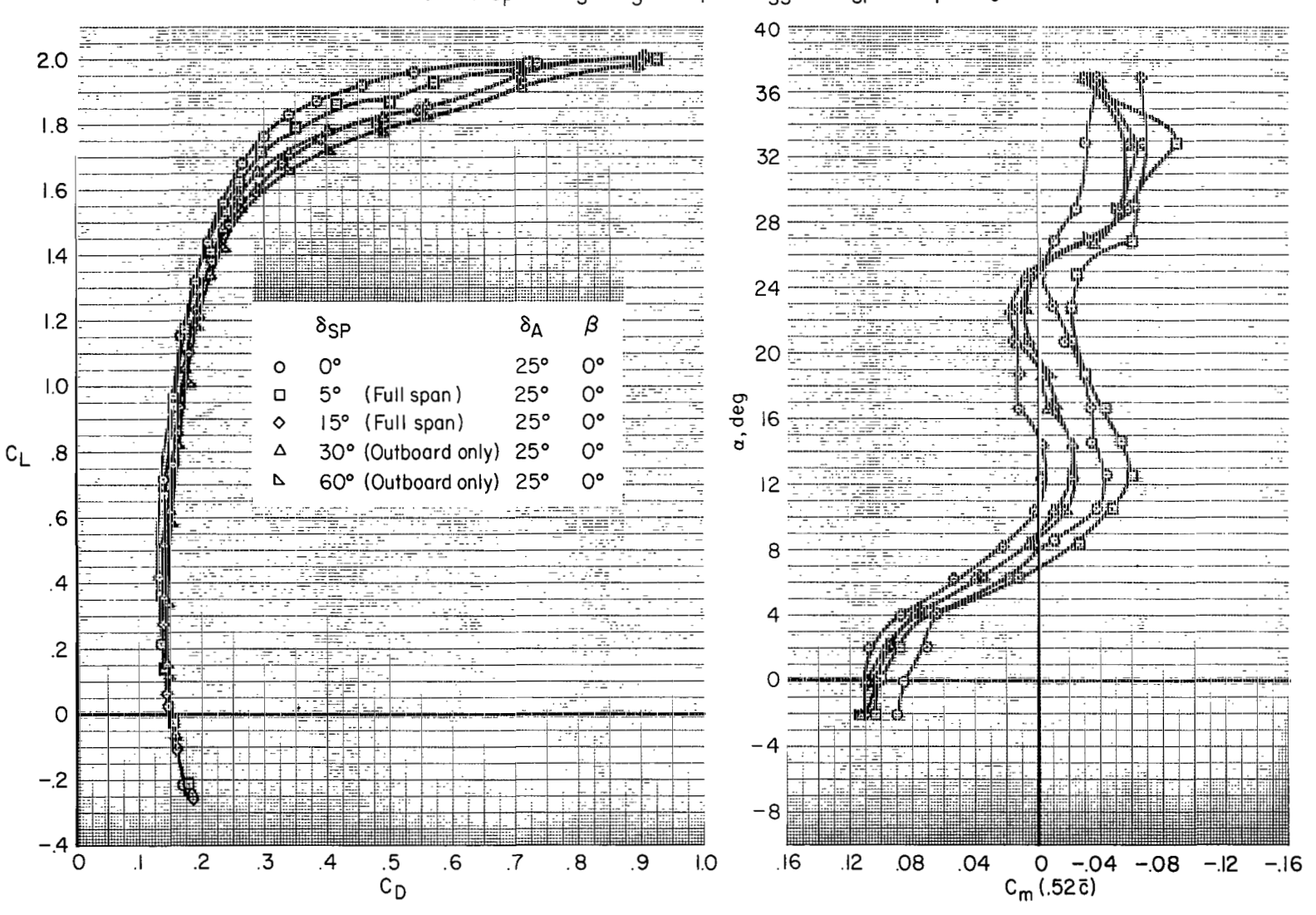

(b) Longitudinal characteristics; C_L vs. C_D, α vs. C_m.

Figure 20.- Continued.

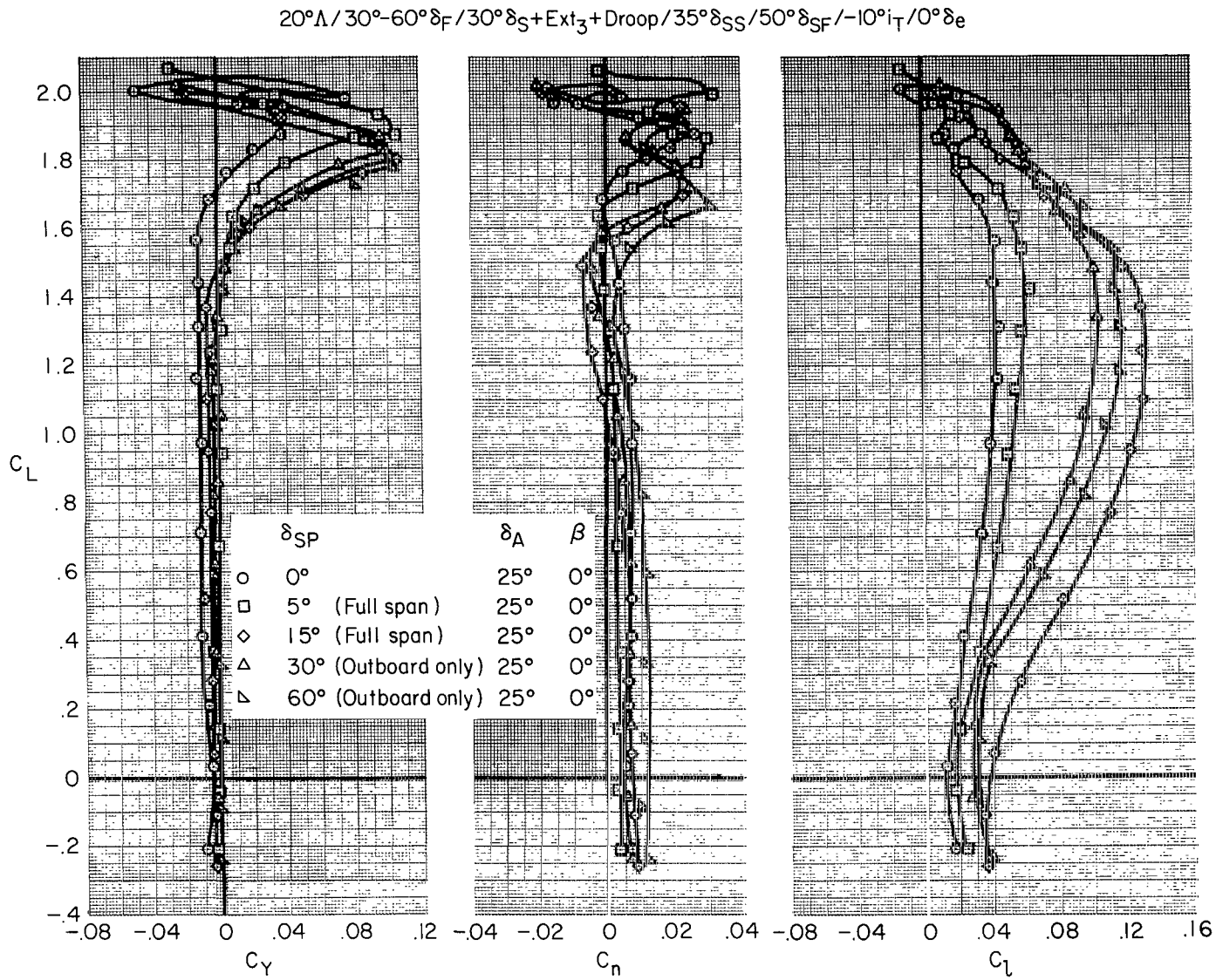

(c) Lateral-directional characteristics showing effect of outboard spoiler panel.

Figure 20.- Continued.

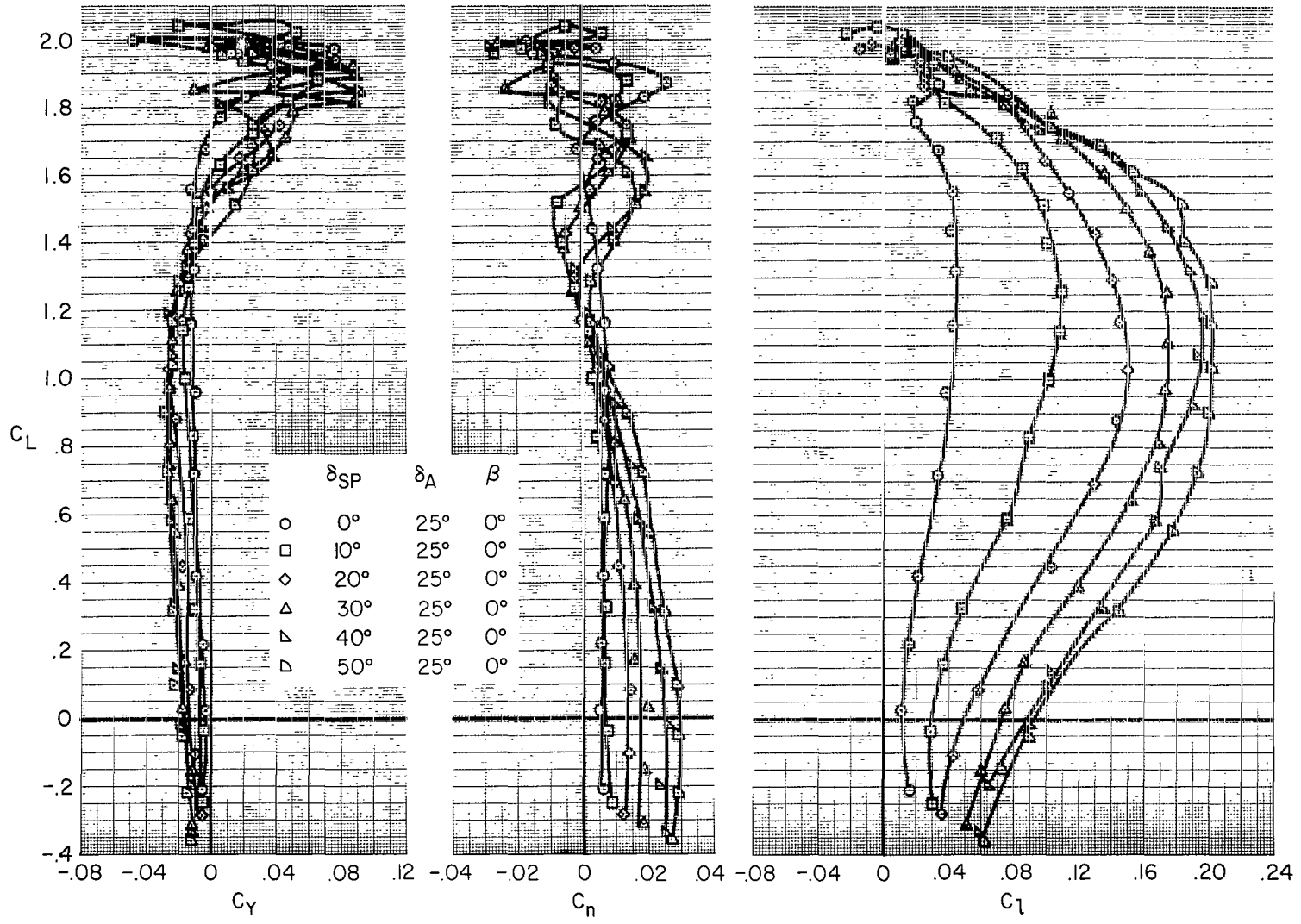

(d) Lateral-directional characteristics of full-span spoiler deflection.

Figure 20.- Concluded.

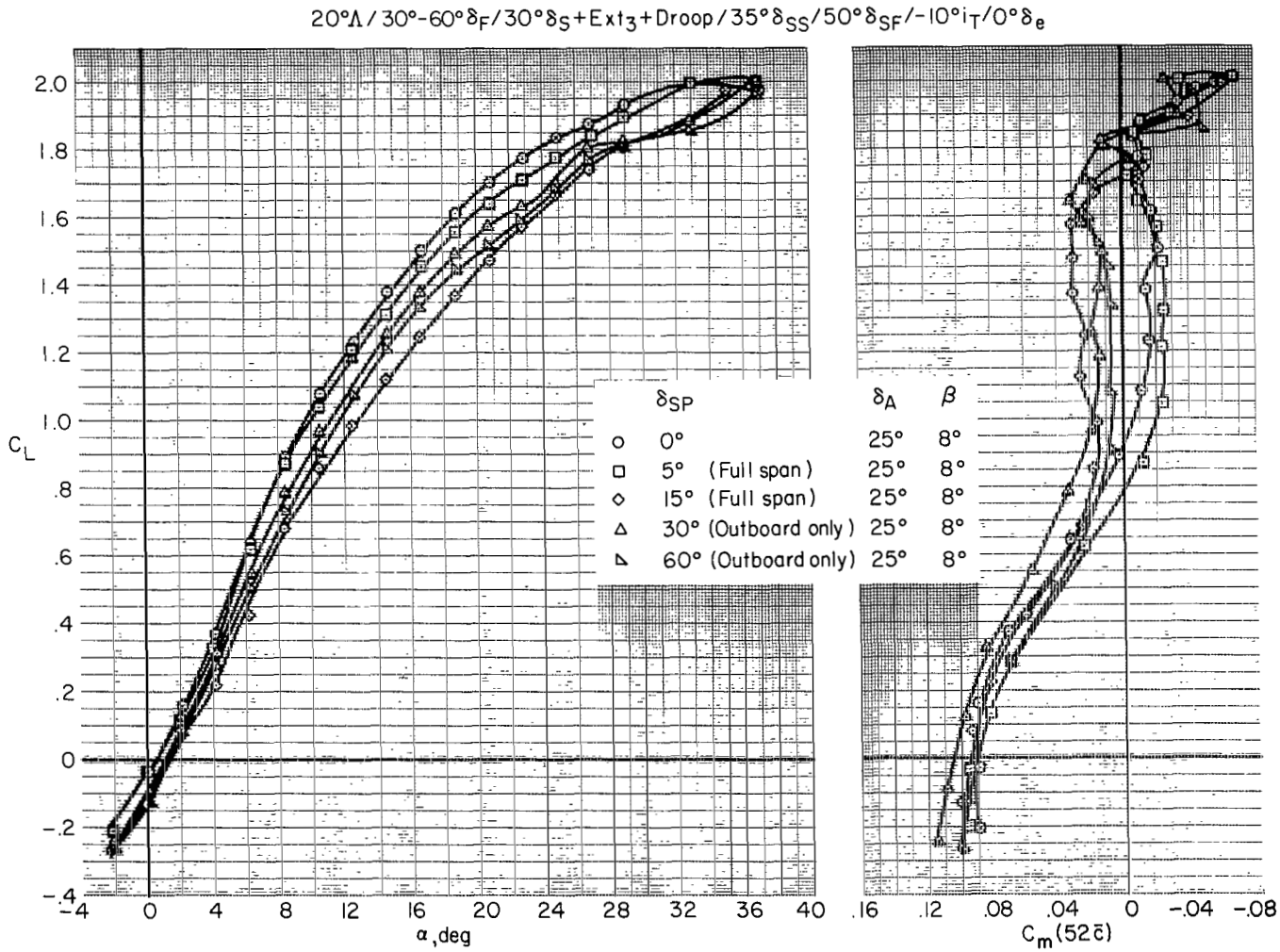

(a) Longitudinal characteristics, C_L vs. α and C_m.

Figure 21.- Effects of spoiler deflection, with 25° positive aileron, 8° sideslip, landing configuration.

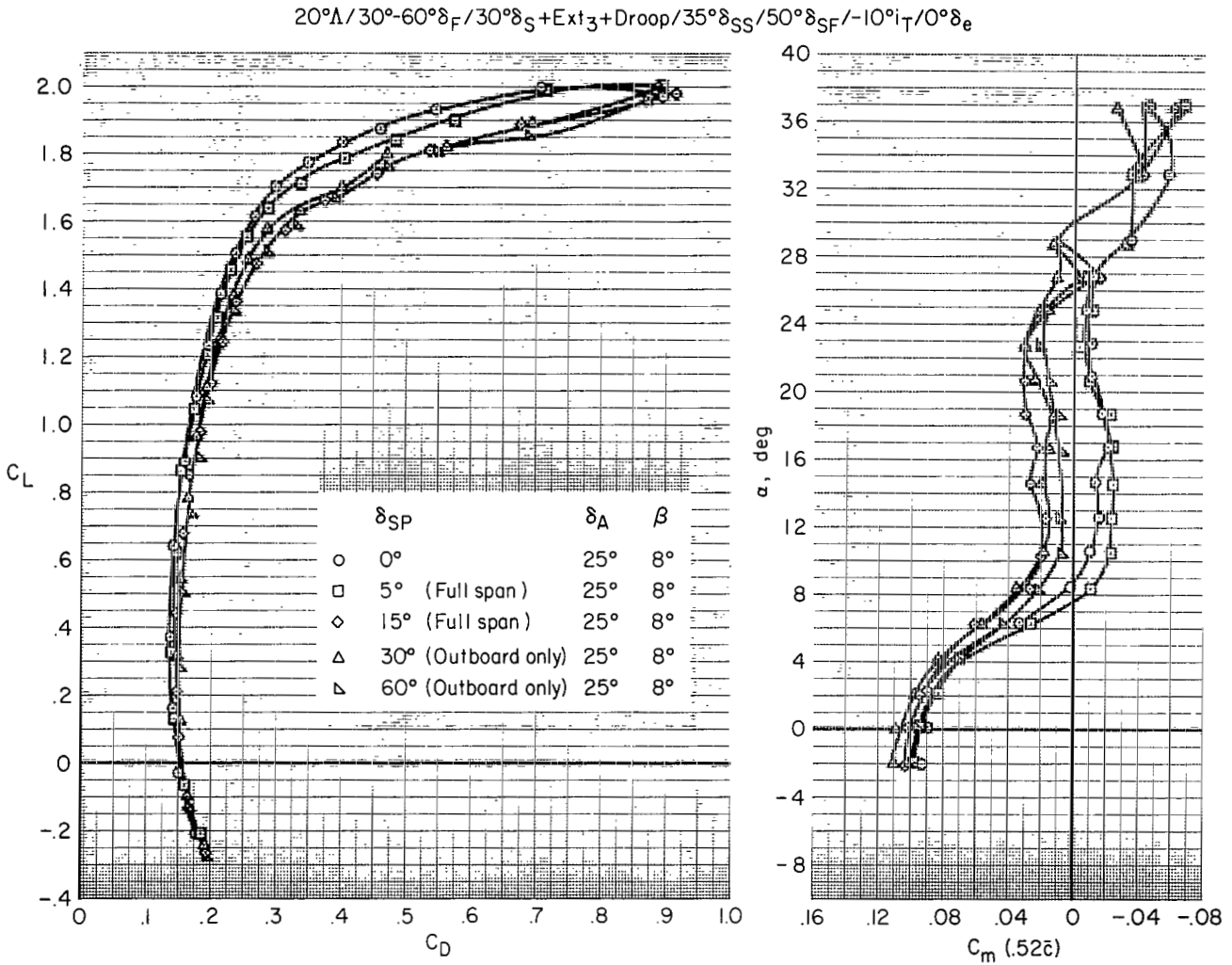

(b) Longitudinal characteristics; C_L vs. C_D, α vs. C_m.

Figure 21.- Continued.

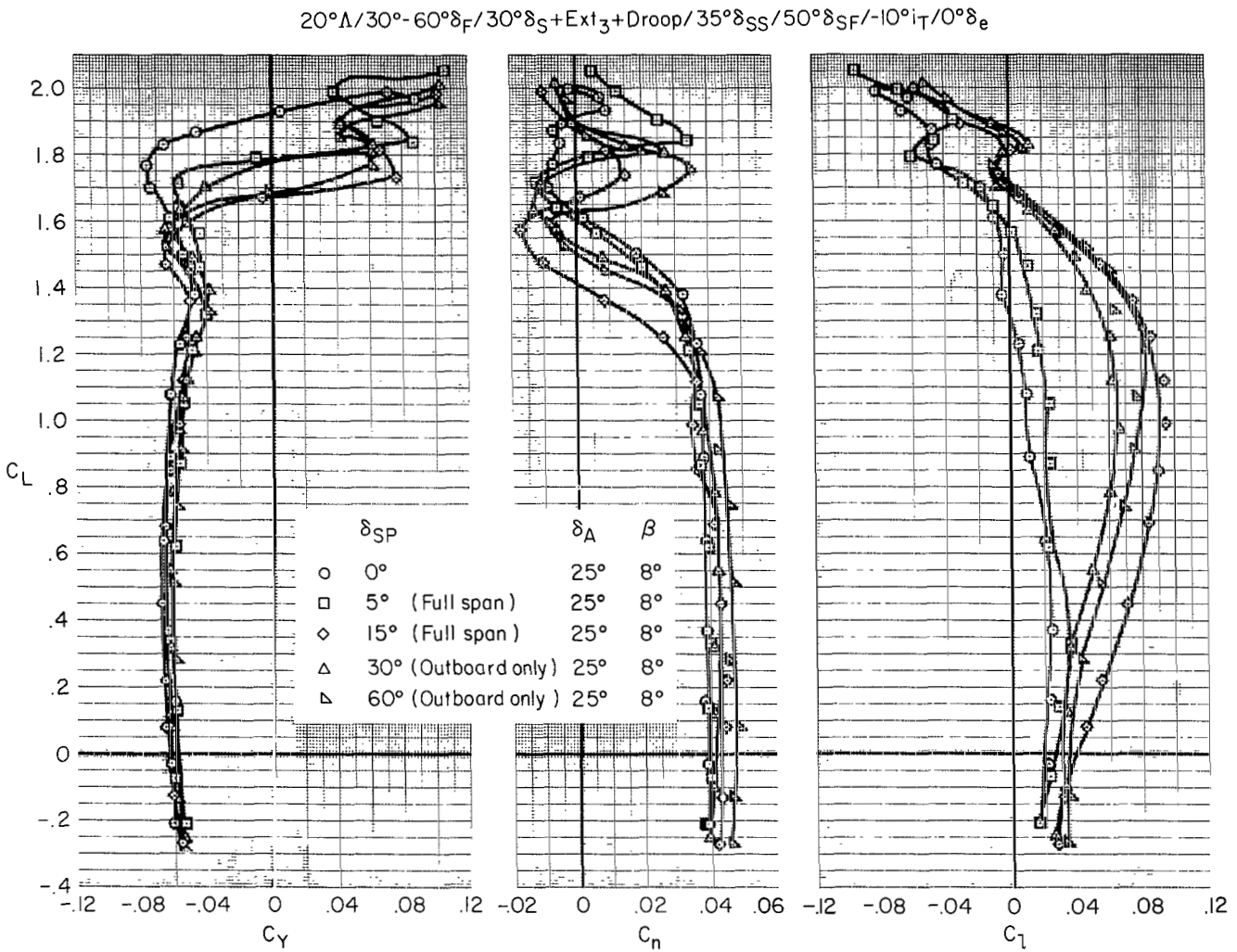

(c) Lateral-directional characteristics showing effect of outboard spoiler.

Figure 21.- Continued.

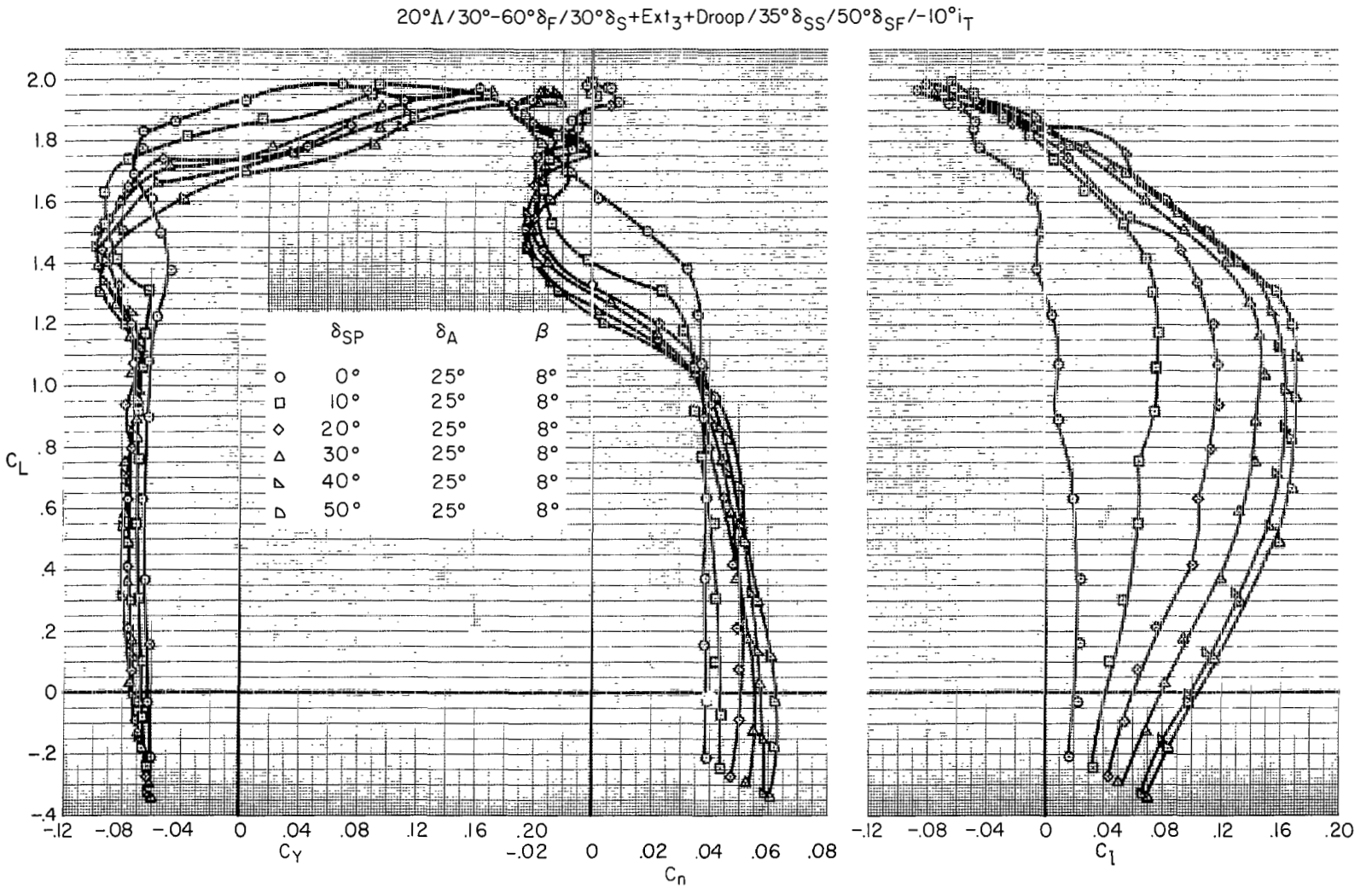

(d) Lateral-directional characteristics of full-span spoiler deflection.

Figure 21.- Concluded.

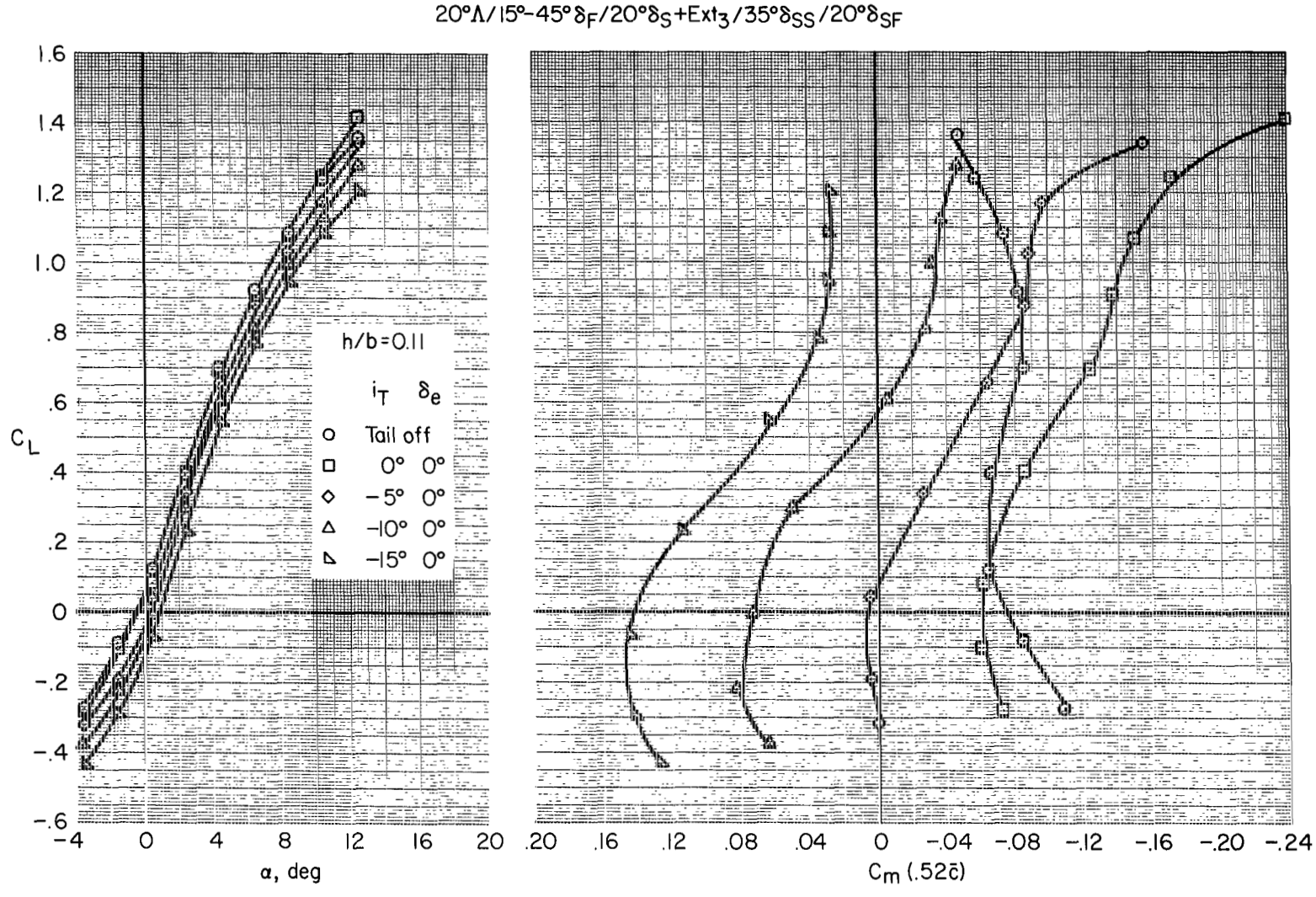

(a) Horizontal-tail incidence, C_L vs. α and C_m.

Figure 22.- Longitudinal characteristics, in ground effect, of horizontal-tail incidence and elevator deflection; take-off configuration.

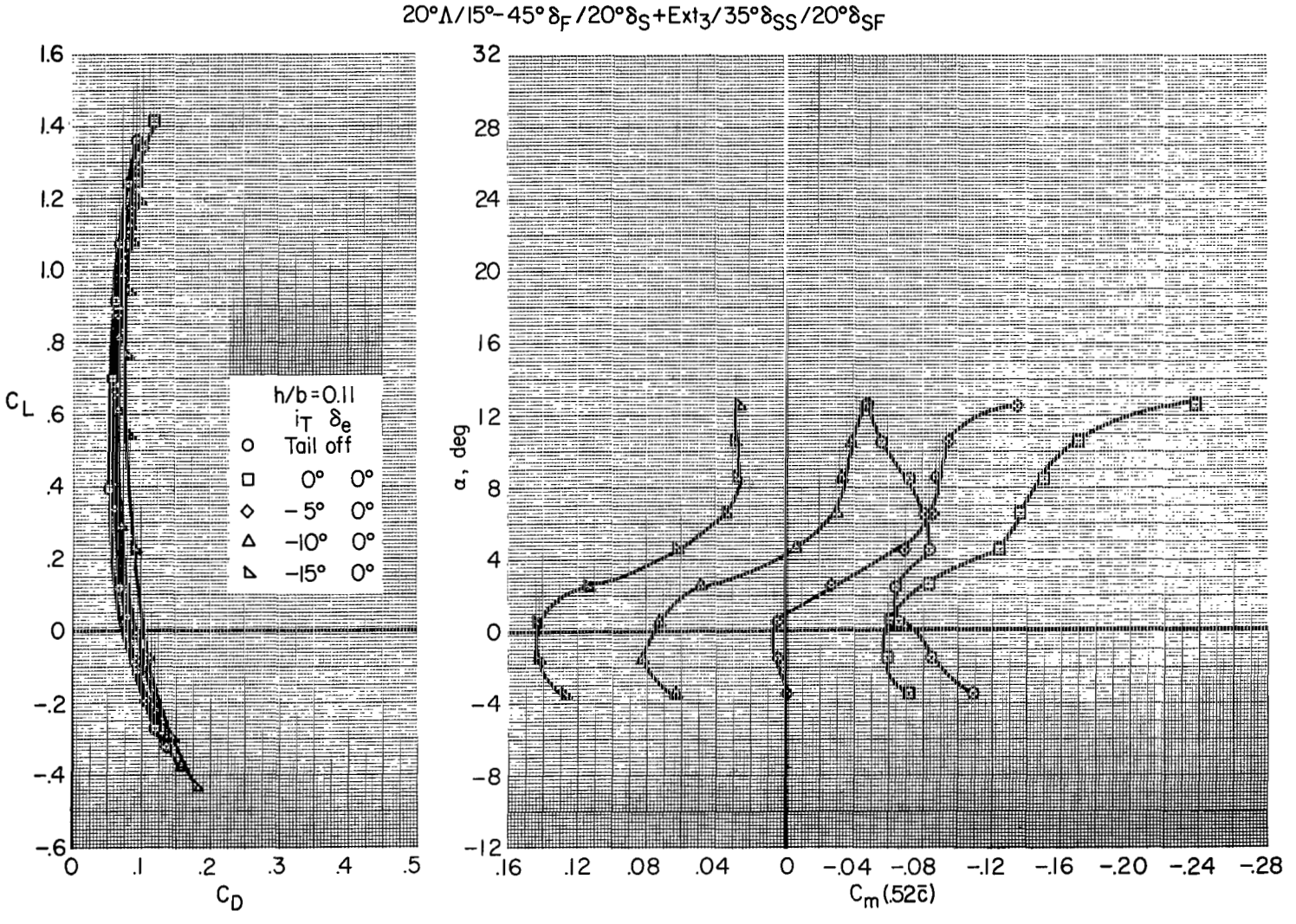

(b) Horizontal-tail incidence; C_L vs. C_D, α vs. C_m.

Figure 22.- Continued.

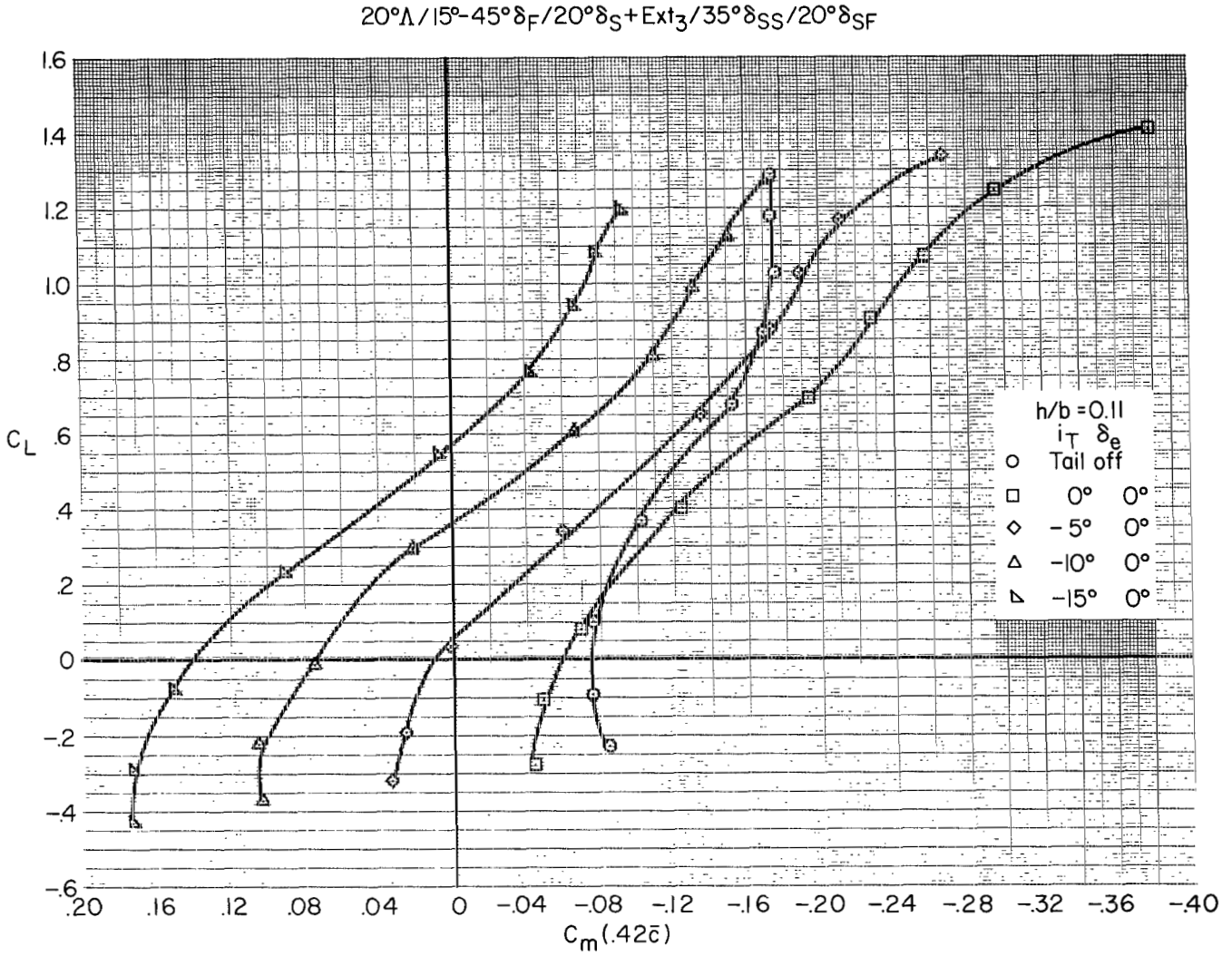

(c) Horizontal-tail incidence, forward moment center location, C_L vs. C_m.

Figure 22.- Continued.

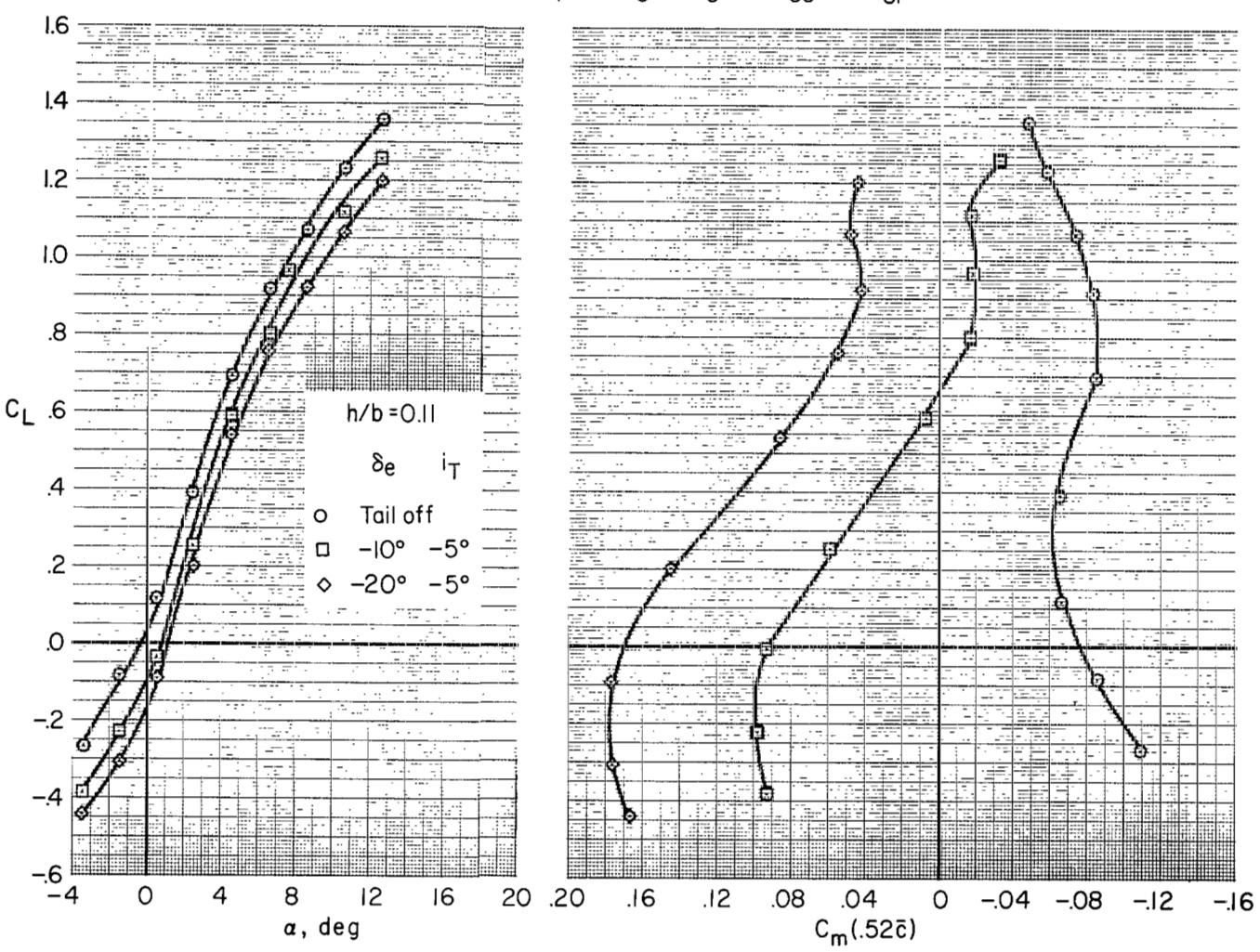

(d) Elevator deflection, C_L vs. α and C_m.

Figure 22.- Continued.

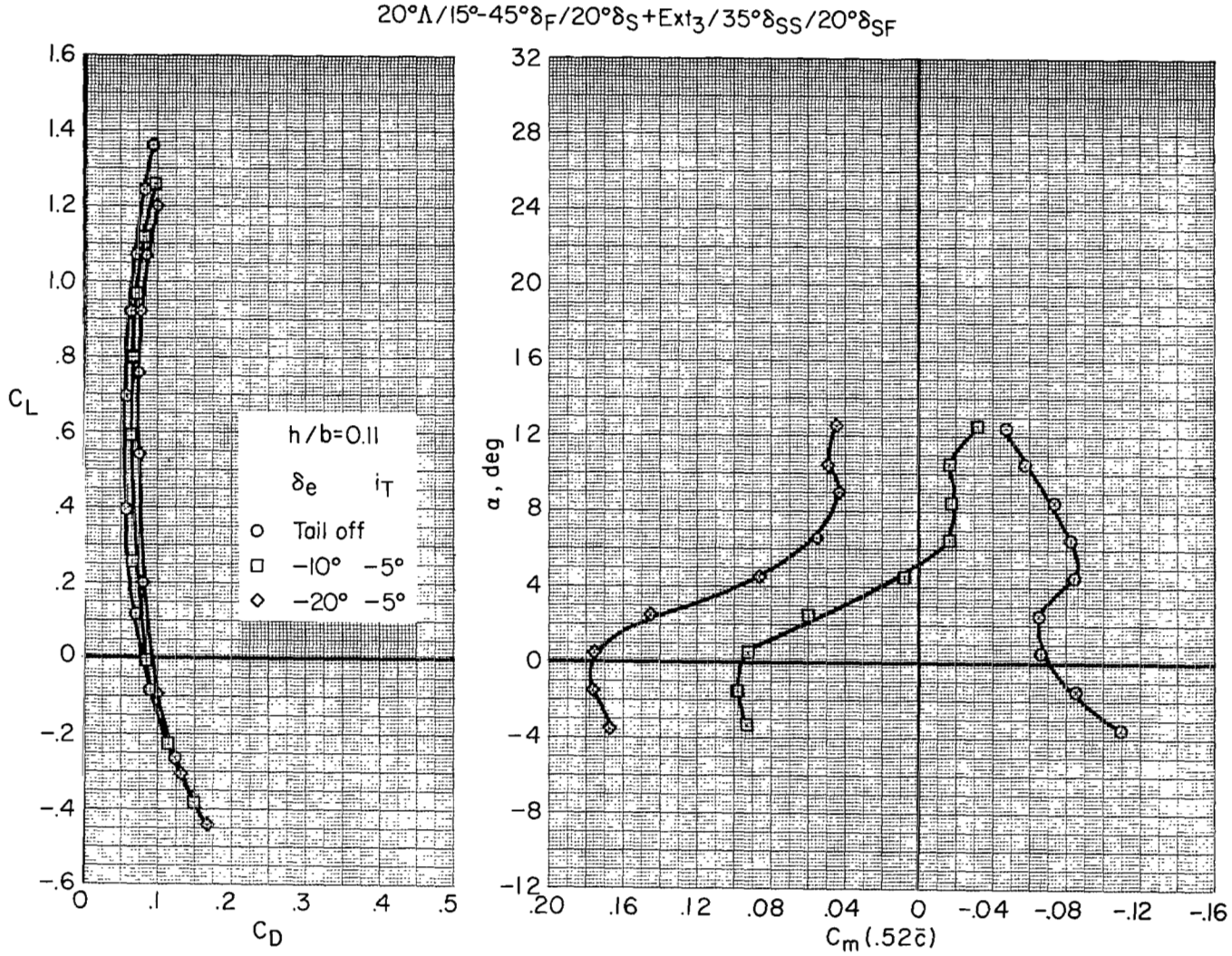

(e) Elevator deflection; C_L vs. C_D, α vs. C_m.

Figure 22.- Continued.

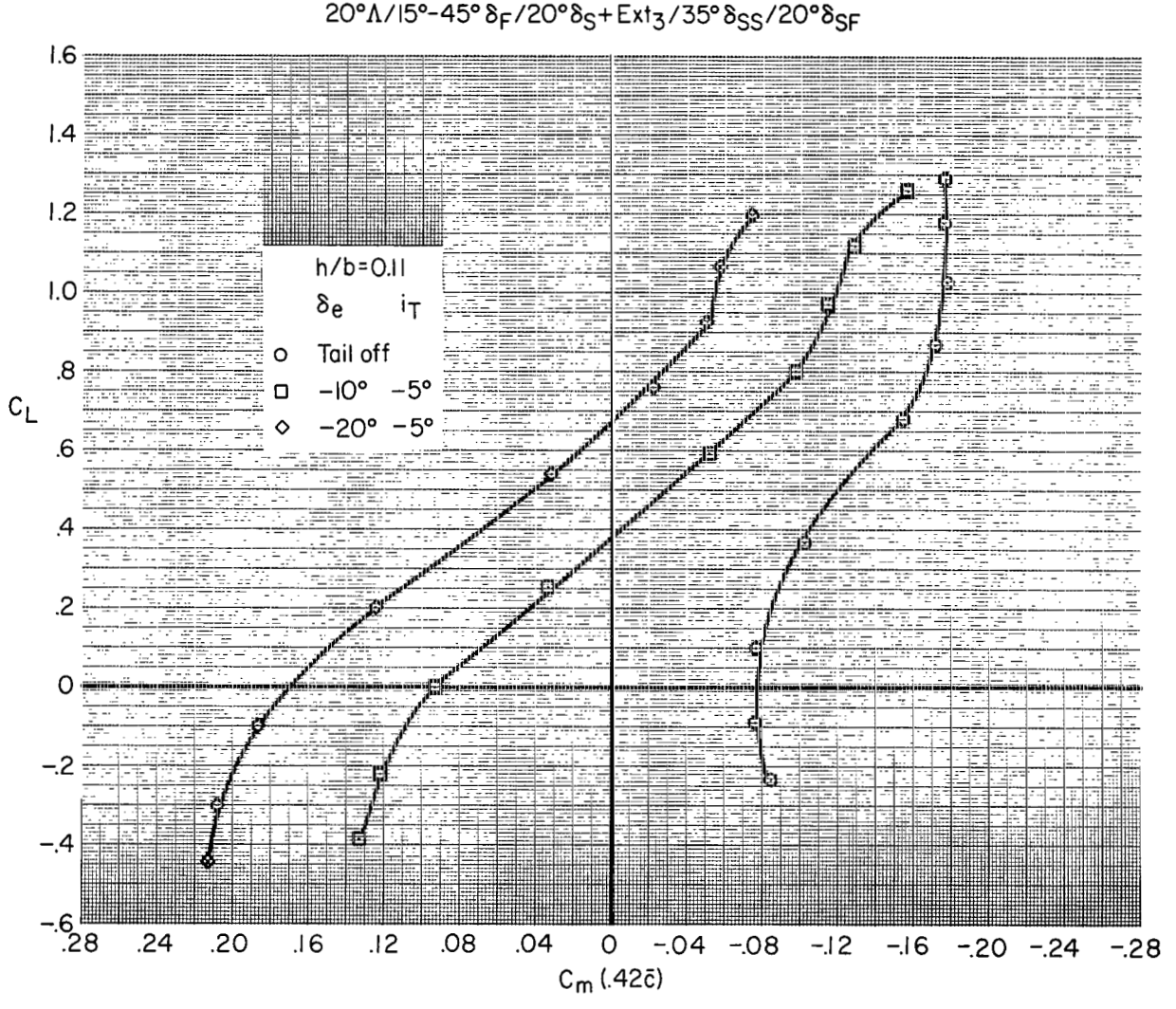

(f) Elevator deflection, forward moment center location; C_L vs. C_m.

Figure 22.- Concluded.

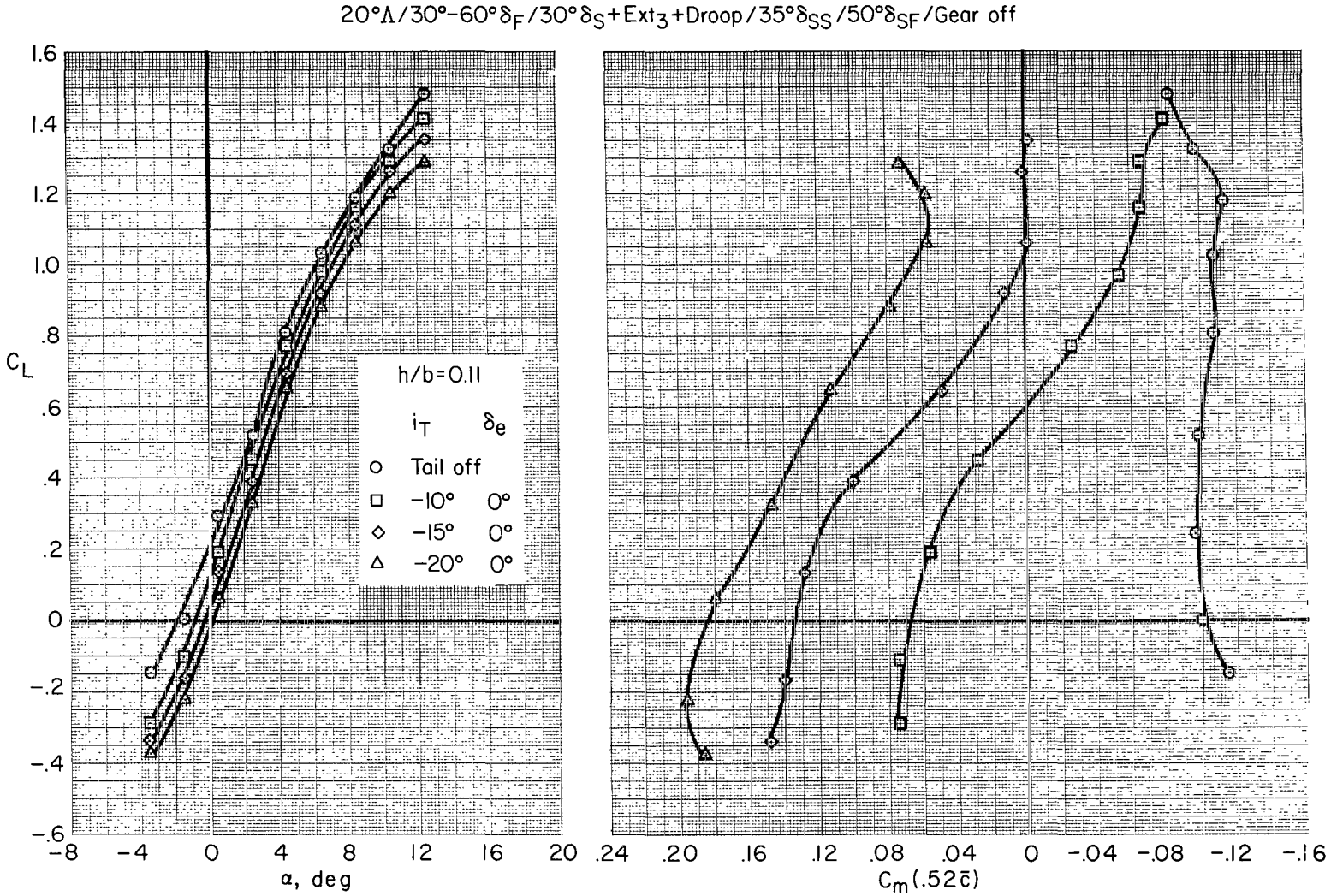

(a) Horizontal-tail incidence, C_L vs. α and C_m.

Figure 23.- Longitudinal characteristics, in ground effect, of horizontal-tail incidence and elevator deflection; landing configuration.

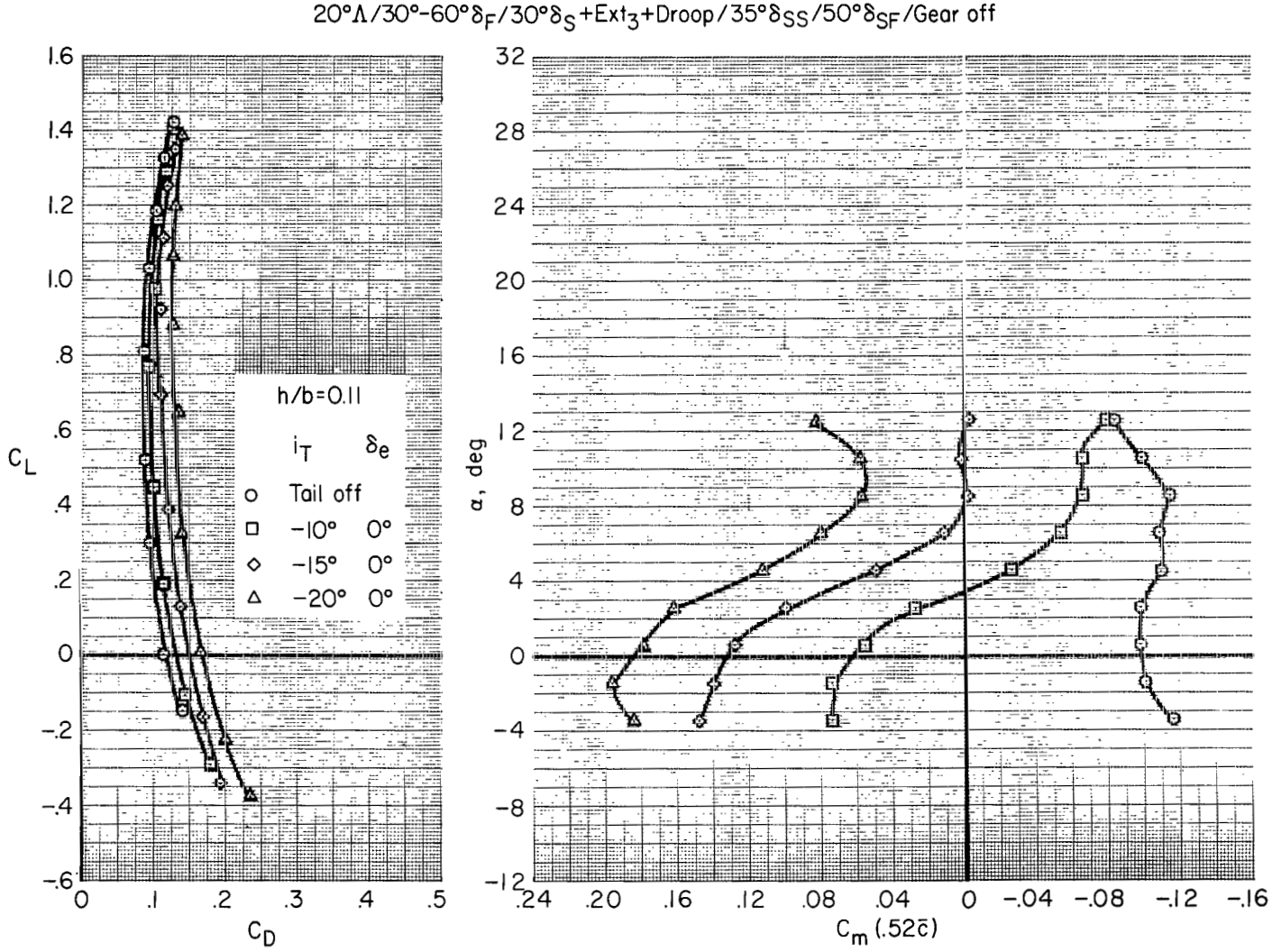

(b) Horizontal-tail incidence; C_L vs. C_D, α vs. C_m.

Figure 23.- Continued.

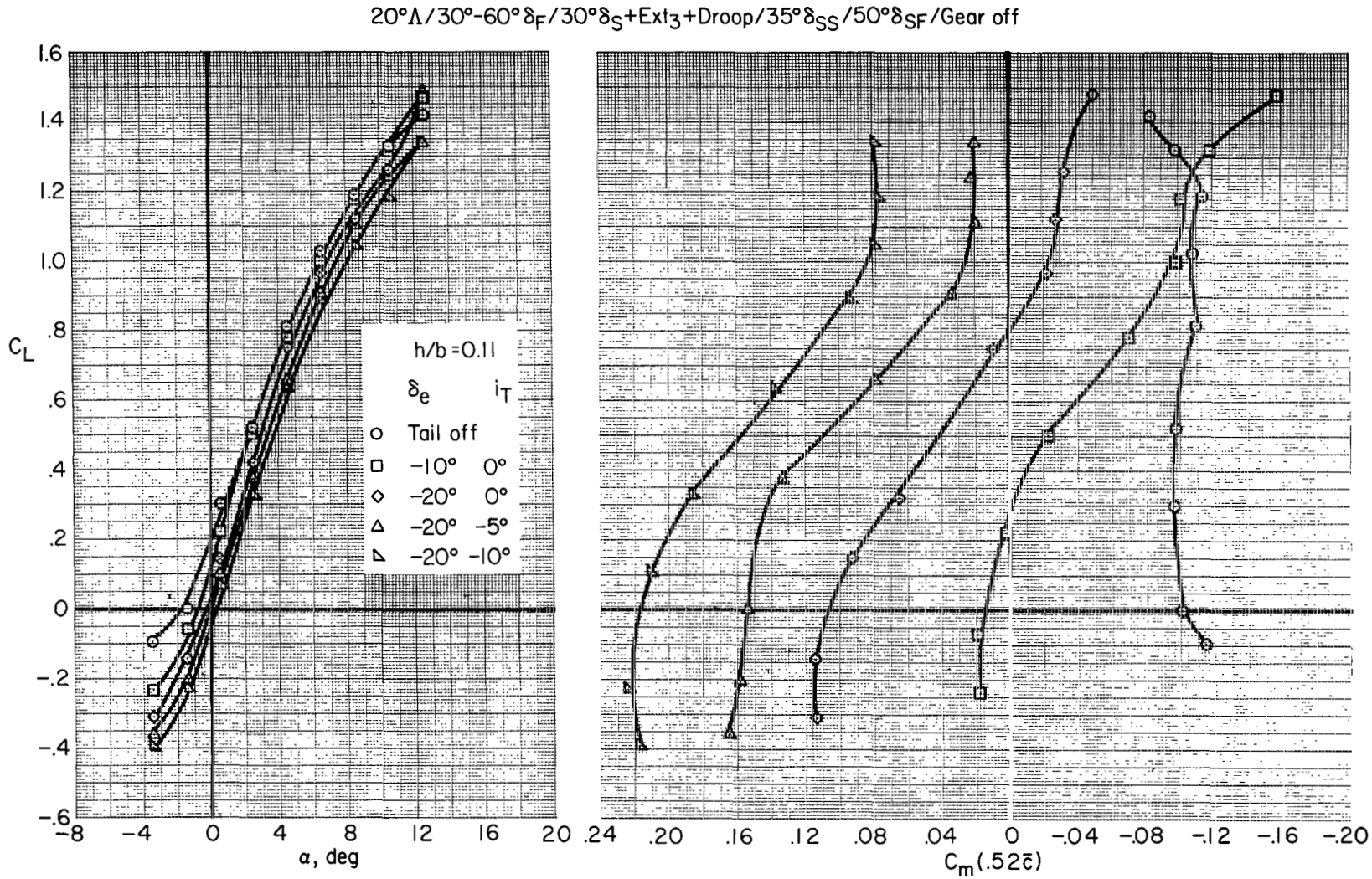

(c) Horizontal-tail incidence and elevator deflection, C_L vs. α and C_m.

Figure 23.- Continued.

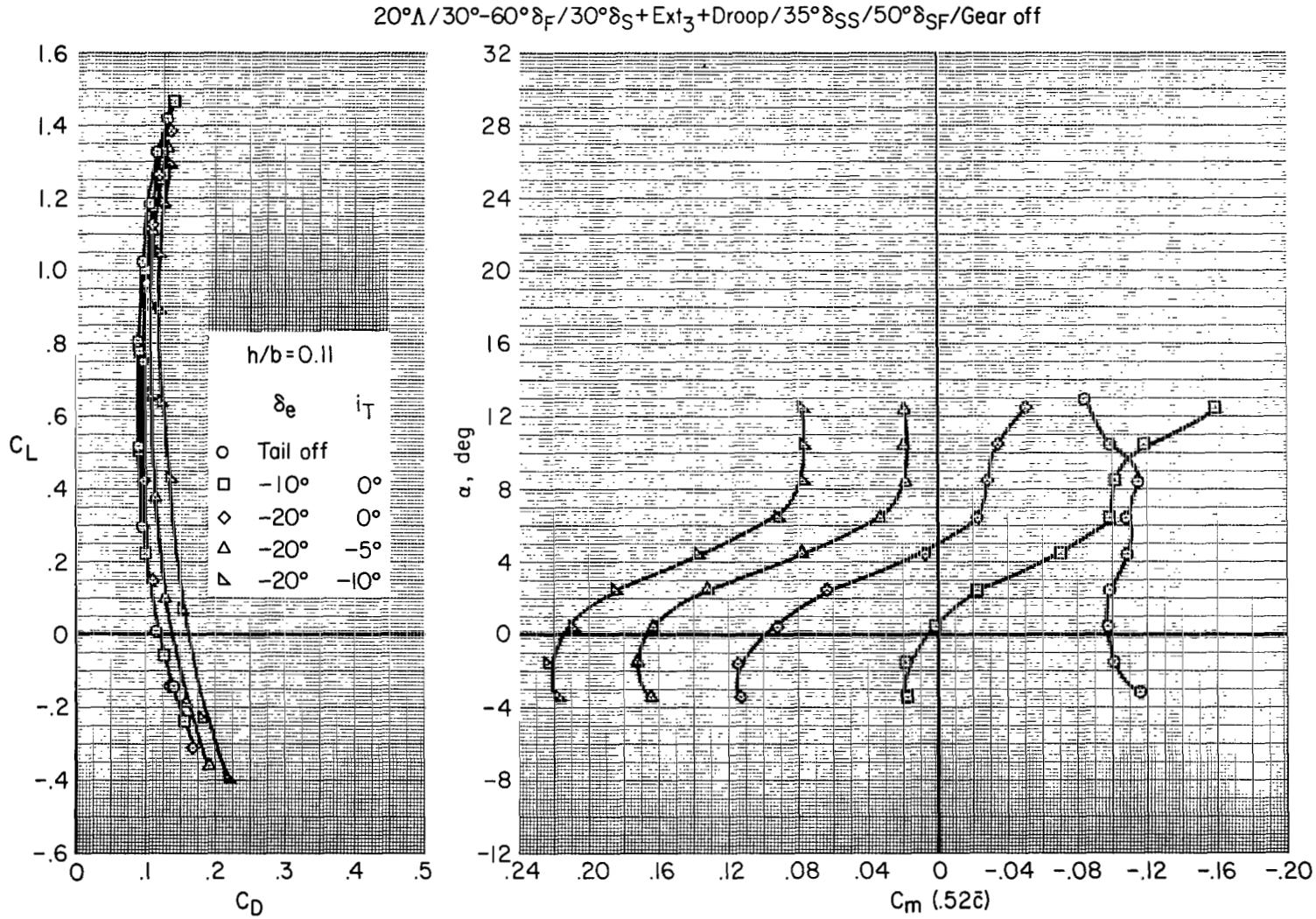

(d) Horizontal-tail incidence and elevator deflection; C_L vs. C_D, α vs. C_m.

Figure 23.- Concluded.

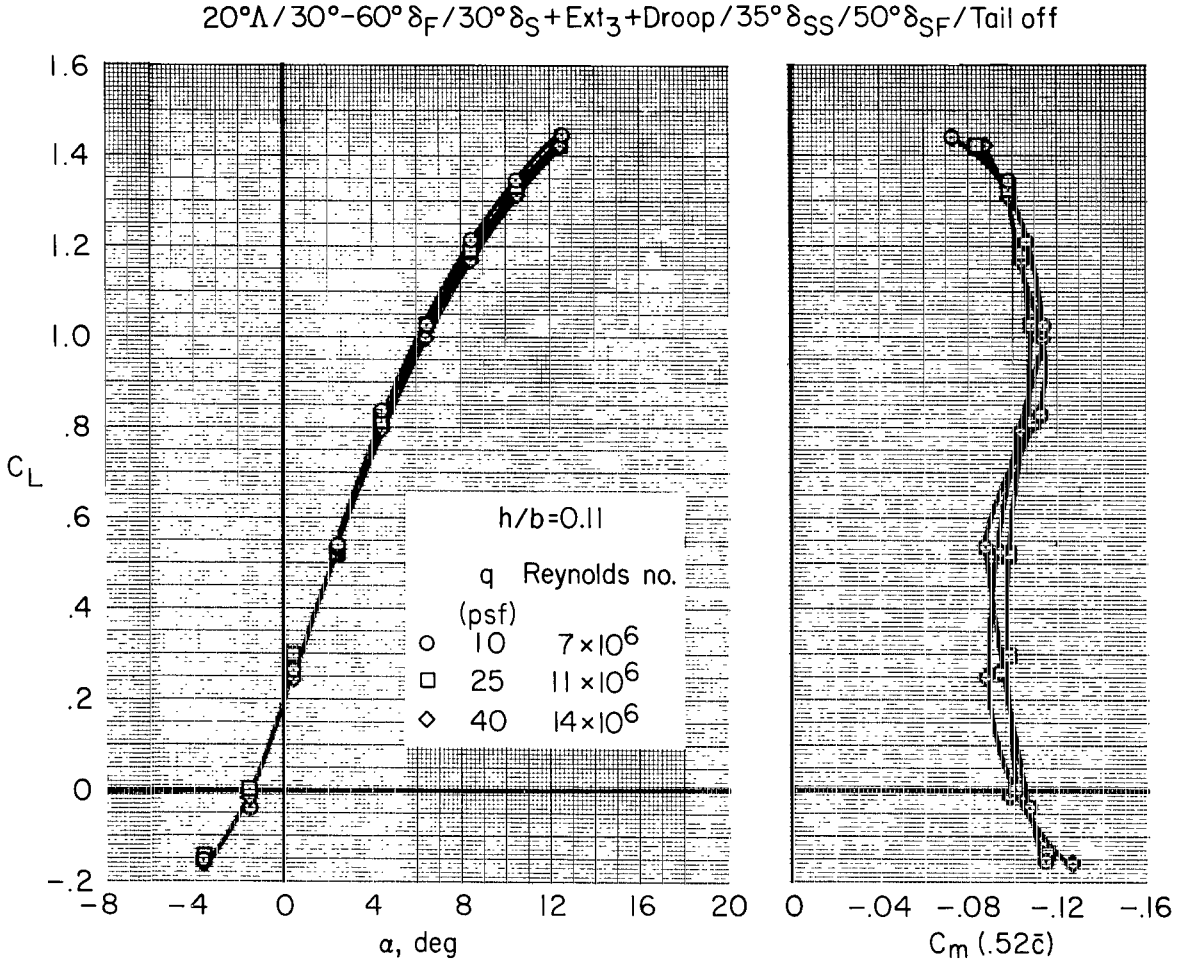

(a) C_L vs. α and C_m

Figure 24.- Effect of Reynolds number on longitudinal characteristics; landing configuration, tail off.

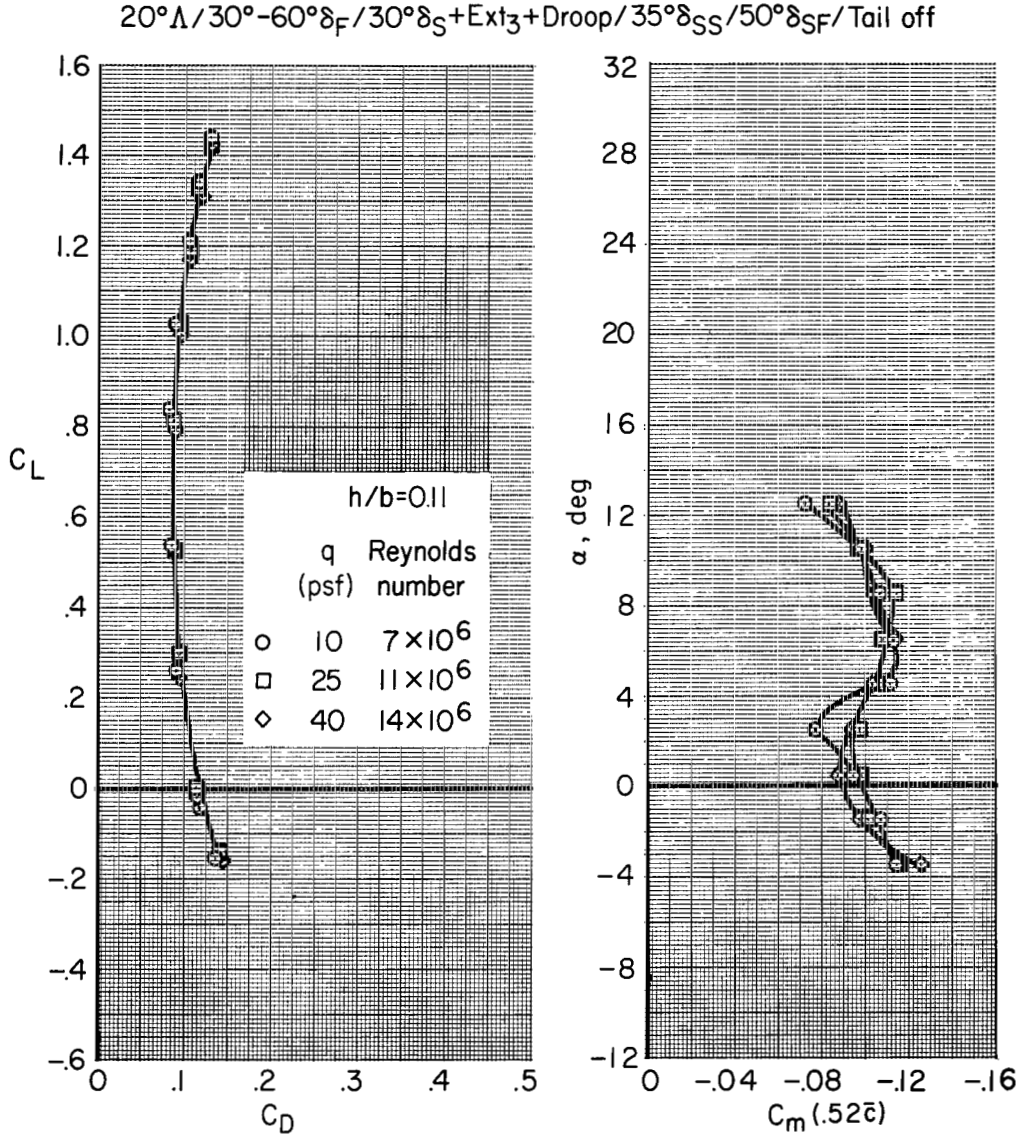

(b) C_L vs. C_D, α vs. C_m

Figure 24.- Concluded.

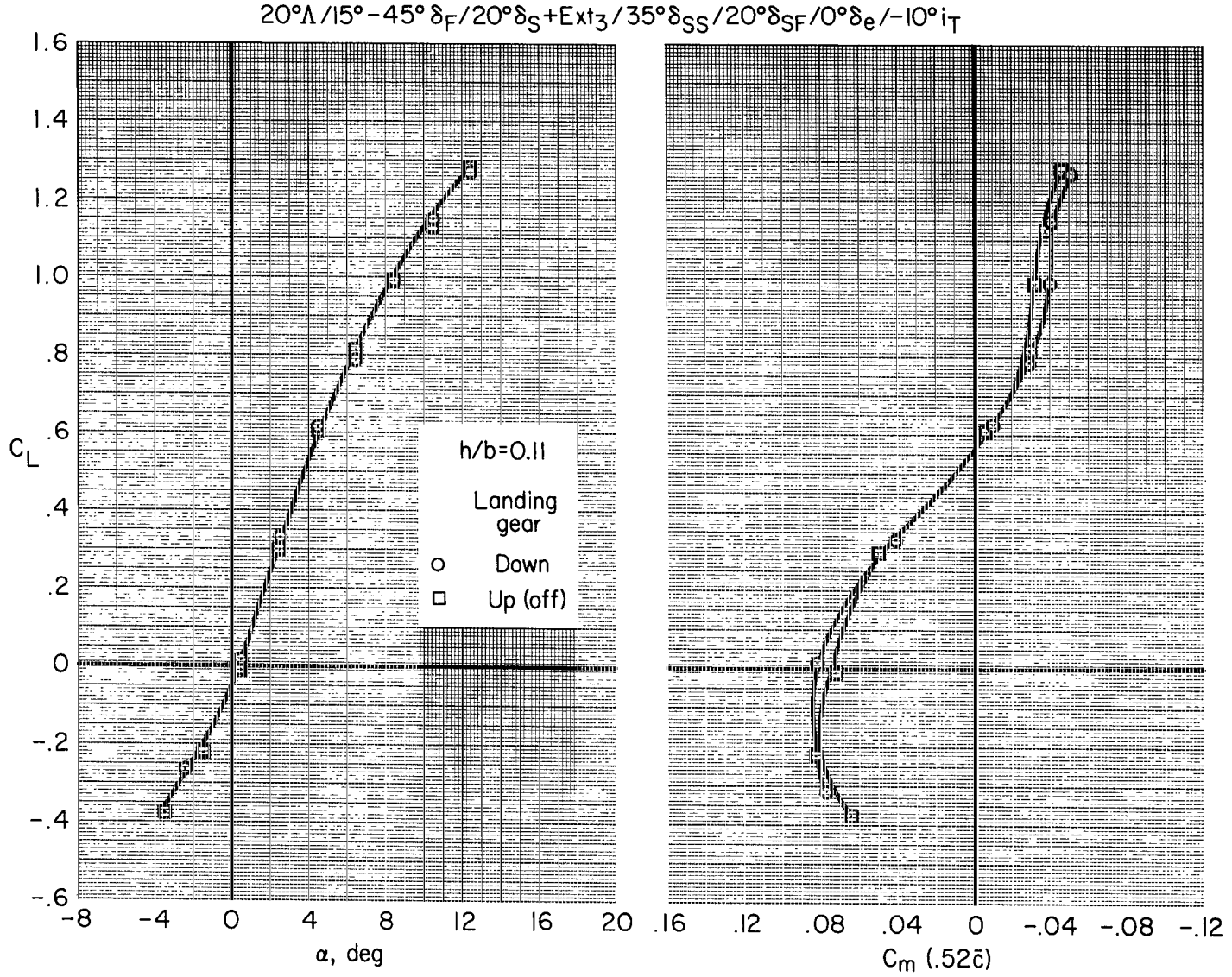

(a) C_L vs. α and C_m

Figure 25.- Effect of landing gear, in ground effect, take-off configuration.

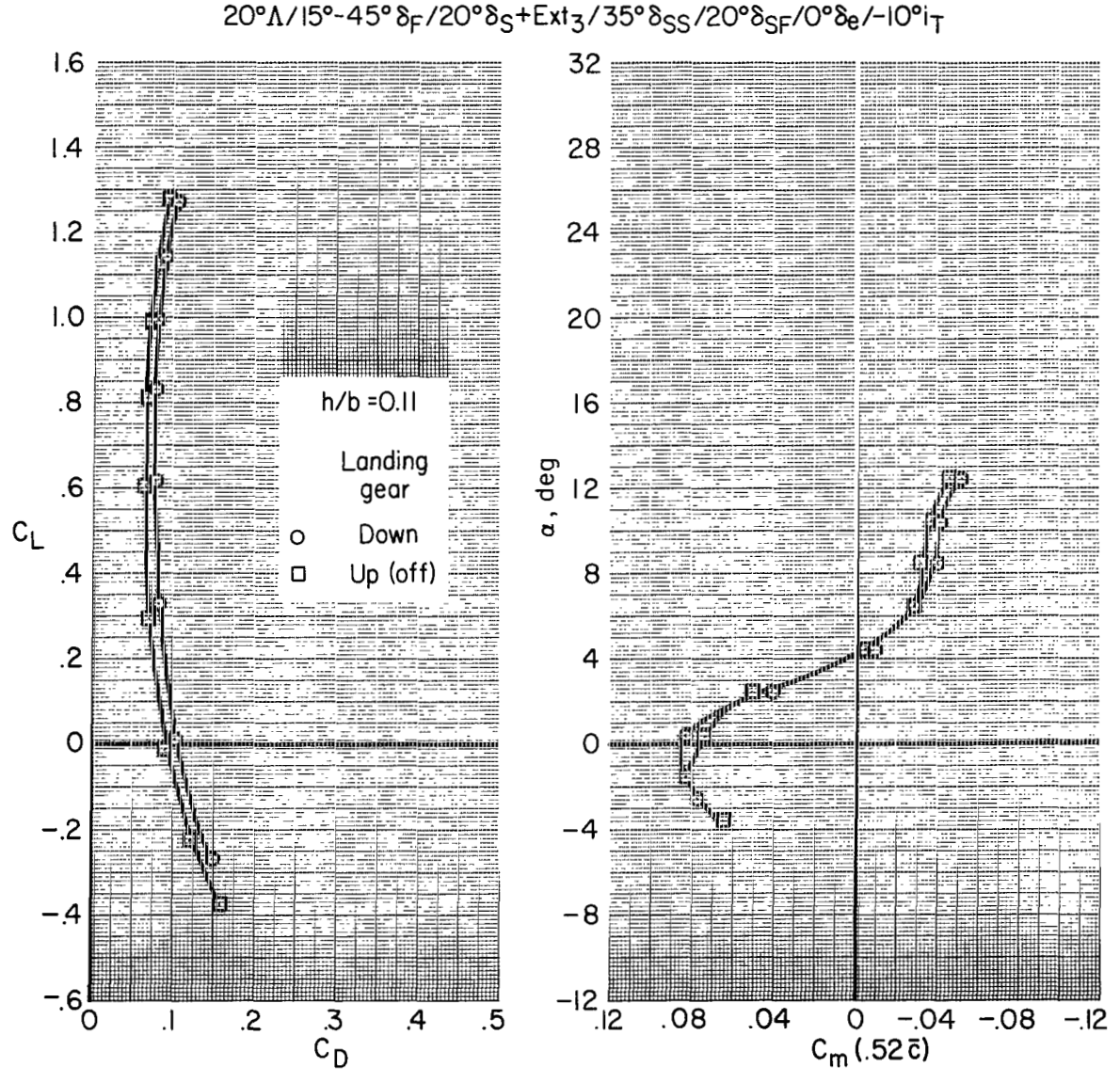

(b) C_L vs. C_D, α vs. C_m

Figure 25.- Concluded.

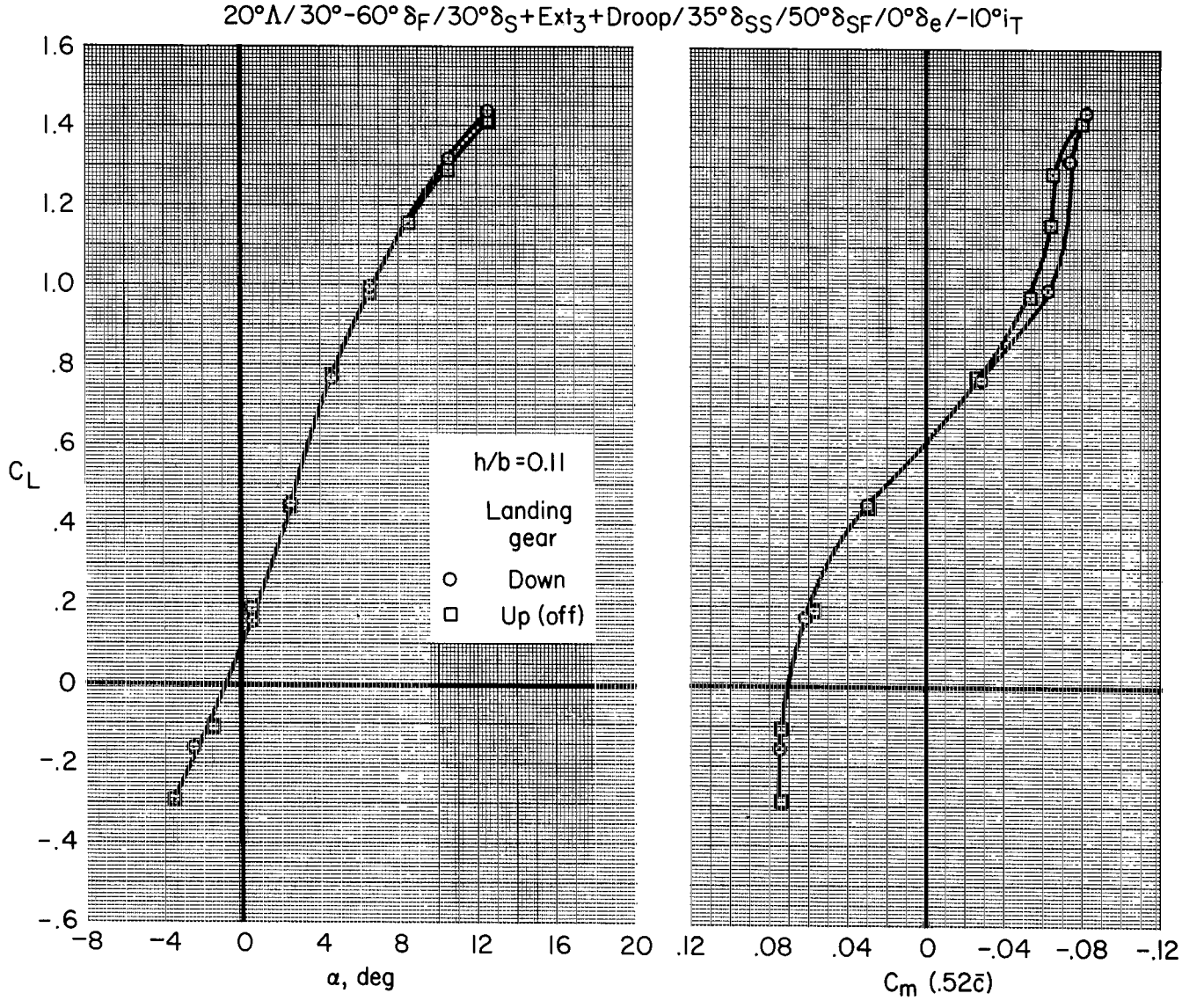

(a) C_L vs. α and C_m

Figure 26.- Effect of landing gear, in ground effect, landing configuration.

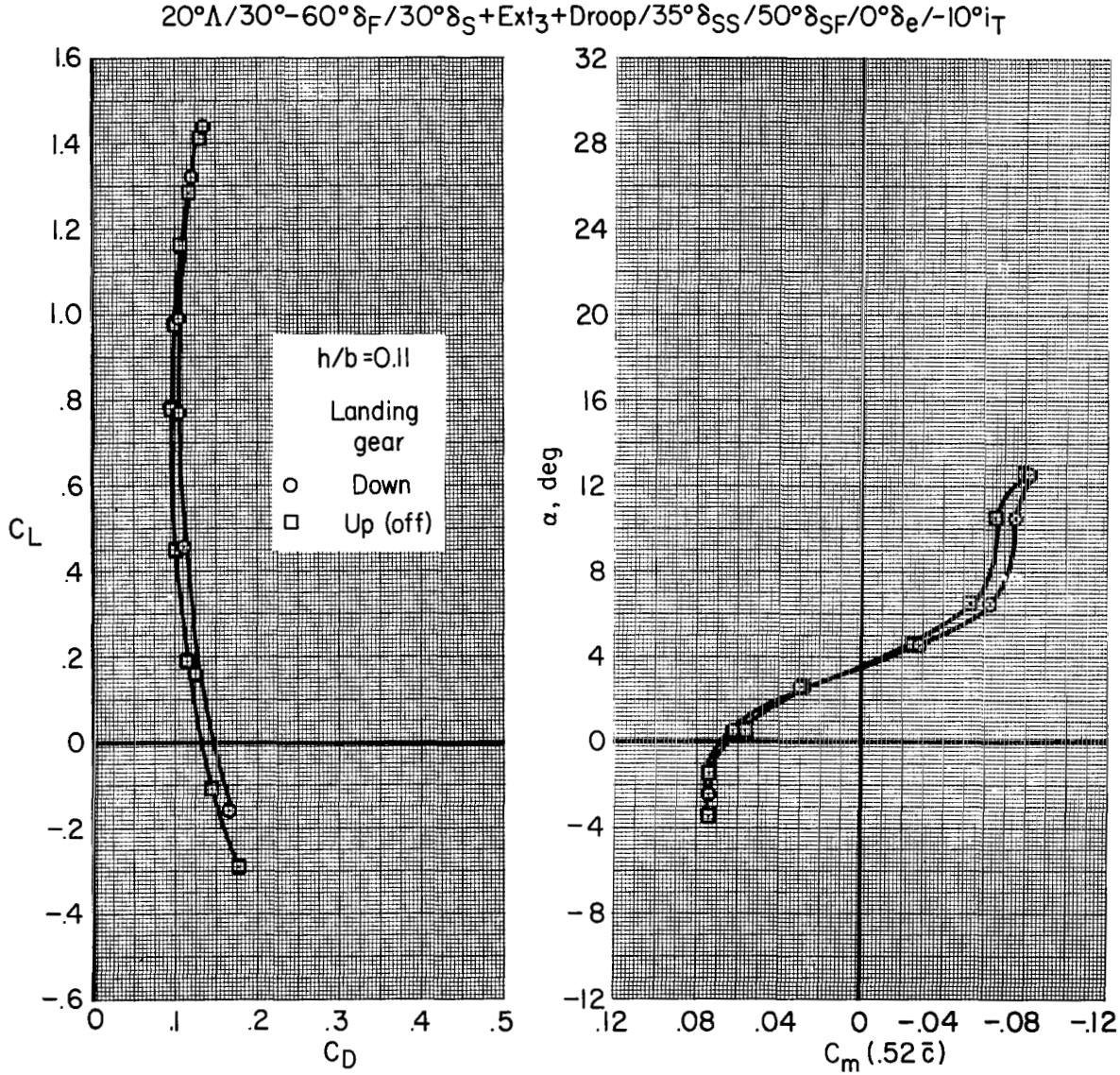

(b) C_L vs. C_D, α vs. C_m

Figure 26.- Concluded.

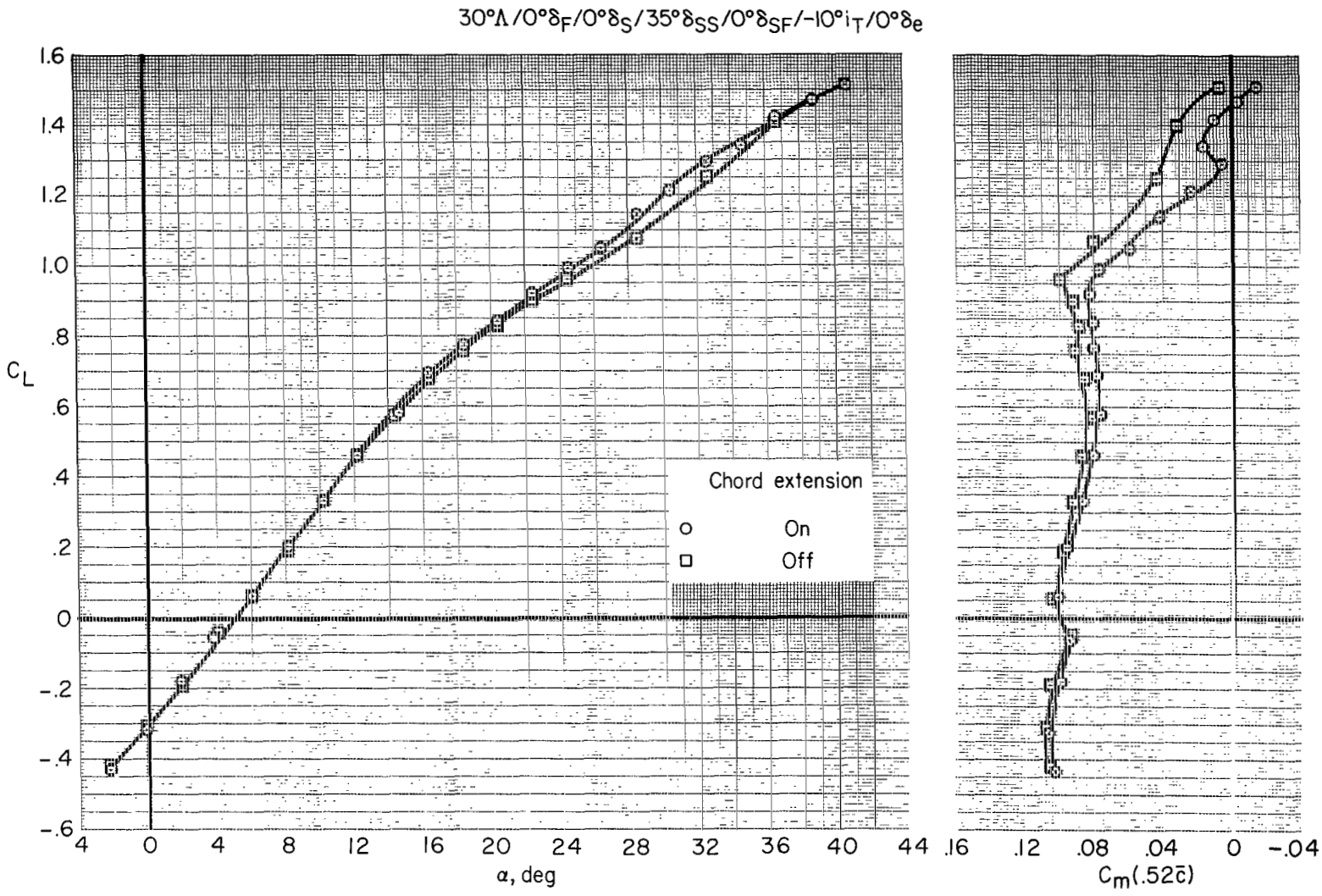

(a) C_L vs. α and C_m

Figure 27.- Effect of wing leading-edge local chord extension; flaps up, slats up, 30° wing sweep.

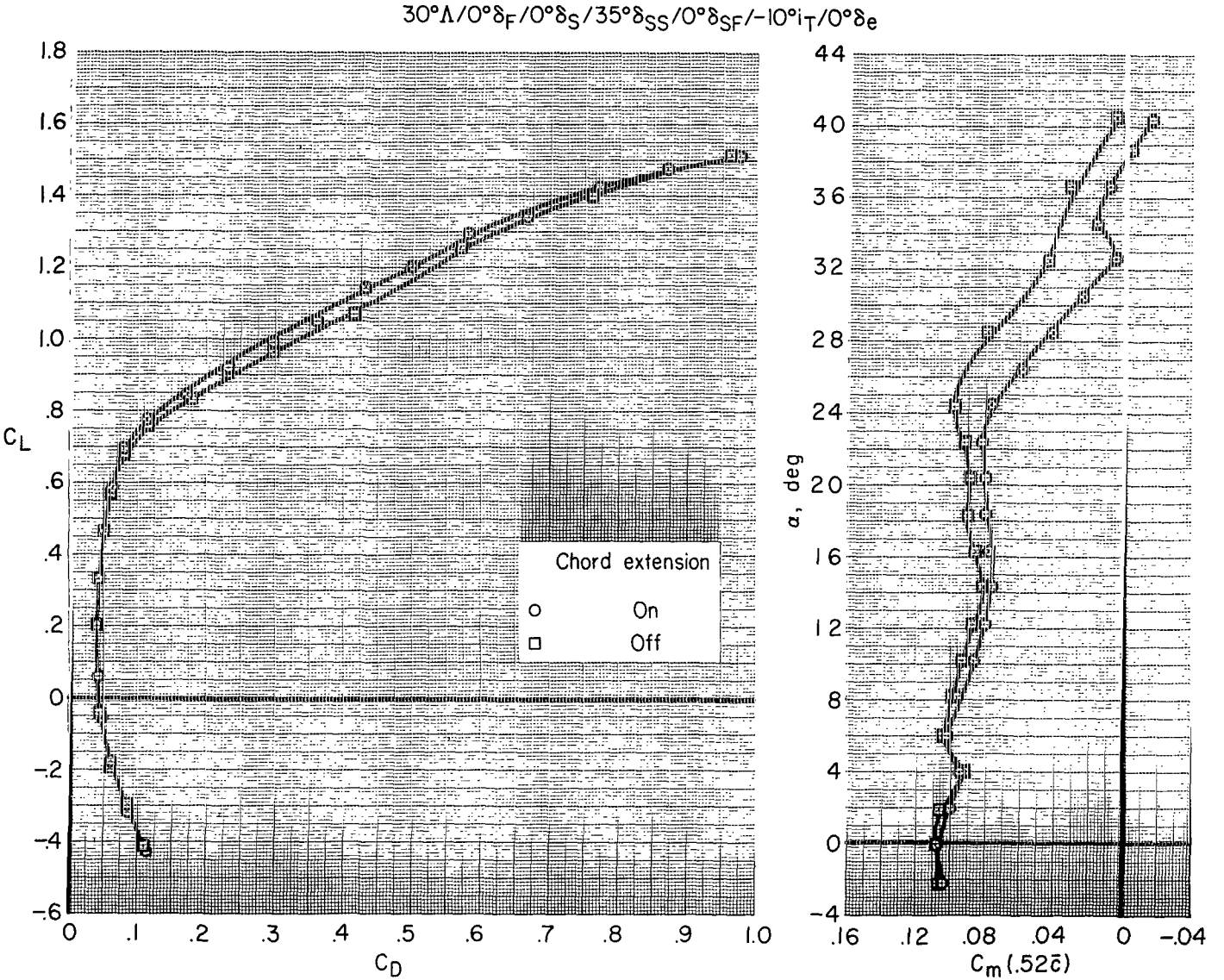

(b) C_L vs. C_D, α vs. C_m

Figure 27.- Concluded.

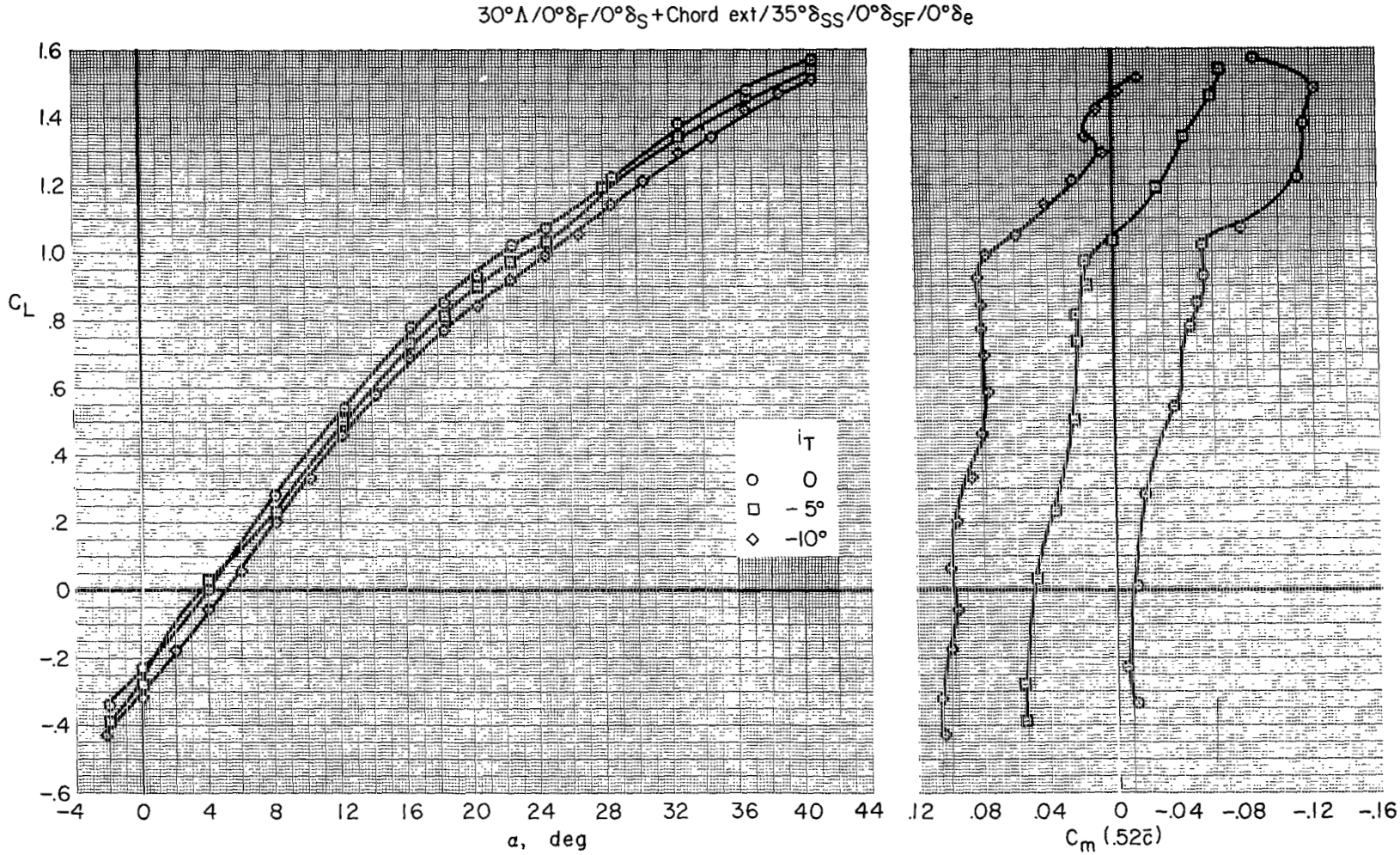

(a) C_L vs. α and C_m

Figure 28.- Longitudinal characteristics of horizontal-tail incidence; 30° wing sweep, flaps up.

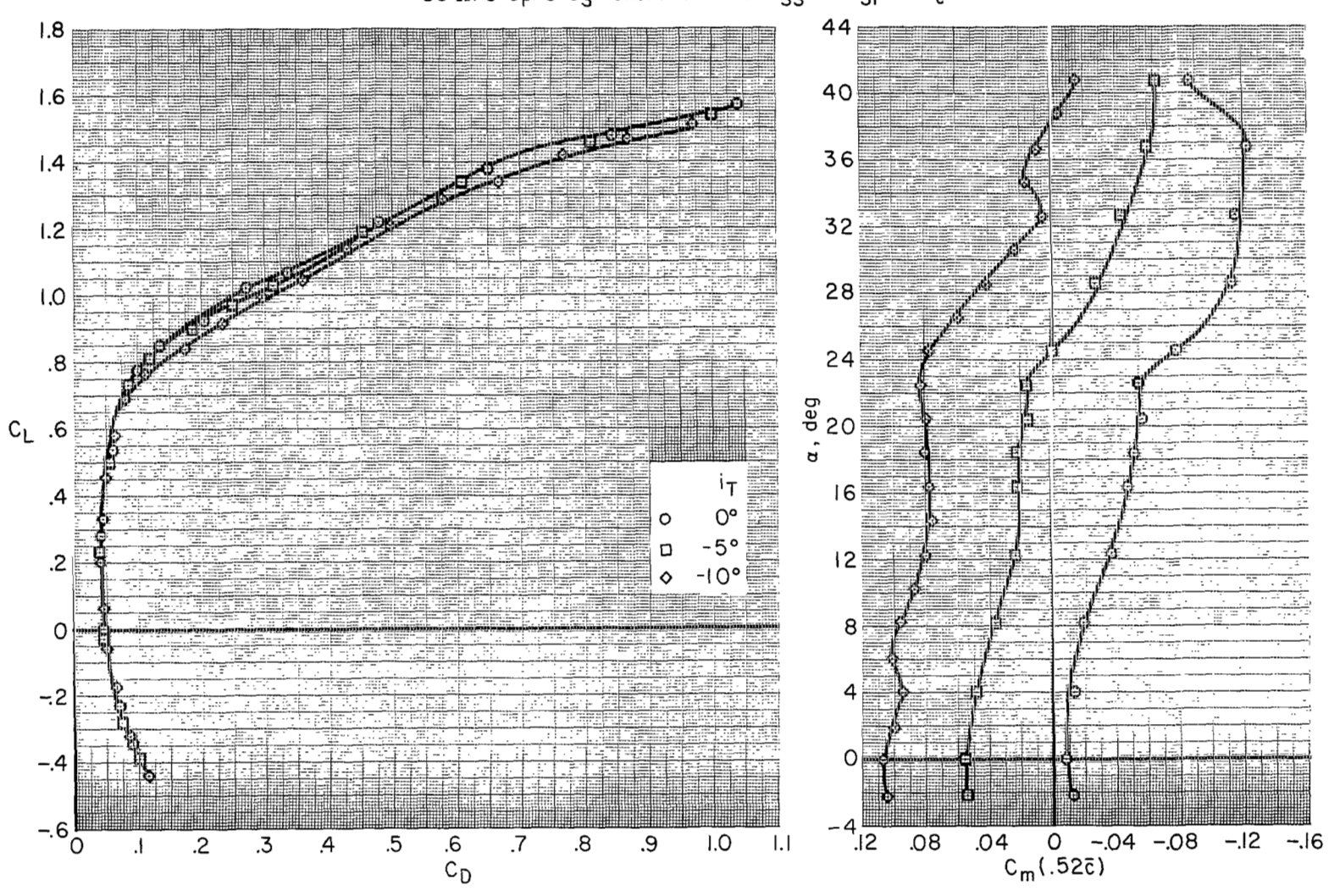

(b) C_L vs. C_D, α vs. C_m

Figure 28.- Concluded.

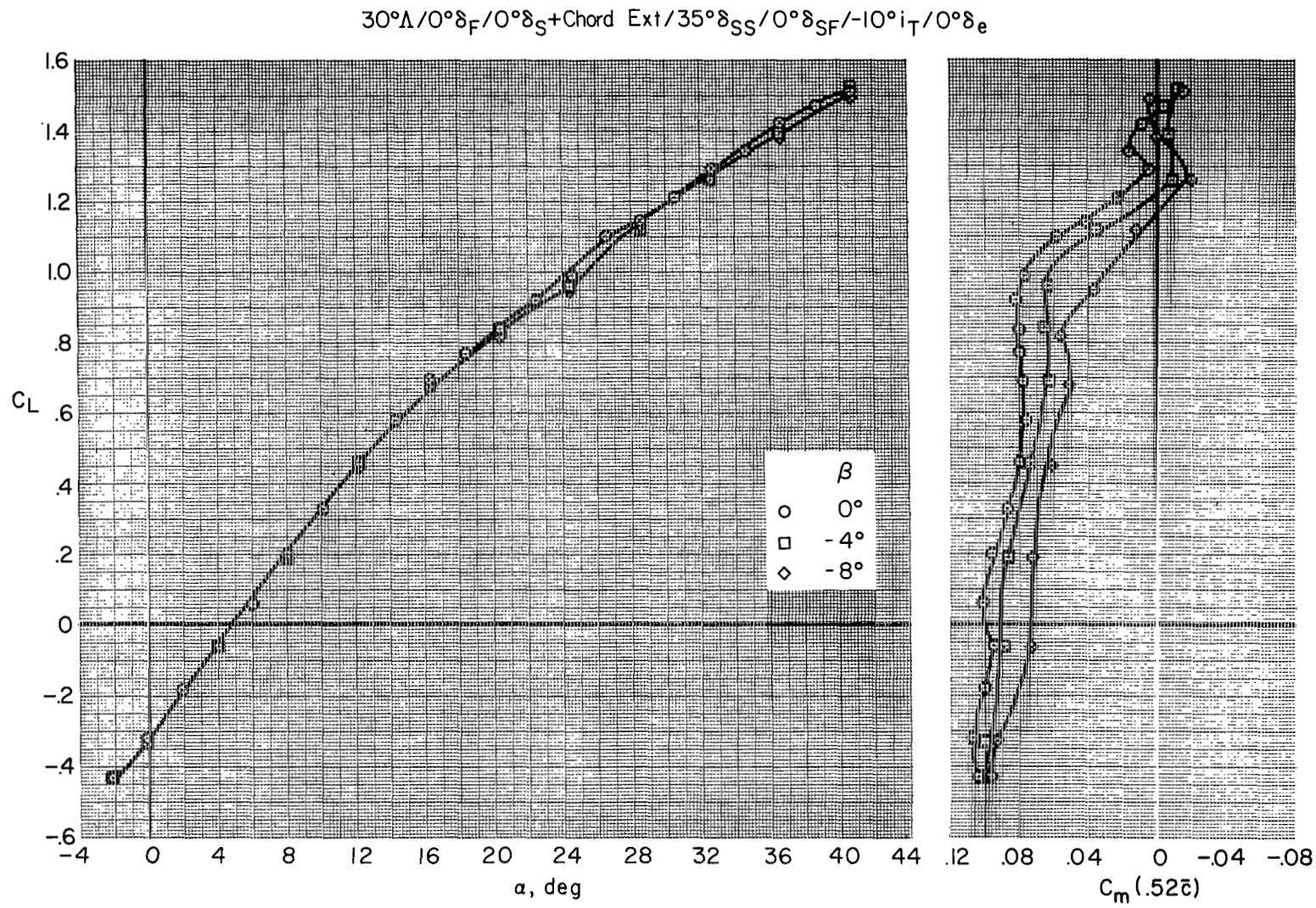

(a) Longitudinal characteristics, C_L vs. α and C_m.

Figure 29.- Characteristics in sideslip; 30° wing sweep, flaps up.

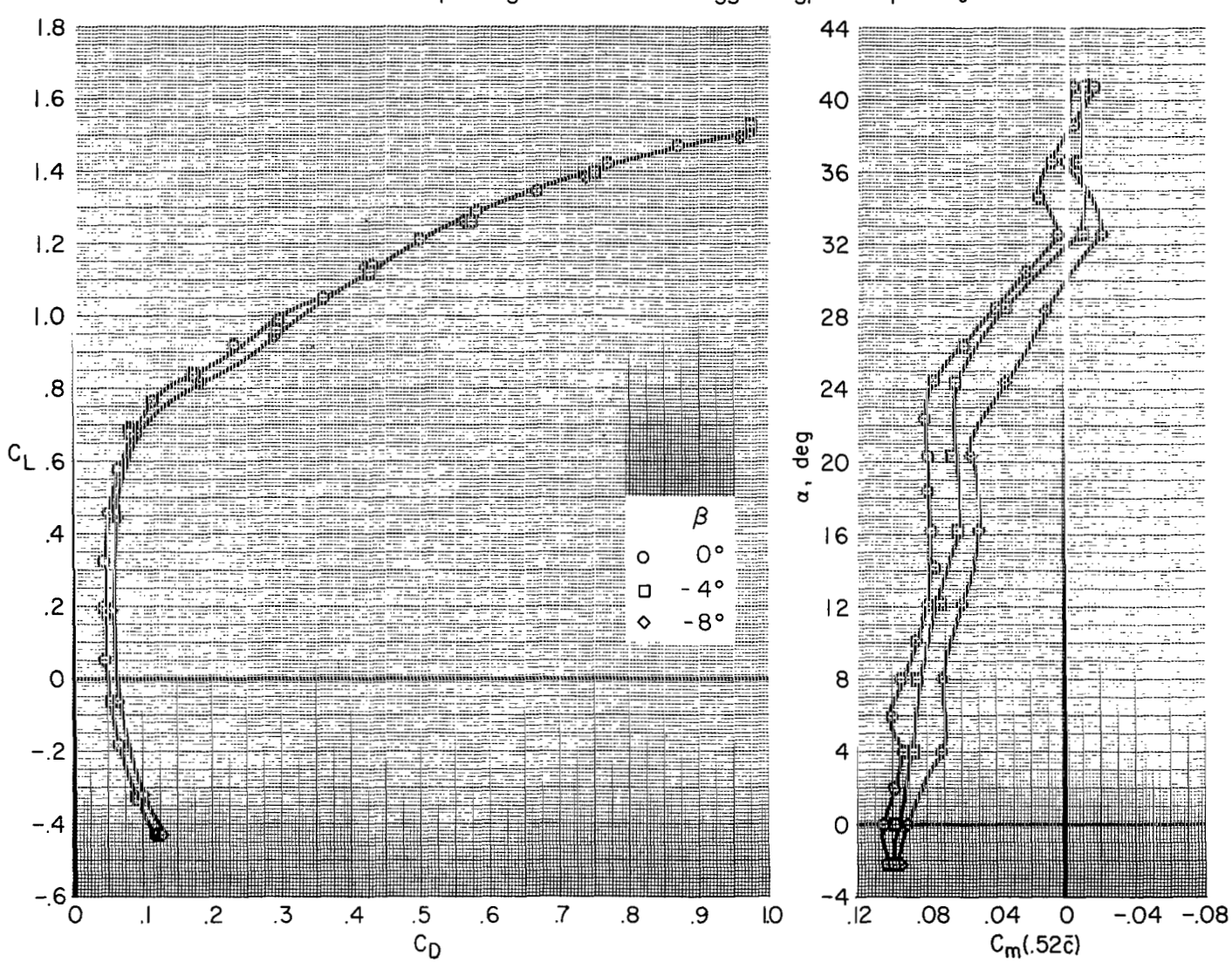

(b) Longitudinal characteristics, C_L vs. C_D, δ vs. C_m

Figure 29.- Continued.

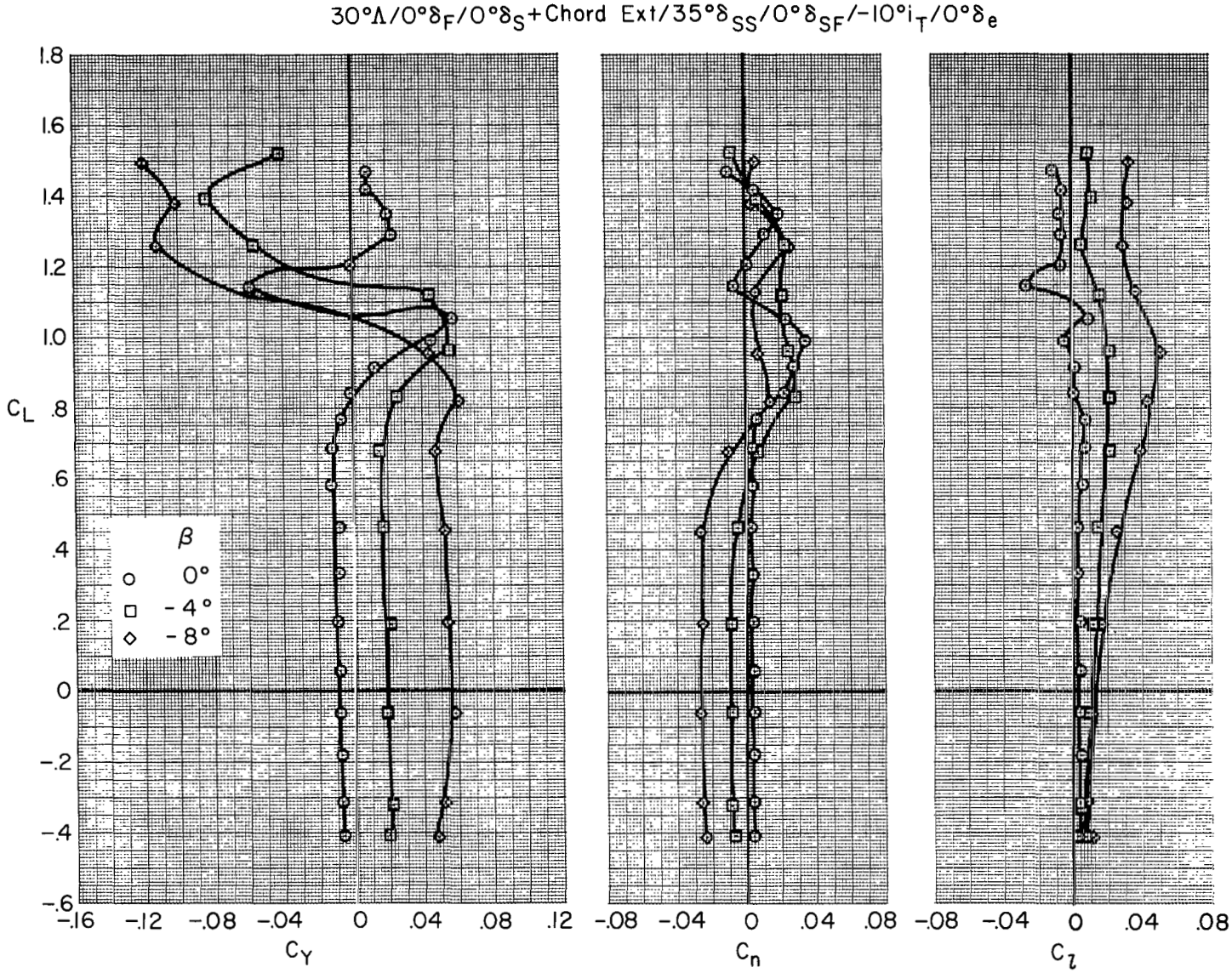

(c) Lateral-directional characteristics.

Figure 29.- Concluded.

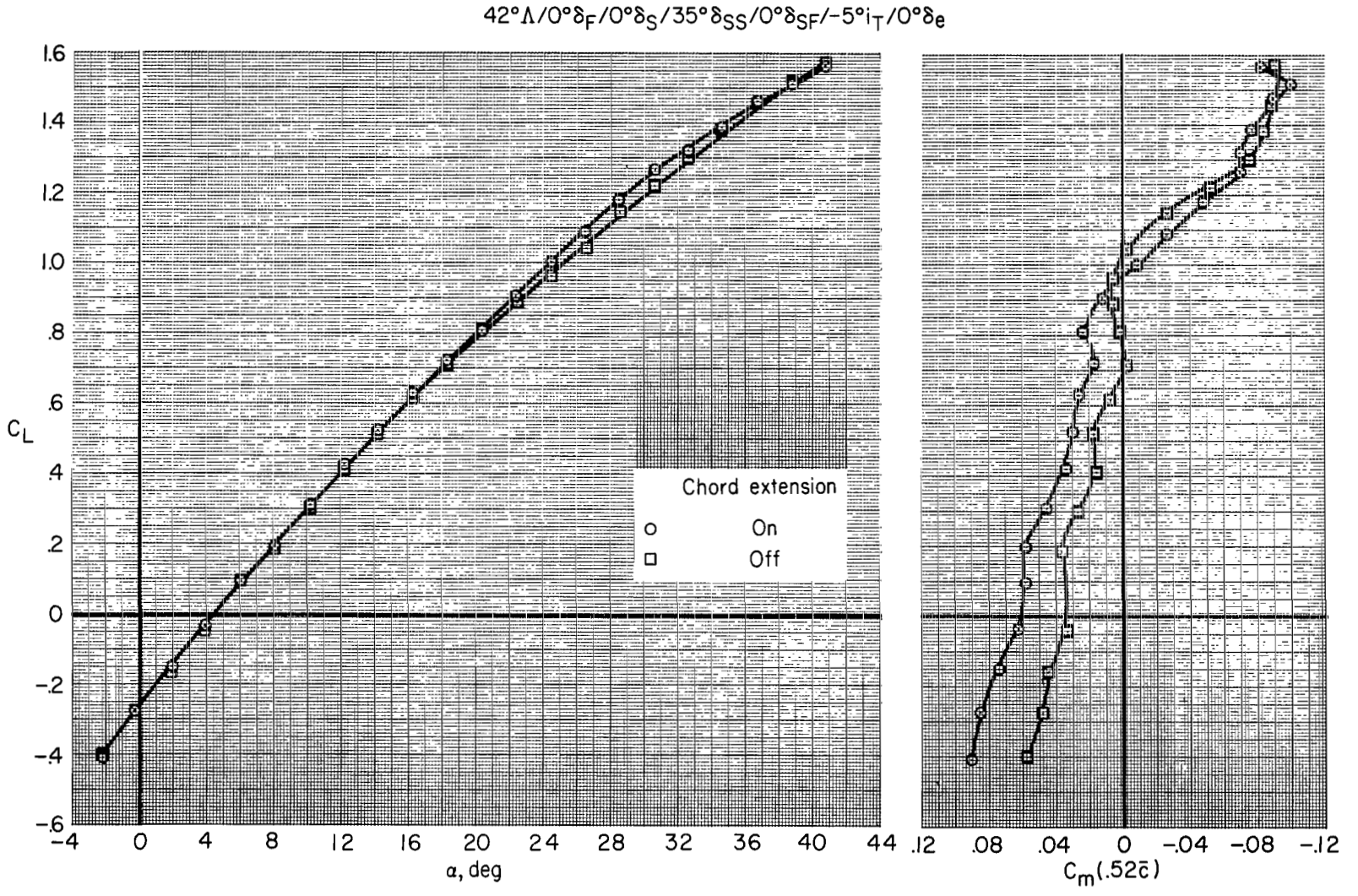

(a) C_L vs. α and C_m

Figure 30.- Effect of wing leading-edge chord extension; 42° wing sweep.

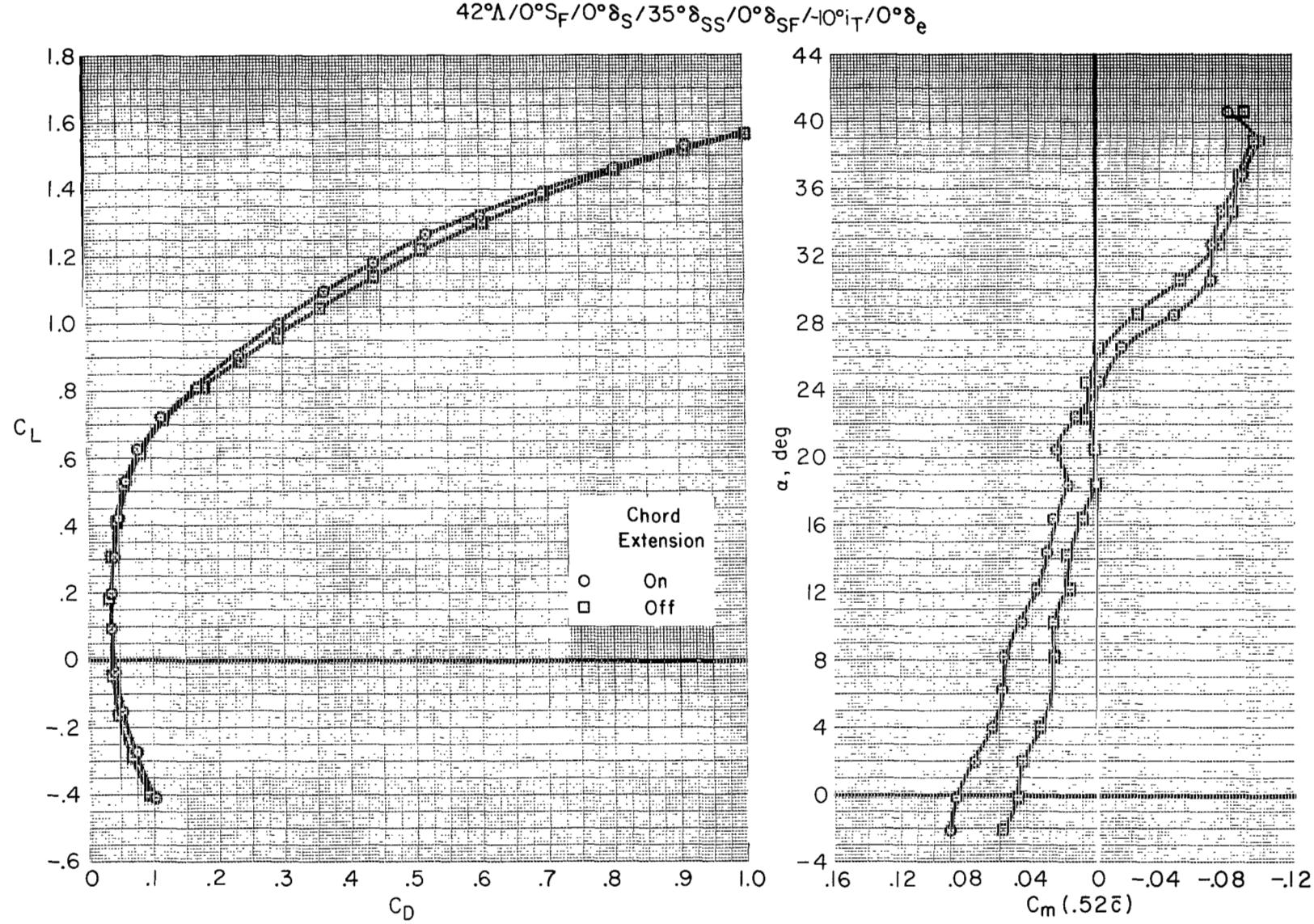

(b) C_L vs. C_D, α vs. C_m

Figure 30.- Concluded.

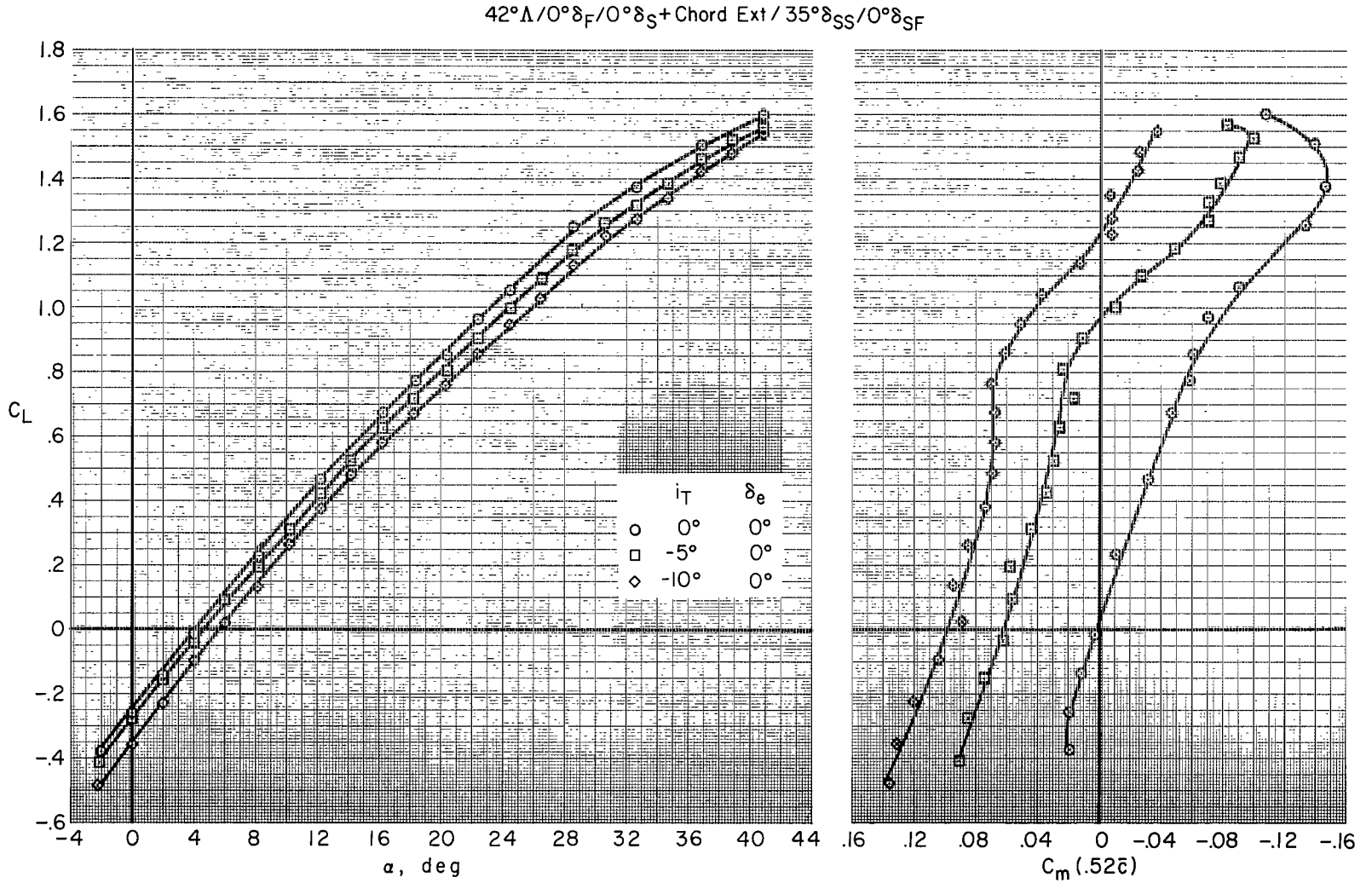

(a) C_L vs. α and C_m

Figure 31.- Effect of horizontal-tail incidence; 42° wing sweep.

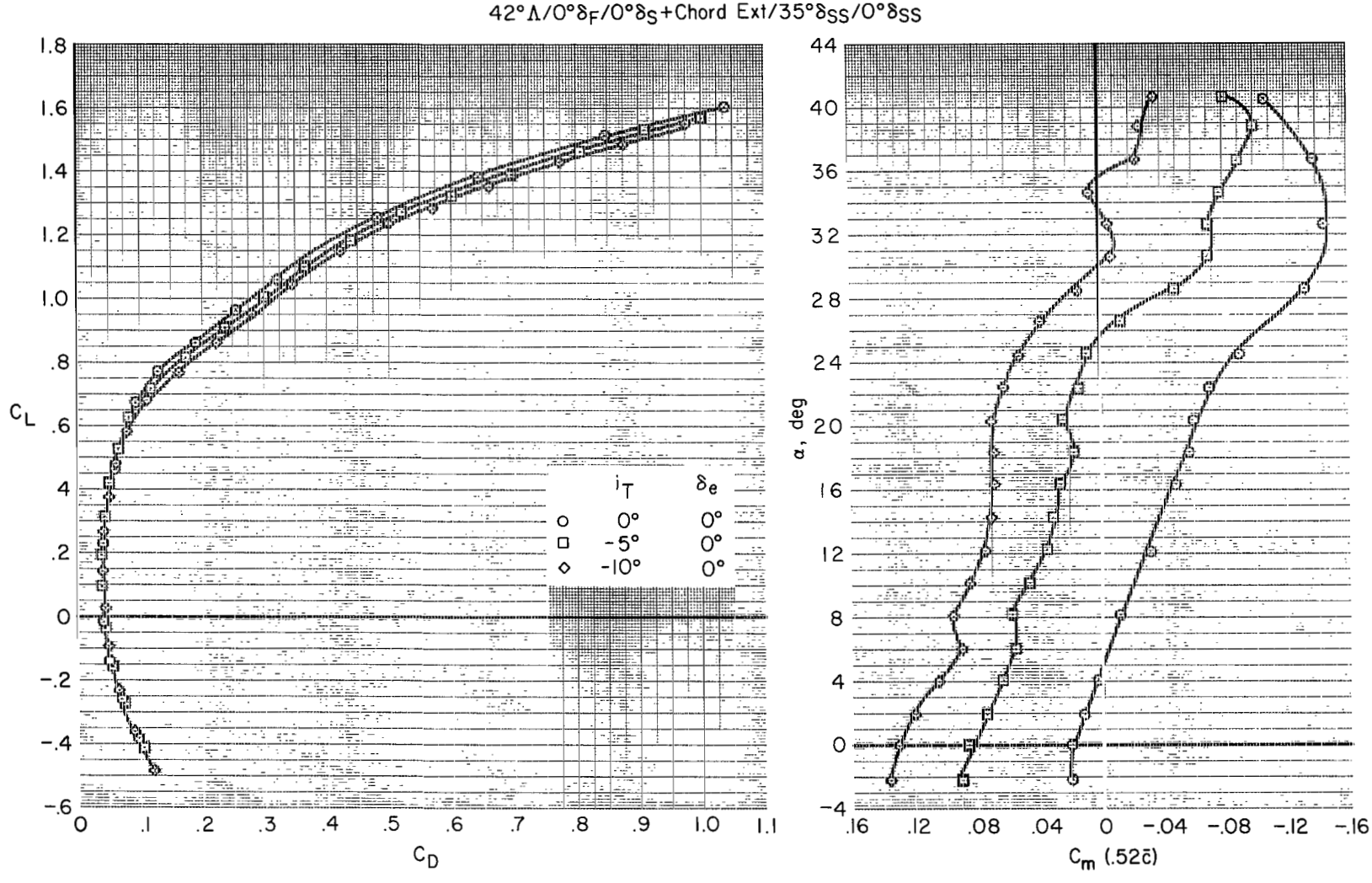

(b) C_L vs. C_D, α vs. C_m

Figure 31.- Concluded.

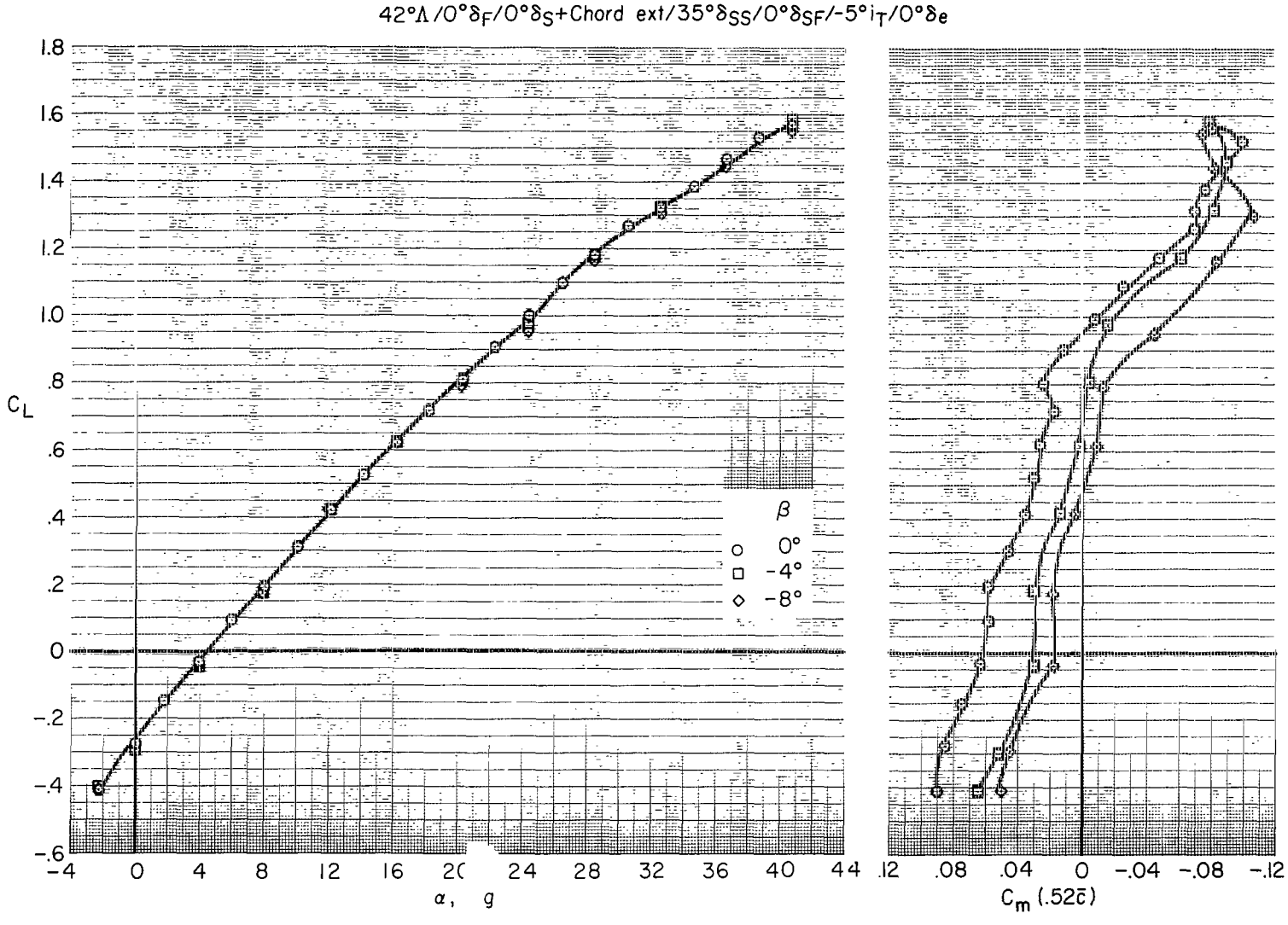

(a) Longitudinal characteristics, C_L vs. α and C_m.

Figure 32.- Characteristics in sideslip; 42° wing sweep.

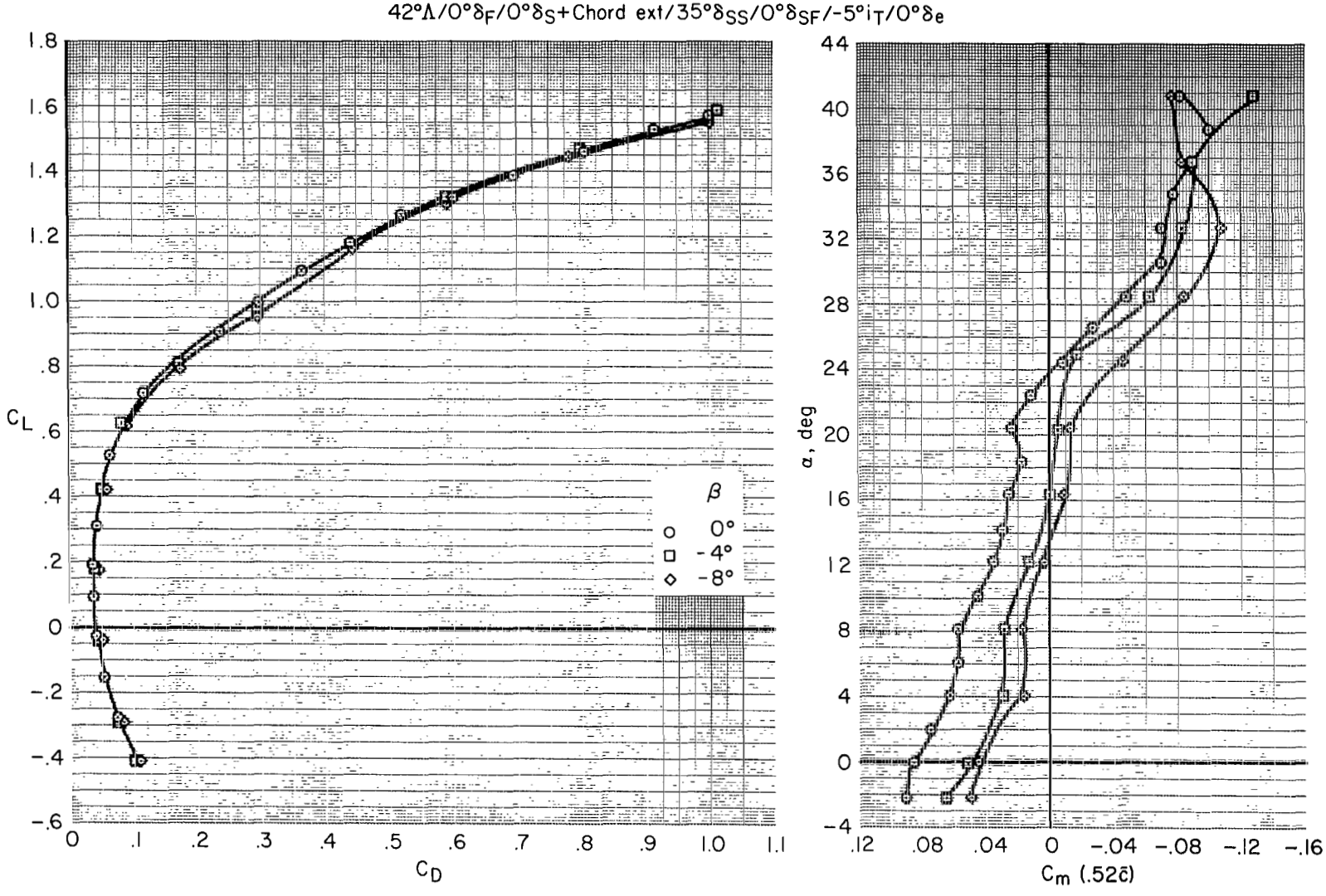

(b) Longitudinal characteristics; C_L vs. C_D, α vs. C_m.

Figure 32.- Continued.

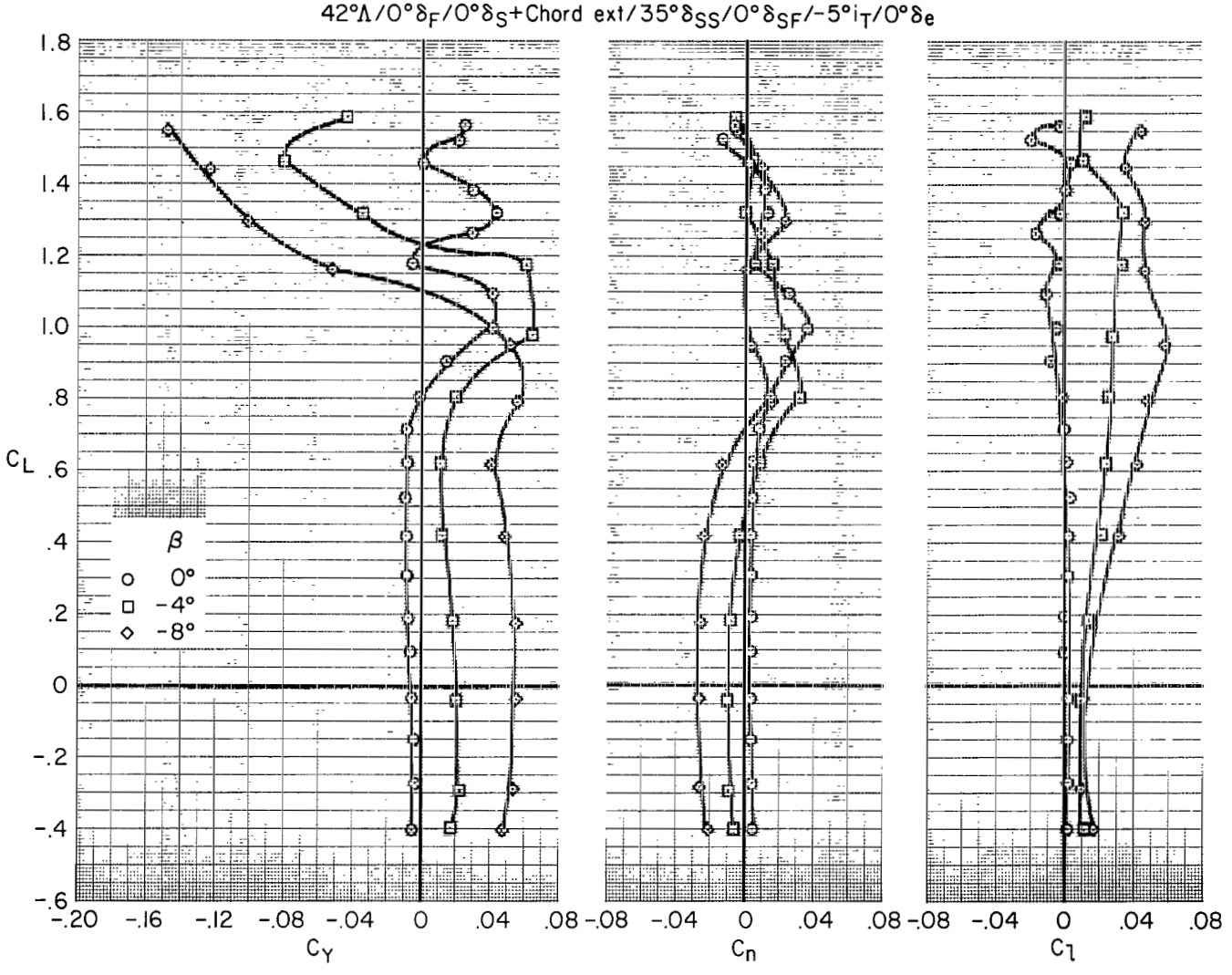

(c) Lateral-directional characteristics.

Figure 32.- Concluded.

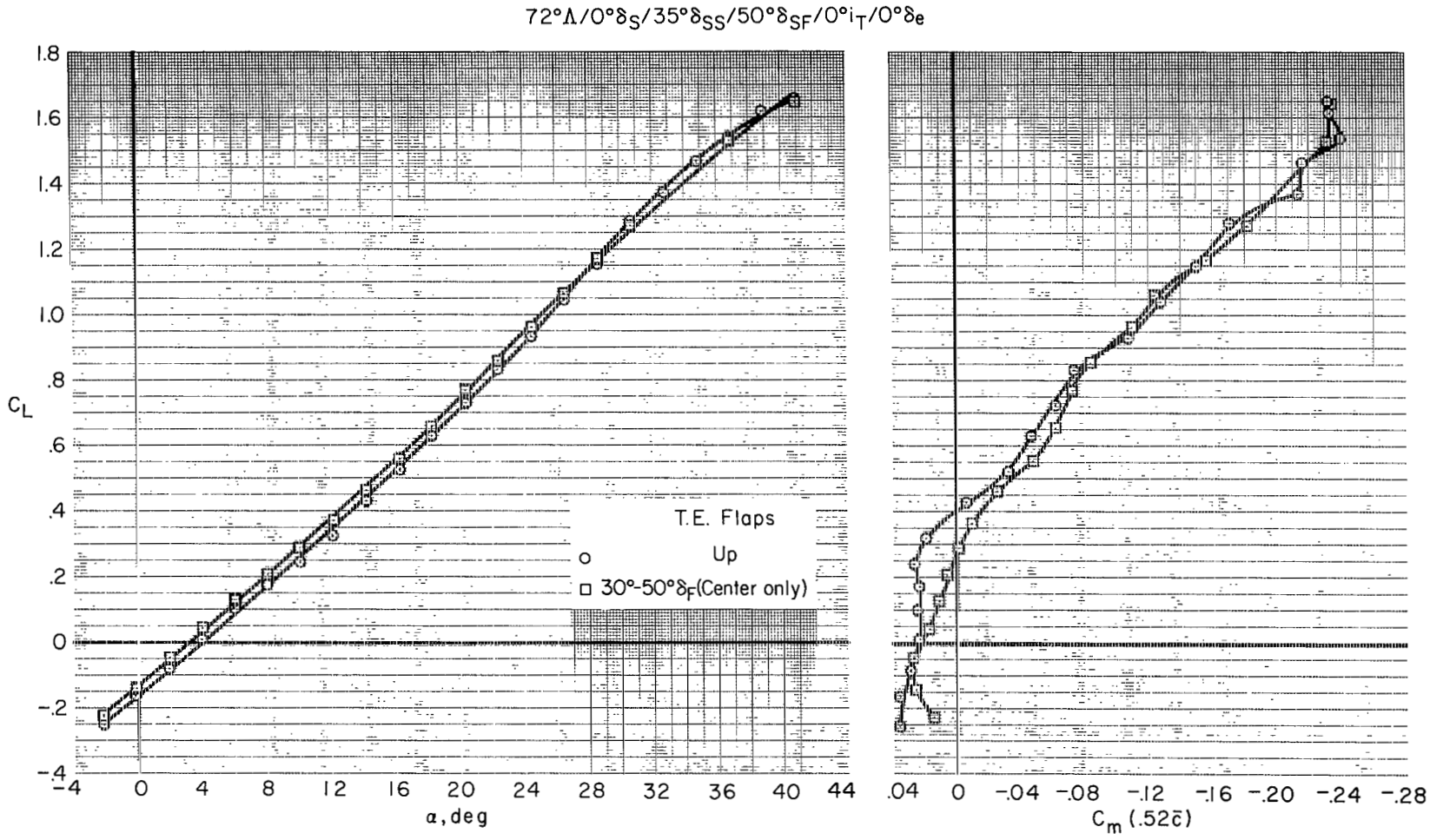

(a) C_L vs. α and C_m

Figure 33.- Effect of wing flap center-section deflection; 72° wing sweep.

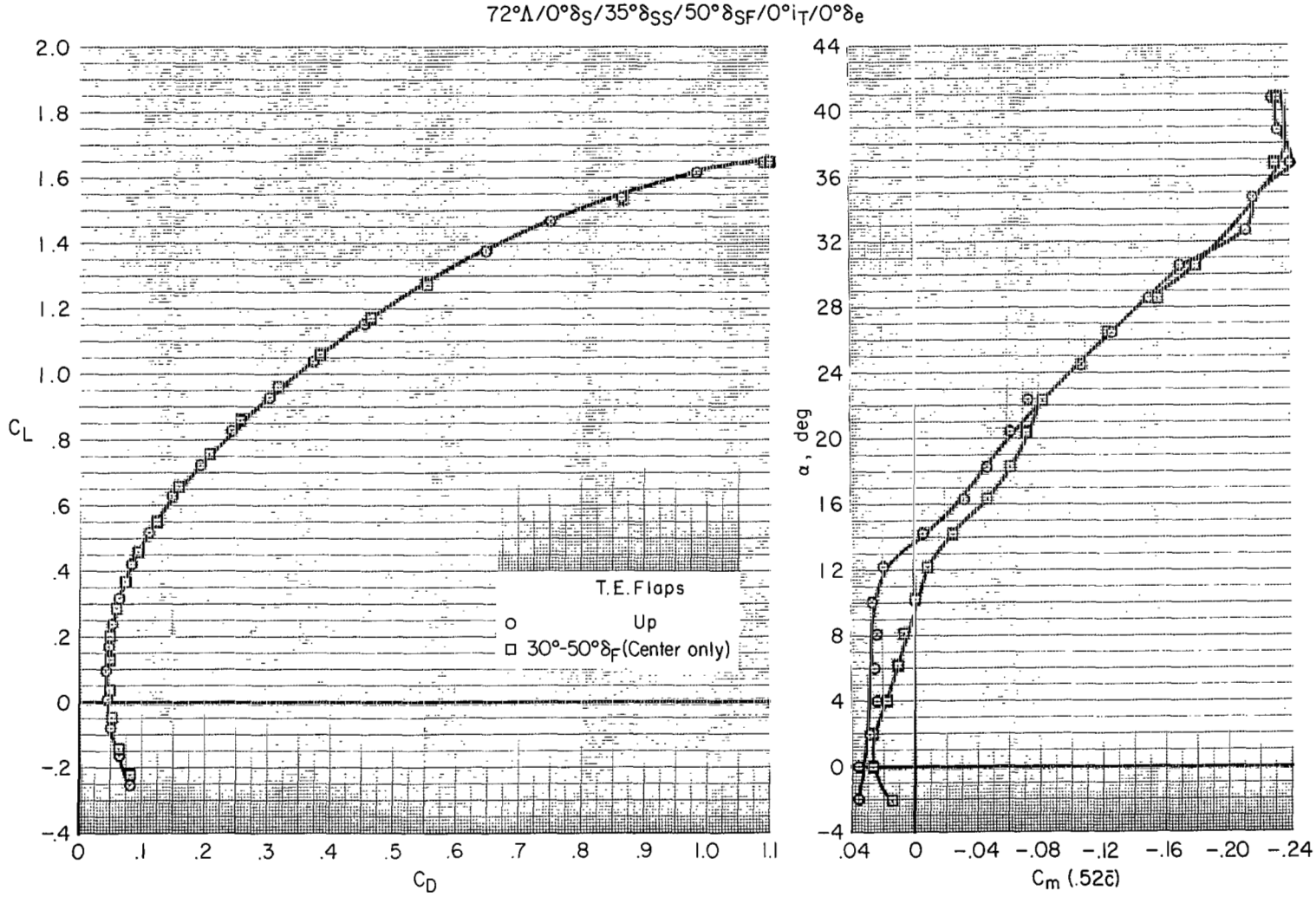

(b) C_L vs. C_D, α vs. C_m

Figure 33.- Concluded.

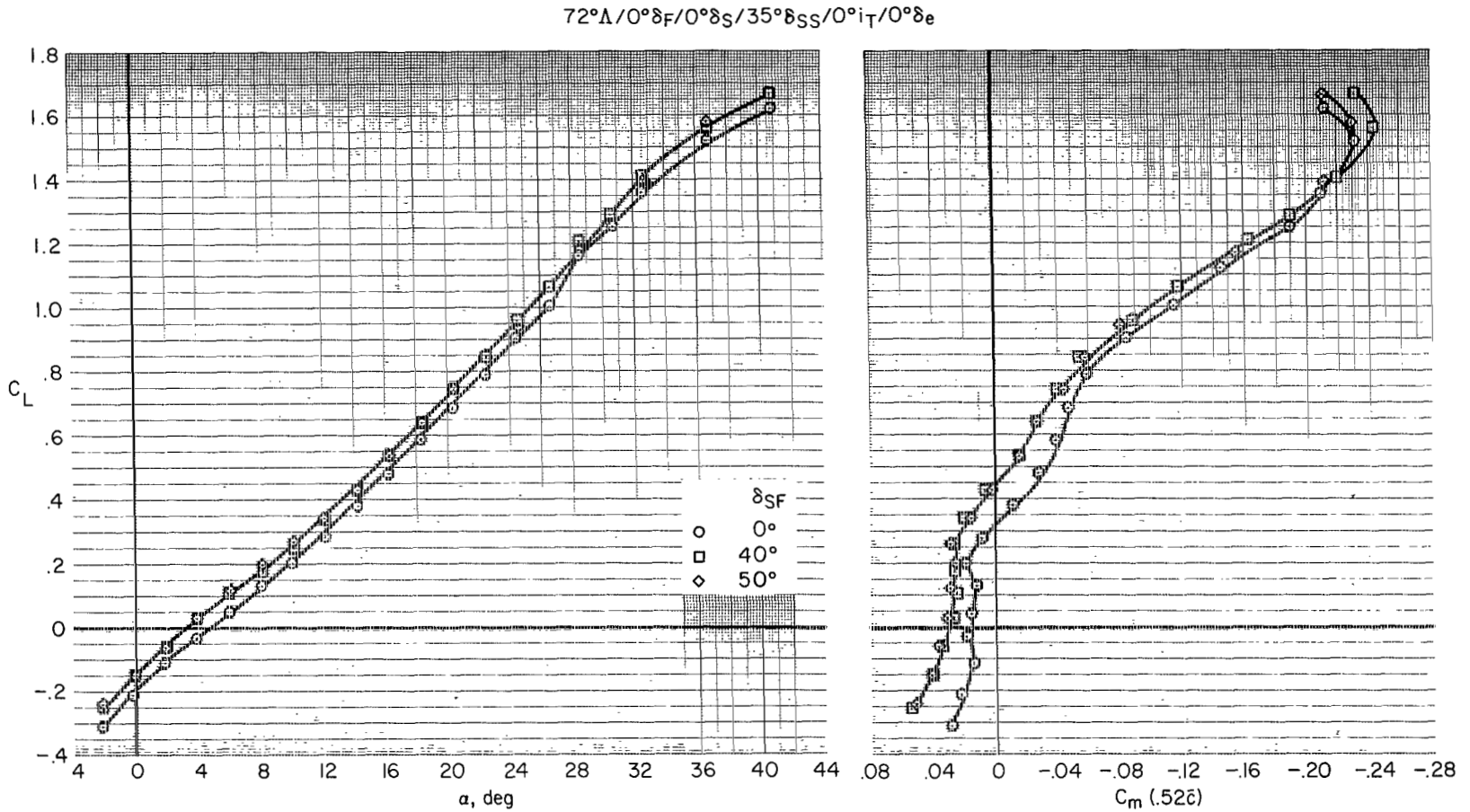

(a) C_L vs. α and C_m

Figure 34.- Effect of strake flap deflection; 72° wing sweep.

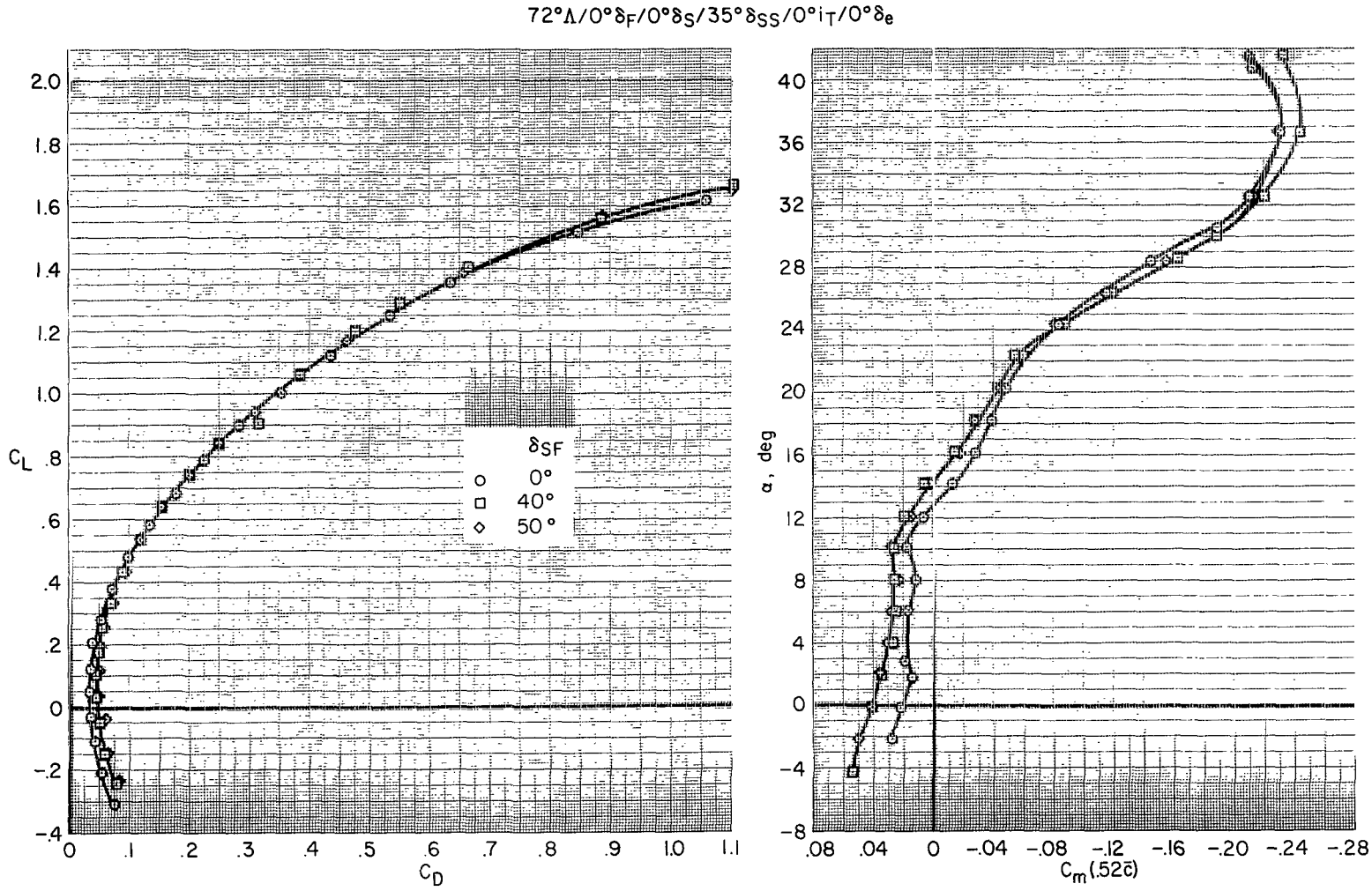

(b) C_L vs. C_D, α vs. C_m

Figure 34.- Concluded.

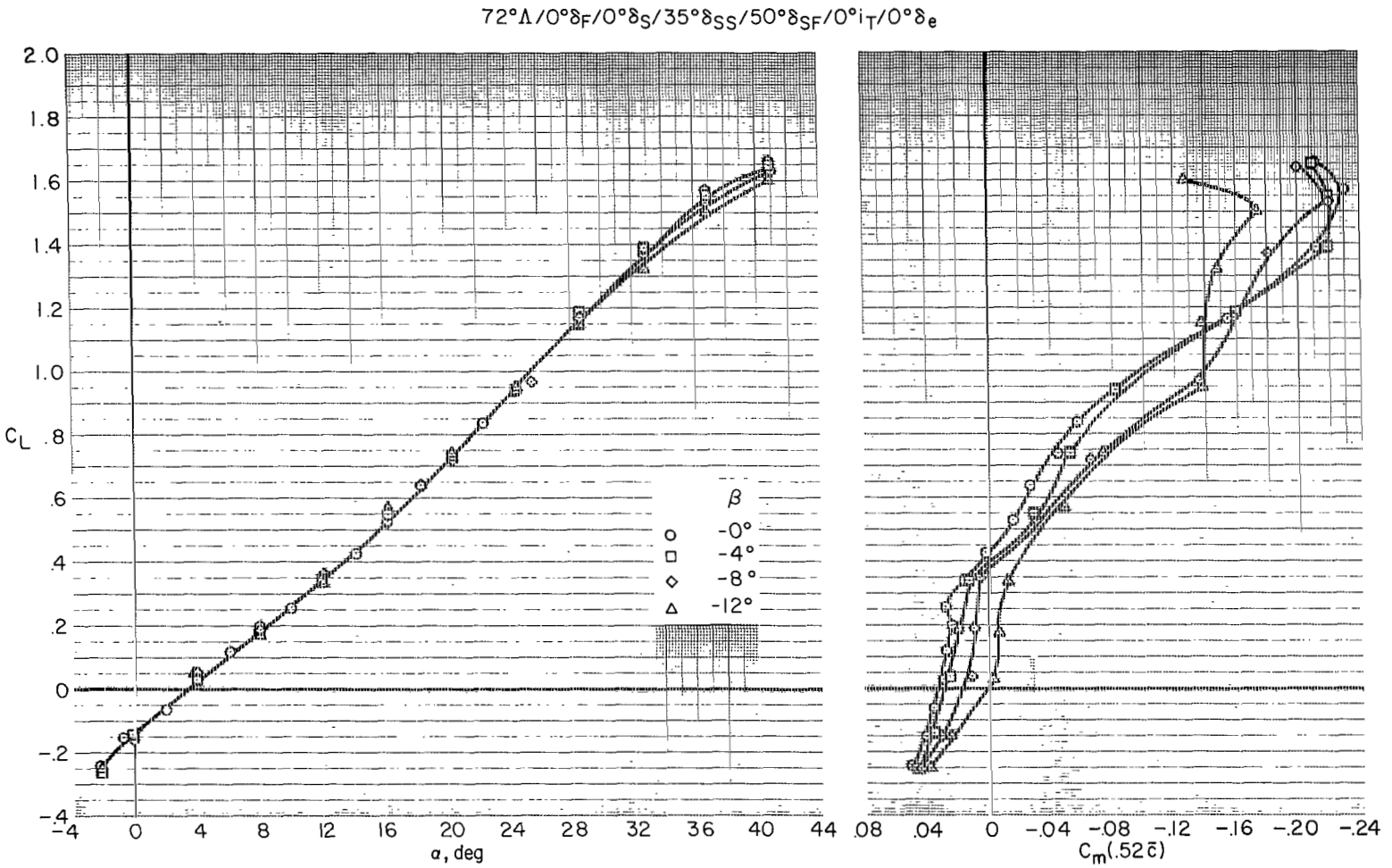

(a) Longitudinal characteristics, C_L vs. α and C_m.

Figure 35.- Characteristics in sideslip; 72° wing sweep.

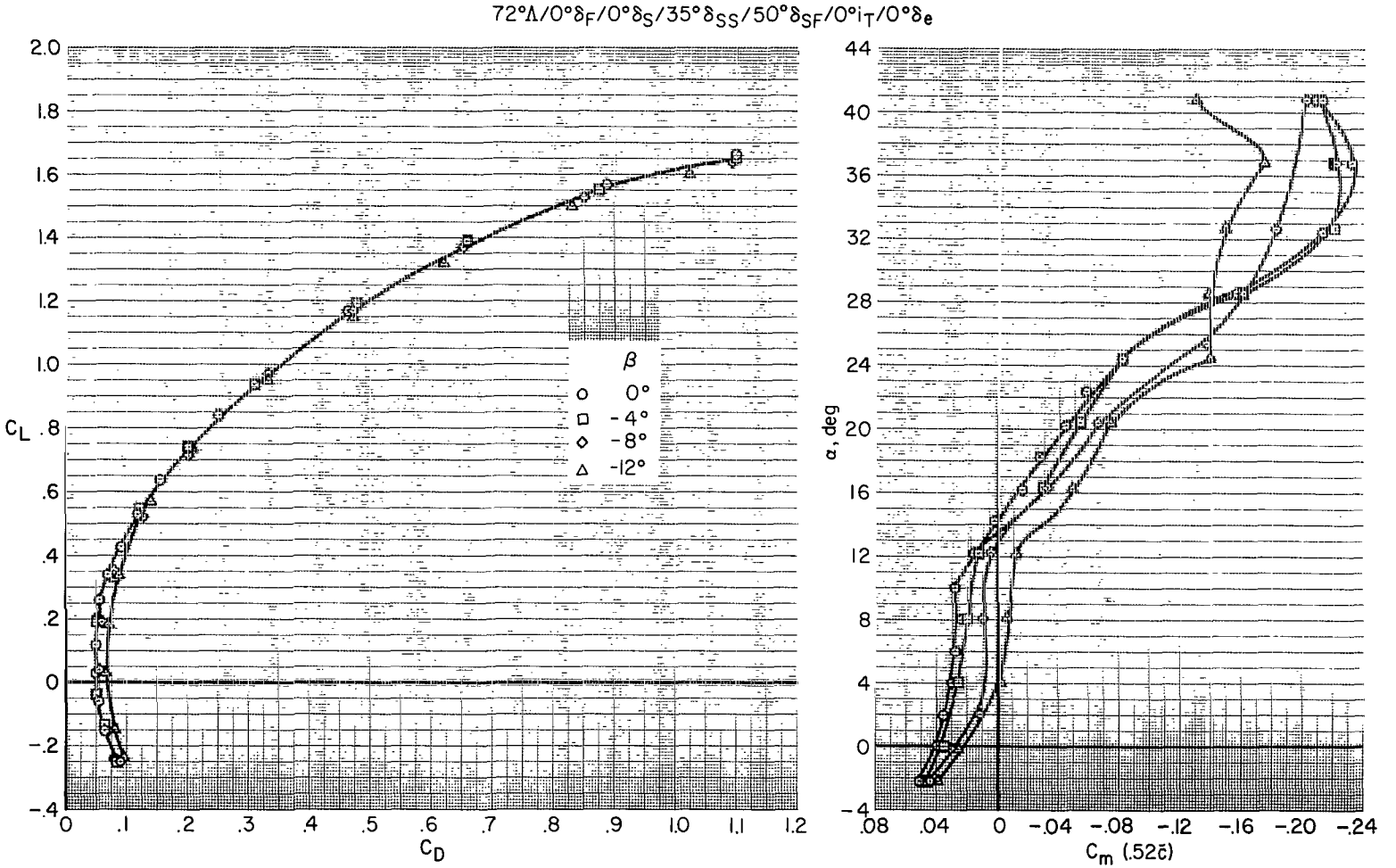

(b) Longitudinal characteristics; C_L vs. C_D, α vs. C_m.

Figure 35.- Continued.

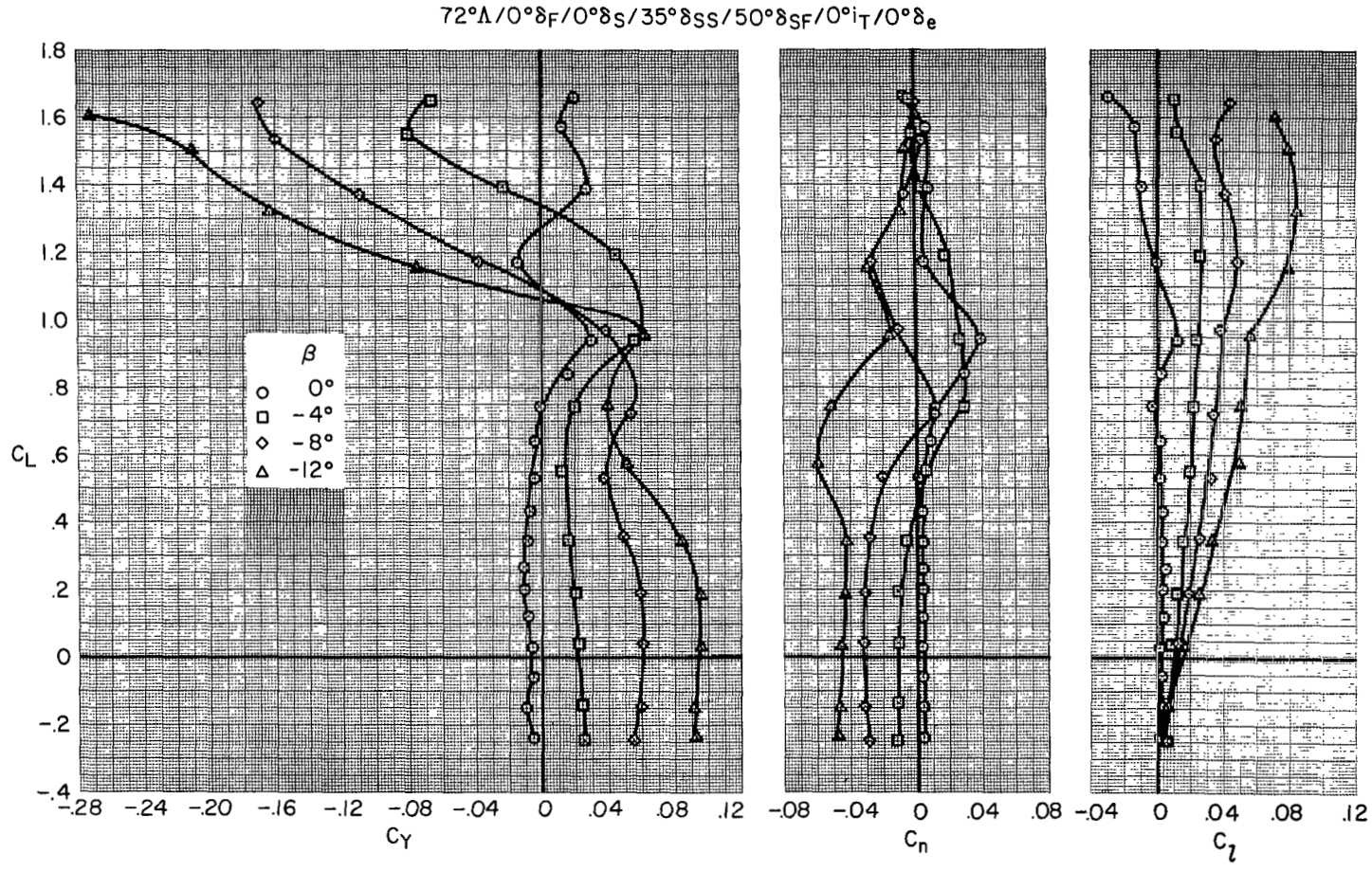

(c) Lateral-directional characteristics.

Figure 35.- Concluded.

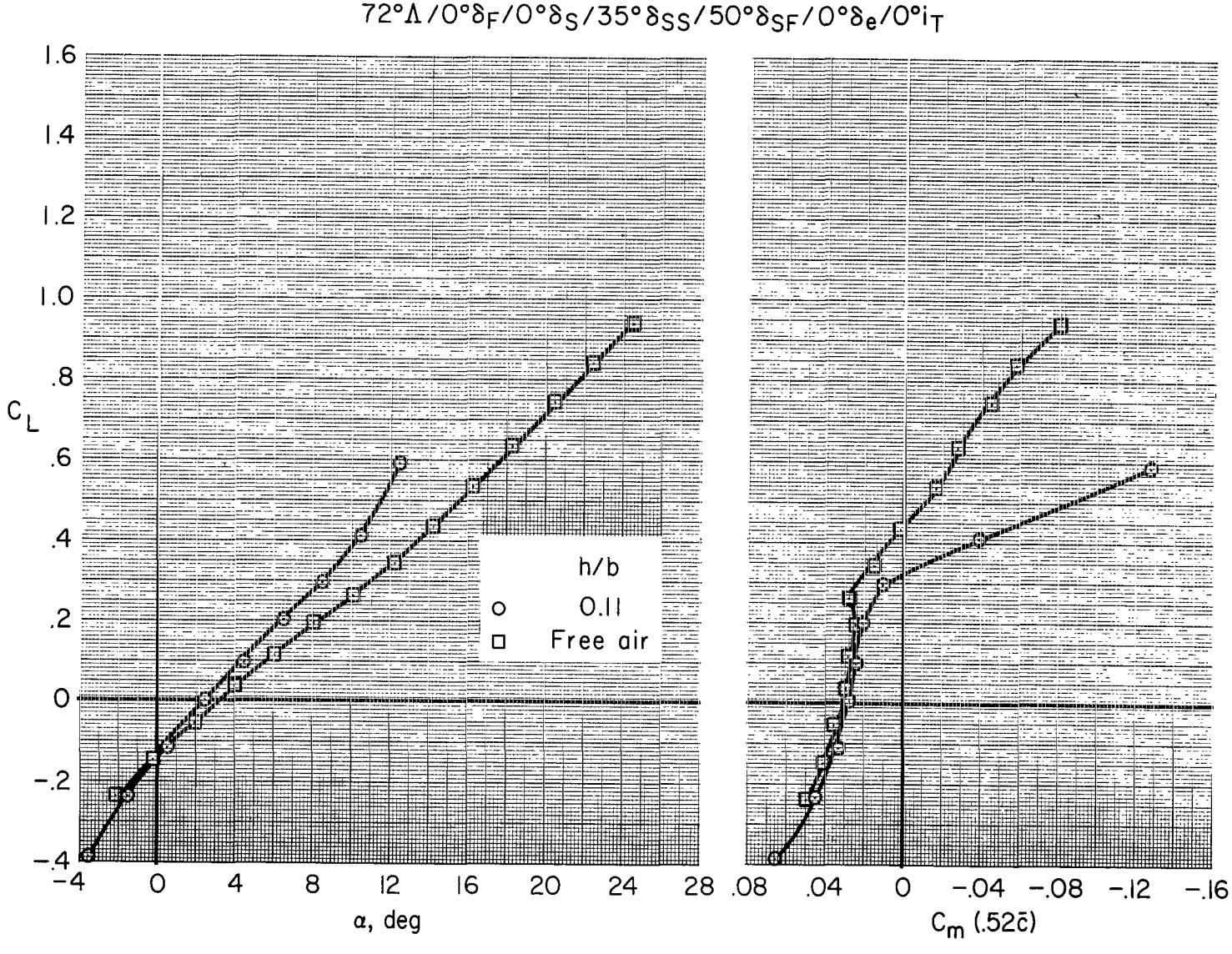

(a) C_L vs. α and C_m

Figure 36.- Effect of ground proximity; 72° wing sweep.

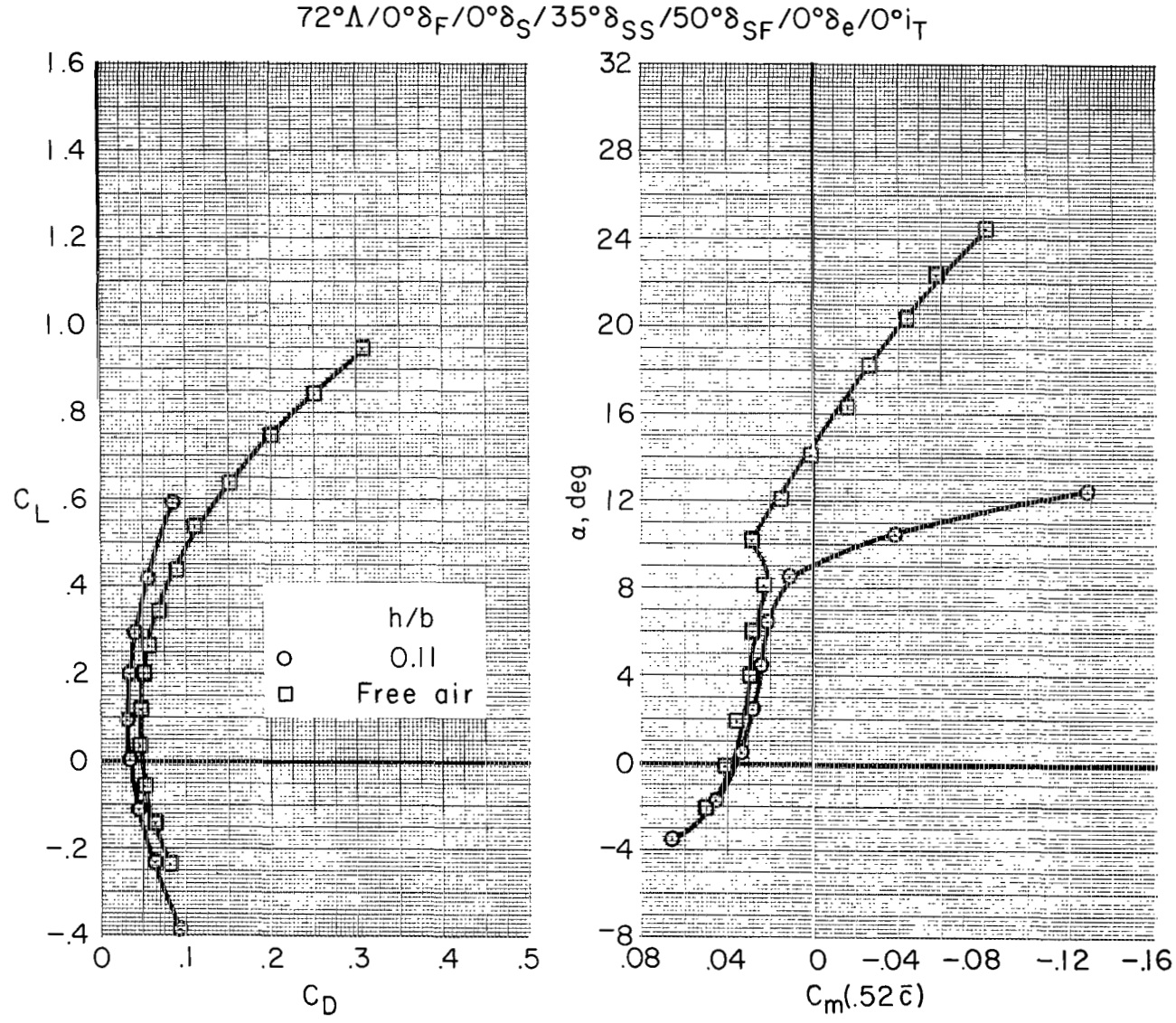

(b) C_L vs. C_D, α vs. C_m

Figure 36.- Concluded.

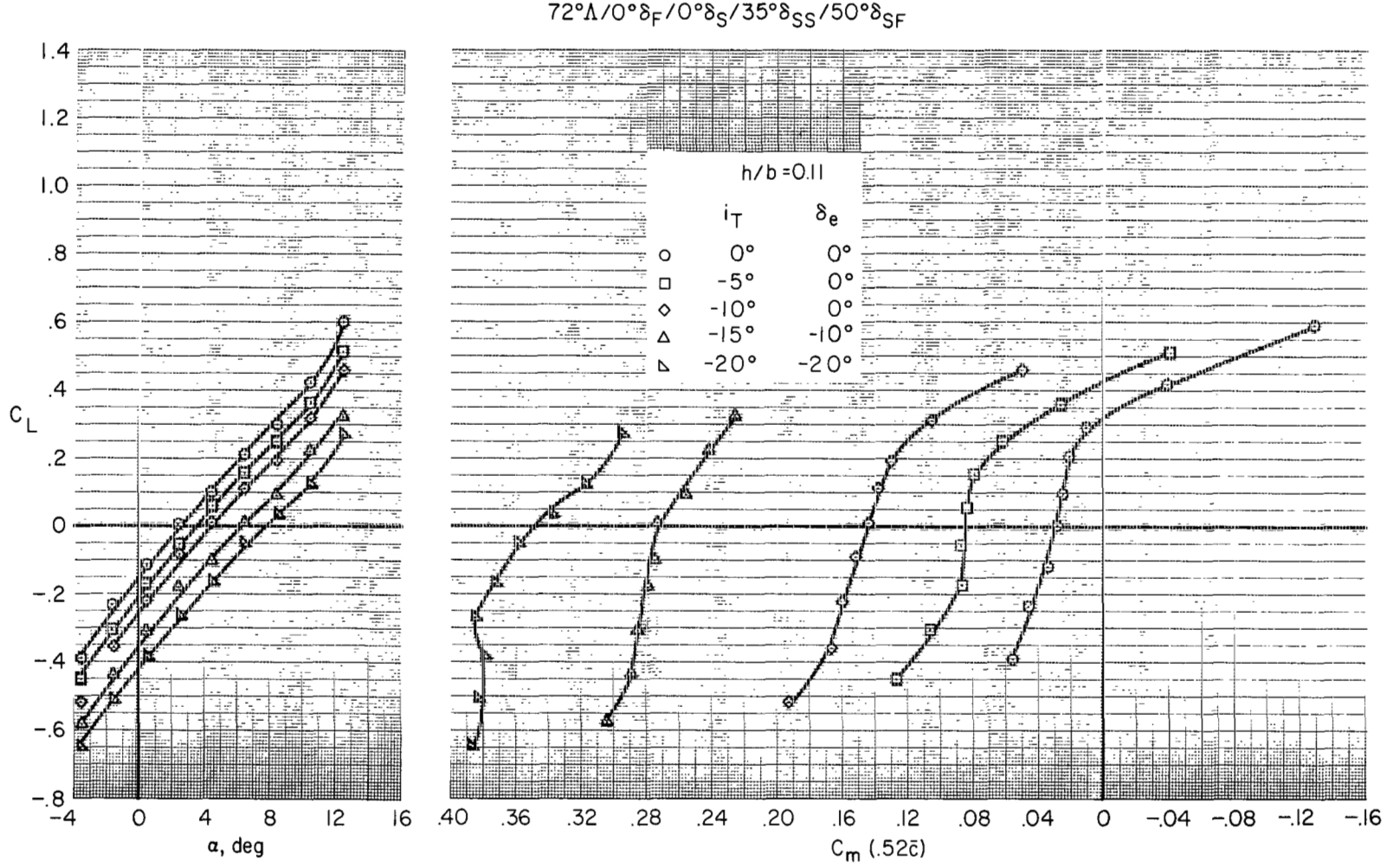

(a) C_L vs. α and C_m

Figure 37.- Effect of horizontal-tail incidence and elevator deflection; 72° wing sweep.

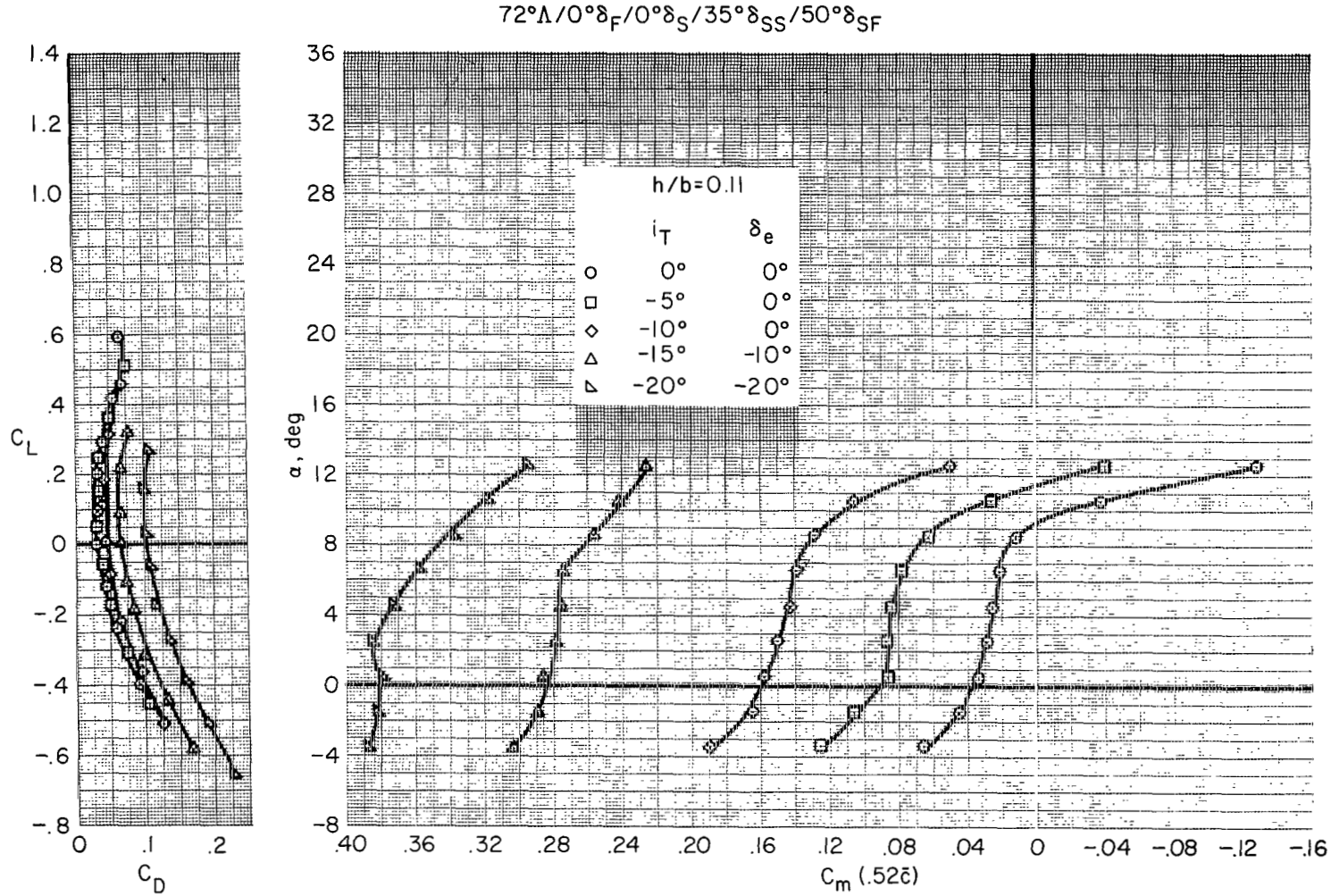

(b) C_L vs. C_D, α vs. C_m

Figure 37.- Concluded.

"The aeronautical and space activities of the United States shall be conducted so as to contribute . . . to the expansion of human knowledge of phenomena in the atmosphere and space. The Administration shall provide for the widest practicable and appropriate dissemination of information concerning its activities and the results thereof."

—NATIONAL AERONAUTICS AND SPACE ACT OF 1958

NASA SCIENTIFIC AND TECHNICAL PUBLICATIONS

TECHNICAL REPORTS: Scientific and technical information considered important, complete, and a lasting contribution to existing knowledge.

TECHNICAL NOTES: Information less broad in scope but nevertheless of importance as a contribution to existing knowledge.

TECHNICAL MEMORANDUMS: Information receiving limited distribution because of preliminary data, security classification, or other reasons.

CONTRACTOR REPORTS: Scientific and technical information generated under a NASA contract or grant and considered an important contribution to existing knowledge.

TECHNICAL TRANSLATIONS: Information published in a foreign language considered to merit NASA distribution in English.

SPECIAL PUBLICATIONS: Information derived from or of value to NASA activities. Publications include conference proceedings, monographs, data compilations, handbooks, sourcebooks, and special bibliographies.

TECHNOLOGY UTILIZATION PUBLICATIONS: Information on technology used by NASA that may be of particular interest in commercial and other non-aerospace applications. Publications include Tech Briefs, Technology Utilization Reports and Notes, and Technology Surveys.

Details on the availability of these publications may be obtained from:

SCIENTIFIC AND TECHNICAL INFORMATION DIVISION

NATIONAL AERONAUTICS AND SPACE ADMINISTRATION

Washington, D.C. 20546